



# **SENSITIVITY TESTS OF A 2-CATEGORY HIBLER ICE MODEL AND COMPARISON TO A 10-CATEGORY HIBLER ICE MODEL BOTH COUPLED TO A COX-BRYAN OCEAN MODEL**

Q. Yao and S.J. Prinsenber

Ocean Sciences Division  
Maritimes Region  
Fisheries and Oceans Canada

Bedford Institute of Oceanography  
P.O. Box 1006  
Dartmouth, Nova Scotia  
Canada B2Y 4A2

1999

## **Canadian Technical Report of Hydrography and Ocean Sciences 201**



Fisheries  
and Oceans

Pêches  
et Océans

Canada

PLEASE DO NOT  
REMOVE FROM  
LIBRARY

RECEIVED

APR 30 1999

INSTITUTE OF  
OCEANOGRAPHY

233453

Canadian Technical Report of  
Hydrography and Ocean Sciences 201

1999

**SENSITIVITY TESTS OF A 2-CATEGORY HIBLER ICE MODEL AND  
COMPARISON TO A 10-CATEGORY HIBLER ICE MODEL BOTH  
COUPLED TO A COX-BRYAN OCEAN MODEL**

by

Q. Yao and S.J. Prinsenber

Ocean Sciences Division  
Maritimes Region  
Department of Fisheries and Oceans

Bedford Institute of Oceanography  
P.O. Box 1006  
Dartmouth, Nova Scotia  
Canada B2Y 4A2

© Public Works and Government Services 1999  
Cat. No. Fs 97-18/201E ISSN 0711-6764

Correct Citation for this publication:

Yao, Q. and S.J. Prinsenberg, 1999. Sensitivity Tests of a 2-Category Hibler Ice Model and Comparison to a 10-Category Hibler Ice Model both Coupled to a Cox-Bryan Ocean Model. Can. Tech. Rep. Hydrogr. Ocean Sci. 201: xii + 108p.

**Table of contents**

<b>Abstract</b>	iv
<b>List of Figures</b>	vi
<b>List of Tables</b>	xi
<b>1. Introduction</b>	
1.1 Model geometry	2
1.2 Initial conditions	2
1.3 Forcing data	3
<b>2. Model simulations and sensitivity tests</b>	5
2.1 The 15-level model	6
2.2 The 17-level model	8
2.3 Vertical mixing coefficient of momentum	9
2.4 Horizontal mixing coefficient	11
2.5 Albedos of water and ice	12
2.6 Ice strength ( $P^*$ )	13
2.7 Wind and air temperature forcing	14
2.8 Multi-category ice-ocean model	17
<b>3. Comparison of model ice and ocean velocity simulations with observations</b>	18
3.1 Ice velocities	18
3.2 Ocean Parameters	26
<b>4. Conclusions</b>	29
<b>Acknowledgment</b>	30
<b>References</b>	31

## ABSTRACT

Yao, Q. and S.J. Prinsenberg, 1999. Sensitivity Tests of a 2-Category Hibler Ice Model and Comparison to a 10-Category Hibler Ice Model both Coupled to a Cox-Bryan Ocean Model. Can. Tech. Rep. Hydrogr. Ocean Sci. 201: xii + 108p.

A full three-dimensional ocean model coupled to ice models using realistic geometry and real atmospheric forcing is used to investigate the coupled ice-ocean model sensitivities to model and forcing parameters in simulating the seasonal evolution of the ice cover along the Canadian East Coast. This study follows the investigations into the ice-ocean processes started with simpler coupled ice-ocean models and documents the tests done with a 2-category ice model before it was replaced by a 10-category ice model.

The coupled ice-ocean model, used along with earlier results, was presented in detail by Ikeda et al. (1996). This manuscript will present results derived with that 15-level ice-ocean model and will present sensitivity tests of a 17-level ice-ocean model. The 2-category ice model simulations are also briefly compared to results obtained with a 10-category ice model.

Sensitivity tests showed that both increasing the number of surface layers and the vertical mixing coefficient affected the ice and surface ocean properties more than the ocean currents at depths where available current observations are underestimated in model simulations. Simulations also showed that the ice extent and ice area are strongly affected by ice and ocean albedos and cloud cover values. These are taken in previous model simulation as being constant or as climatic norms, suggesting that seasonal variable albedo values or derived values should be used in future simulations. Major improvements in model simulations were achieved in ice concentration by changing to a 10-category ice model and in ice extent by changing to an improved initial oceanographic data set.

## RÉSUMÉ

Yao, Q. and S.J. Prinsenberg, 1999. Sensitivity Tests of a 2-Category Hibler Ice Model and Comparison to a 10-Category Hibler Ice Model both Coupled to a Cox-Bryan Ocean Model. Can. Tech. Rep. Hydrogr. Ocean Sci. 201: xii + 108p.

On utilise un modèle océanique tridimensionnel complet couplé à des modèles des glaces comprenant une géométrie réaliste et un forçage atmosphérique réel pour étudier à quel point les résultats du modèle couplé glaces-océan sont sensibles aux variations du modèle et des paramètres de forçage dans la simulation de l'évolution saisonnière de la couverture glacielle sur la côte est du Canada. Cette recherche fait suite aux études des processus glaces-océan démarrées avec des modèles couplés glaces-océan et documente les tests effectués avec un modèle des glaces à deux catégories qui a été depuis remplacé par un modèle des glaces à 10 catégories.

Le modèle couplé glaces-océan, utilisé avec les résultats antérieurs, a été présenté en détail par Ikeda *et al.* (1996). Ce manuscrit présentera les résultats obtenus à partir de ceux du modèle glaces-océan à 15 niveaux, ainsi que les tests de sensibilité d'un modèle glaces-océan à 17 niveaux. Les simulations du modèle de glaces à 2 catégories sont également comparés rapidement aux résultats obtenus avec un modèle à 10 catégories.

Les tests de sensibilité ont montré qu'en augmentant le nombre de couches de surface et le coefficient de mélange vertical, on modifiait davantage les propriétés de la glace et de l'océan superficiel que les courants océaniques à des profondeurs où les observations de courants disponibles sont sous-estimées dans les modélisations. Les simulations ont aussi montré que l'extension et la superficie de la glace sont fortement influencées par les albédos de la glace et de l'océan et par les valeurs des couvertures nuageuses. Dans les simulations des précédents modèles, ces paramètres sont représentés par des constantes ou des normales climatologiques, ce qui suggère qu'il faudrait prendre, dans les simulations futures, les valeurs saisonnières variables de l'albédo ou des valeurs dérivées de celles-ci. On a obtenu de meilleures modélisations des concentrations des glaces en adoptant un modèle de glaces à 10 catégories et de l'extension de la glace en utilisant un ensemble initial de données océanographiques amélioré.

**List of Figures:**

Fig. 1.1 Extent of the model domain.	A1
Fig. 1.2 Model's representation of bottom topography using 15 depth layers.	A2
Fig. 2.1 Weekly time series data of ice extent, ice area and ice volume for the 1991/92 ice season for the Labrador and Newfoundland Shelf area.	A3
Fig. 2.2 Time series simulated by the 2-category model with 15 ocean layers for the 1991/92 ice season.	A4
Fig. 2.3a Daily mean ice velocity and mixing layer's ocean velocity simulated by the 2-category model with 15 ocean layers for Jan. 29, 1992.	A5
Fig. 2.3b Daily mean ice velocity and mixing layer's ocean velocity simulated by the 2-category model with 15 ocean layers for Feb. 25, 1992.	A6
Fig. 2.3c Daily mean ice velocity and mixing layer's ocean velocity simulated by the 2-category model with 15 ocean layers for Mar. 29 1992.	A7
Fig. 2.4 Daily mean ECMWF winds for different 3 days at 6 locations.	A8
Fig. 2.5 Time series simulated by the 2-category model with 17 ocean layers for the 1991/92 ice season for Labrador and Newfoundland Shelf area.	A9
Fig. 2.6a <sub>1</sub> Daily mean ice velocity and ocean velocity averaged over layers 1, 2 and 3 simulated by the 2-category model with 17 ocean layers for Jan. 29, 1992.	A10
Fig. 2.6a <sub>2</sub> Daily mean ocean velocities of the surface and second layers simulated by the 2-category model with 17 ocean layers for Jan. 29, 1992.	A11
Fig. 2.6a <sub>3</sub> Daily mean ocean velocities of the third and fourth layers simulated by the 2-category model with 17 ocean layers for Jan. 29, 1992.	A12
Fig. 2.6b <sub>1</sub> Daily mean ice velocity and ocean velocity averaged over layers 1, 2 and 3 simulated by the 2-category model with 17 ocean layers for Feb. 25, 1992.	A13
Fig. 2.6b <sub>2</sub> Daily mean ocean velocities of the surface and second layers simulated by the 2-category model with 17 ocean layers for Feb. 25, 1992.	A14
Fig. 2.6b <sub>3</sub> Daily mean ocean velocities of the third and fourth layers simulated by the 2-category model with 17 ocean layers for Feb. 25, 1992.	A15

Fig. 2.6c <sub>1</sub> Daily mean ice velocity and ocean velocity averaged over layers 1, 2 and 3 simulated by the 2-category model with 17 ocean layers for Mar. 29, 1992.	A16
Fig. 2.6c <sub>2</sub> Daily mean ocean velocities of the surface and second layers simulated by the 2-category model with 17 ocean layers for Mar. 29, 1992.	A17
Fig. 2.6c <sub>3</sub> Daily mean ocean velocities of the third and fourth layers simulated by the 2-category model with 17 ocean layers for Mar. 29, 1992.	A18
Fig. 2.7a Station locations for which ocean current data is available for comparison with model simulations (from Narayanan et al., 1996). Station numbers are also used to indicate grid locations for which sensitivity test results are shown.	A19
Fig. 2.7b <sub>1</sub> Model ocean speeds at stations 18, 19 and 21 of the basic and test 2 for Feb. 29 to Mar. 29, 1992. Depth range of level 4 is from 30 to 50m and for level 6 from 70 to 100m.	A20
Fig. 2.7b <sub>2</sub> Model ocean speeds at stations 22, 24, 27 and 28 of the basic and test 2 for Feb. 29 to Mar. 29, 1992. Depth range of level 4 is from 30 to 50m and for level 6 from 70 to 100m.	A21
Fig. 2.8a Simulated time series of ice extent, ice area and ice volume of test case 2 for the 1991/92 ice season.	A22
Fig. 2.8b Simulated ice equivalent thickness of basic and test case 2 for Mar.16, 1992.	A23
Fig. 2.8c Simulated temperature and salinity profiles at locations 1, 2, and 3 (locations shown on Fig. 2.8b) of basic and test case 2 for Mar 16, 1992.	A24
Fig. 2.9 Simulated time series of test 3, 4 and basic cases for 1991/92 ice season.	A25
Fig. 2.10a Model ocean speeds at stations 18, 19 and 21 of the basic and test 3 for Feb. 29 to Mar. 29, 1992.	A26
Fig. 2.10b Model ocean speeds at stations 22, 24, 27 and 28 of the basic and test 3 for Feb. 29 to Mar. 29, 1992.	A27
Fig. 2.11a Model ocean speeds at stations 18, 19 and 21 of the basic and test 4 for Feb. 29 to Mar. 29, 1992.	A28
Fig. 2.11b Model ocean speeds at stations 22, 24, 27 and 28 of the basic and test 4 for Feb. 29 to Mar. 29, 1992.	A29
Fig. 2.12 Simulated time series of ice extent, ice area and ice volume of albedo test case 5 for the 1991/92 ice season.	A30

Fig. 2.13 Simulated time series of ice extent, ice area and ice volume of albedo test case 6 for the 1991/92 ice season.	A31
Fig. 2.14 Simulated time series of ice extent, ice area and ice volume of albedo test case 7 for the 1991/92 ice season.	A32
Fig. 2.15 Weekly time series data of ice extent, ice area and ice volume for the 1971/72 ice season for the Labrador and Newfoundland Shelf area.	A33
Fig. 2.16 Simulated time series of ice extent and ice volume of P* test case 15.1 and 15.2 for the 1971/72 ice season.	A34
Fig. 2.17 Simulated time series of ice extent and ice volume of P* test case 17.1 and 17.2 for the 1971/72 ice season.	A35
Fig. 2.18 Simulated time series of wind and air temperature tests for 2 wind cases compared to basic case of the 1991/92 ice season.	A36
Fig. 2.19 Simulated time series of wind and air temperature tests for 2 air temperature cases compared to basic case of the 1991/92 ice season.	A37
Fig. 2.20 Daily mean ice velocity examples for 2 air temperature cases on Apr 16, 1992.	A38
Fig. 2.21 Daily mean wind distribution for Apr 16, 1992.	A39
Fig. 2.22a Alongshore components of daily ice transport averaged across Hamilton Bank for wind and basic cases between Dec. 1 1991 to Mar. 29, 1992.	A40
Fig. 2.22b Alongshore component of daily ice transport averaged across Hamilton Bank for wind and basic cases between Mar 30, 1992 to May 28.	A41
Fig. 2.23a Offshore components of daily ice transport averaged across Hamilton Bank for wind and basic cases between Dec. 1 1991 to Mar. 29, 1992.	A42
Fig. 2.23b Offshore component of daily ice transport averaged across Hamilton Bank for wind and basic cases between Mar 30, 1992 to May 28.	A43
Fig. 2.24a Alongshore components of daily ice transport averaged across Hamilton Bank for air temperature and basic cases between Dec. 1 1991 to Mar. 29, 1992.	A44
Fig. 2.24b Alongshore component of daily ice transport averaged across Hamilton Bank for air temperature and basic cases between Mar 30, 1992 to May 28.	A45

Fig. 2.25a Offshore components of daily ice transport averaged across Hamilton Bank for air temperature and basic cases between Dec. 1 1991 to Mar. 29, 1992.	A46
Fig. 2.25b Offshore component of daily ice transport averaged across Hamilton Bank for air temperature and basic cases between Mar 30, 1992 to May 28.	A47
Fig. 2.26 Comparison of 2- and 10-category ice models for 1991/92 ice season.	A48
Fig. 2.27 Comparison of ice concentration by 2- and 10-category ice models for Feb. 26, 1992.	A49
Fig. 3.1 Comparison of daily mean ice velocities of beacon data and model simulations for Mar. 8, 1992.	A50
Fig. 3.2 Comparison of daily mean ice velocities of beacon data and model simulations for Mar. 9, 1992.	A51
Fig. 3.3 Comparison of daily mean ice velocities of beacon data and model simulations for Mar. 11, 1992.	A52
Fig. 3.4 Comparison of daily mean ice velocities of beacon data and model simulations for Mar. 13, 1992.	A53
Fig. 3.5 Comparison of daily mean ice velocities of image data and model simulations for Feb. 23, 1992.	A54
Fig. 3.6 Comparison of daily mean ice velocities of image data and model simulations for Mar. 8, 1992.	A55
Fig. 3.7 Comparison of daily mean ice velocities of image data and model simulations for Apr. 17, 1992.	A56
Fig. 3.8 Comparison of daily mean ice velocities of image data and model simulations for Apr. 18, 1992.	A57
Fig. 3.9a Ice velocity scatter plot of beacon data and model simulations for Feb., 1992.	A58
Fig. 3.9b Ice velocity scatter plot of image data and model simulations for Feb., 1992.	A59
Fig. 3.10a Ice velocity scatter plot of beacon data and model simulations for Mar., 1992.	A60

Fig. 3.10b Ice velocity scatter plot of image data and model simulations for Mar., 1992.	A61
Fig. 3.11a Ice velocity scatter plot of beacon data and model simulations for Apr. 1992.	A62
Fig. 3.11b Ice velocity scatter plot of image data and model simulations for Apr. 1992.	A63
Fig. 3.12 Ice velocity scatter plot of beacon data and model simulations for Feb. 22 to May 22, 1994.	A64
Fig. 3.13a Comparison of daily mean ocean velocities and speeds of MCM data and model simulations at Station 15 for Feb. 29 to Mar. 29, 1992.	A65
Fig. 3.13b Comparison of daily mean ocean velocities and speeds of MCM data and model simulations at Station 18 for Feb. 29 to Mar. 29, 1992.	A66
Fig. 3.13c Comparison of daily mean ocean velocities and speeds of MCM data and model simulations at Station 19 for Feb. 29 to Mar. 29, 1992.	A67
Fig. 3.13d Comparison of daily mean ocean velocities and speeds of MCM data and model simulations at Station 30 for Feb. 29 to Mar. 29, 1992.	A68
Fig. 3.13e Comparison of daily mean ocean velocities and speeds of MCM data and model simulations at Station 40 for Feb. 29 to Mar. 29, 1992.	A69
Fig. 3.14 March 1992 salinity and temperature profiles from Hamilton Bank stations 1-3, and from Cartwright Saddle stations 4-6.	A70
Fig. 3.15 Initial temperature and salinity profiles used by the model at stations 1-6.	A71
Fig. 3.16 March 1992 model simulated temperature and salinity profiles at stations 1-6.	A72
Fig. 3.17 Comparison of weekly data and 10-category ice models for 1991/92 ice season.	A73
Fig. 3.18 Comparison of ice concentration weekly data and 10-category ice models for Feb. 26, 1992.	A74
Fig. 3.19 Concentrations of 10-category ice model for Jan. 30, Feb. 29, Mar. 30 and Apr. 29, 1992.	A75

## List of Tables

Table 1.1 Model parameters used in the 15- and 17-level ice-ocean models.	3
Table 2.1 Comparison of the vertical mixing coefficients of momentum used in the basic cases of the 15-level and the 17-level ocean model.	8
Table 2.2 Ice and ocean speeds of basic case at station #40, Hamilton Bank slope.	9
Table 2.3 Ice and ocean speeds of test case 1 at station #40, Hamilton Bank slope.	9
Table 2.4 Horizontal mixing coefficients of test cases 3 and 4.	11
Table 2.5 Water and ice albedo values for simulation tests 5 through 7.	12
Table 2.6 Values of ice strength ( $P^*$ ) for test cases using 15- and 17-level ocean model.	13
Table 2.7 1991/92 monthly mean ice transports (along-shore), averaged across Hamilton Bank for the basic and four test cases (unit: $\text{km}^3/\text{day}/\text{km}$ ).	16
Table 2.8 1991/92 monthly mean ice transports (offshore), averaged across Hamilton Bank for the basic and four test cases (unit: $\text{km}^3/\text{day}/\text{km}$ ).	16
Table 2.9 Ice thickness categories of the 10-category ice model.	17
Table 3.1 Number of grid's daily ice velocities for each day available from beacon-derived velocity observations.	18
Table 3.2 Number of grid's daily ice velocities for each day available from image-derived velocity data sets.	19
Table 3.3a Correlation results of model versus observed ice beacon velocities for the total ice season covering 79 days (476 samples) between Feb. and April, 1992.	21
Table 3.3b Correlation results of model versus observed ice beacon velocities for February, 1992 covering 18 days (64 samples).	21
Table 3.3c Correlation results of model versus observed ice beacon velocities for March, 1992 covering 31 days (247 samples).	22
Table 3.3d Correlation results of model versus observed ice beacon velocities for April, 1992 covering 30 days (165 samples).	22

Table 3.4a Correlation results of model versus image-derived ice velocities for February to April, 1992 covering 6 days (622 samples).	23
Table 3.4b Correlation results of model versus image-derived ice velocities for February, 1992 covering 1 day (140 samples).	23
Table 3.4c Correlation results of model versus image-derived ice velocities for March, 1992 covering 1 day period (148 samples).	24
Table 3.4d Correlation results of model versus image-derived ice velocities for April, 1992 covering 4 days (334 samples).	24
Table 3.5 Correlation results of model versus observed ice beacon velocities for March to May, 1994 covering 68 days (170 samples).	25
Table 3.6 Model depth levels.	26
Table 3.7. Location and depth of MCM data and model layers used for comparison with the available east and north components of ocean velocity, U and V, and ocean temperatures and salinities, T and S. (* data period is to March 29 only; locations of stations were shown on Fig. 2.7a).	27
Table 3.8 Model parameters used in the final version of the 10-category ice-ocean coupled model whose simulations are shown in Figs. 3.17 and 3.18.	29

## 1. INTRODUCTION

The ice-ocean modelling work at the Bedford Institute for the Labrador Shelf has progressed by systematically adding more physics in several numerical models. Ikeda et al. (1988) first applied Hibler's ice model to the Labrador Shelf with a fixed-thickness ocean mixed layer. It revealed that interannual variability in the ice cover is highly correlated with air temperature but that sea ice over the southern shelf (south of  $55^{\circ}\text{N}$ ) is transported from the north. Results suggested that sea ice is advected from north of  $55^{\circ}\text{N}$  but the ice extent south of  $55^{\circ}\text{N}$  is controlled thermodynamically. An active mixed-layer model was added to this particular ice-ocean model (Yao and Ikeda, 1990); it showed that vertical heat flux associated with convective mixing suppresses ice growth. However, their ocean currents, which could transport ice and heat laterally, were prescribed but not simulated in the model. Mysak et al. (1991), using a reduced gravity ocean model to study the mechanisms controlling the offshore ice edge location, found that the ice edge position is determined by a heat balance between atmospheric cooling and onshore heat flux associated with wind-driven Sverdrup flow. Finally, Ikeda (1991) expanded his earlier coupled ice-ocean model with idealized geometry and atmospheric heat forcing as well as limited circulation dynamics (cross-shelf geostrophy). It was found that the southward along-shelf current induces an onshore secondary circulation, which carries significant heat and reduces ice growth. The results indicated that a full 3-D ocean model was required (i.e. Ikeda et al., 1996) to investigate seasonal ice evolution and oceanic processes. The processes important for ice cover evolution include wind-driven ice movement as well as oceanic processes such as seasonal mixed-layer development, shelf circulation and cross-shelf exchanges associated with topographic (banks and saddles) effects on the Labrador Current.

This report uses a 2-category Hibler ice model coupled to a Cox-Bryan ocean model as described in Ikeda et al. (1996) to examine the seasonal advance and retreat of the ice cover over the Labrador Shelf. The coupled model also examines the dynamic and thermodynamic roles of the shelf/slope water on the ice cover extent and thickness. The model is an ice model developed by Hibler (1979) coupled with the ocean general circulation model developed by Bryan and Cox (Bryan, 1969). After a short description of the 2-category model, its controlling parameters and initial and forcing conditions, the manuscript describes sensitivity tests in section 2 including a brief comparison of the 2- and 10-category ice models. Sensitivity tests for 10-category ice type model will not be included in this report. In section 3 the model ice drifts and ocean currents are compared with ice and ocean observations.

## 1.1 Model geometry

The model's domain (Fig. 1.1) uses spherical coordinates and extends from  $39.75^{\circ}$  to  $65.25^{\circ}$  in the north-south direction and from the Canadian east coast ( $64.5^{\circ}$  W) to nearly to European coast ( $15.5^{\circ}$ W) in the east-west direction. The latitudinal grid scale is uniformly  $0.25^{\circ}$ , and the longitudinal grid scale varies from  $0.5^{\circ}$  (west to  $39.5^{\circ}$ ) to  $1^{\circ}$  (east to  $39.5^{\circ}$ ). Fig. 1.1 shows the location of the 1000 meter bathymetric contour, which along the Labrador and Newfoundland shelves can be taken as the location of the Labrador current, the major southward moving current along the Canadian northern coast. Results of the model will only be shown for a sub-area called the analysis field (Fig. 1.1). This area is of major concern to forecasters providing ice and ocean information to the shipping industry. It is also the area where most of our ice and ocean observations have been collected and form a basis to validate the model. Realistic bottom topography is implemented based on the 1/12-degree global data. The vertical coordinates are discretized into 15 levels with thickness of 30, 50, 70, 100, 130, 160, 230, 280, 350, 4x500, and 2x300m, see Fig. 1.2. When 17 levels are used, the first 30m level is split up into three levels each 10m thick while the others remain the same as those of the 15-level model.

## 1.2 Initial conditions

The models are initialized on December 1 (model day #1) with the basin-scale fall ocean temperature and salinity as compiled by Levitus (1982). Since this data is greatly smoothed in the horizontal plane, it was modified with fresher and colder water over the Labrador Shelf to a depth of 250 meters. This is done to reflect the colder, low salinity shelf water that enters the domain in the north from the Arctic through Davis Strait. The temperatures in levels 1, 2, 3, and 4 of the 15-level model are reduced respectively by  $2^{\circ}\text{C}$ ,  $1.5^{\circ}\text{C}$ ,  $1^{\circ}\text{C}$  and  $0.5^{\circ}\text{C}$ ; and the salinities by 1ppt, 0.75ppt, 0.5ppt and 0.25ppt. A 17-level ocean model was generated from the 15-level model by separating the first 30m level of the 15-level into three equal 10m levels. Levels 1, 2, and 3 of the 17-level model kept the same initial temperature and salinity conditions as level 1 of 15-level model, i.e. the temperature were reduced by  $2^{\circ}\text{C}$  and the salinity by 1ppt. Other initial temperature and salinity values for layers deeper than 30m remained the same. In areas where the reduced temperature became below the freezing point ( $-1.8^{\circ}\text{C}$ ), the temperature was reset to the freezing point. To represent the freshwater flux from Davis and Hudson Straits, the salinity for the area representing the boundary to Hudson Strait and Davis Strait ( $60^{\circ}\text{N}$  to  $65^{\circ}\text{N}$  and  $62^{\circ}\text{W}$  to  $64.5^{\circ}\text{W}$ ) remained fixed to the initial state. This salinity profile could be varied seasonally if the approximate seasonal variation was available, but is for now kept constant. At December 1, the starting date of model simulations, all grids in the model domain are set to be ice-free and their ice and ocean velocities are initiated to be zero.

### 1.3 Forcing data

The model simulates the annual advance and retreat of the Labrador Shelf pack ice over a 180-day period starting from Dec. 1. Simulations for the 1968/69, 1970/71 and 1971/72 ice seasons were described in Ikeda et al. (1996). In this report, the model will simulate the pack ice properties the 1991/92 and 1993/94 ice seasons for which ice and ocean observations are available.

The model is forced by 12 hourly atmospheric data (geostrophic wind, air temperature and dew point) at a  $2.5^\circ \times 2.5^\circ$  grid obtained from the European Centre for Medium-range Weather Forecasting (ECMWF). The data is bi-linearly interpolated to the model grid and temporally interpolated from the 12-hour interval to the time step of the model.

Parameter	Basic	Range
number of levels	15 (17)	
ice salinity	5 ppt	
ice strength (P*)	$5 \times 10^3$ Pa ( $5 \times 10^3(1+0.1xH_{ice})$ )	$5 \times 10^3 - 20 \times 10^3$
air-ice drag coefficient	$2 \times 10^{-3}$	
ice-water drag coefficient	$5 \times 10^{-3}$ ( $10 \times 10^{-3}$ )	
air-water drag coefficient	$1 \times 10^{-3}$	
specific heat	$4.2 \times 10^3$ J/°C kg	
latent heat of fusion of ice	$3.36 \times 10^5$ J/kg	
turning angle, wind	25°	10° for 10 category model
turning angle, water	25°	10° for 10 category model
freezing point	-1.8°C	
ice albedo	0.5/0.75 (0.5)	0.5 - 0.9
water albedo	0.1/0.75 (0.1)	0.1 - 0.9
precipitation	$4 \times 10^{-8}$ ms <sup>-1</sup> (0)	
clouds	0.9	0.6 - 0.9
coefficient of horizontal mixing of U, V	$1 \times 10^3$ m <sup>2</sup> s <sup>-1</sup>	$0.2 \times 10^3 - 1 \times 10^3$
coefficient of horizontal mixing of T, S	$0.2 \times 10^3$ m <sup>2</sup> s <sup>-1</sup>	$0.1 \times 10^3 - 0.2 \times 10^3$
coefficient of vertical mixing of U, V	$2 \times 10^{-4}$ m <sup>2</sup> s <sup>-1</sup> ( $100 \times 10^{-4}$ for level 1-3, $2 \times 10^{-4}$ for others)	$100 \times 10^{-4} - 200 \times 10^{-4}$ for level 1-3 and level 1-6
coefficient of vertical mixing of T, S	$1 \times 10^{-4}$ m <sup>2</sup> s <sup>-1</sup> ( $10 \times 10^{-4}$ for level 1-3, $1 \times 10^{-4}$ for others)	
sensible heat flux coeff.	$1.3 \times 10^{-3}$	
latent heat flux coeff.	$1.1 \times 10^{-3}$	
time step	1200 s (600 s)	
minimum ice thickness	0.5 m	

Table 1.1 Model parameters used in the 15- and 17-level ice-ocean models.

Due to the lack of data, cloudiness is read into the model as climatic norms and then used with air temperatures and dew points to calculate the heat fluxes of the long- and short-wave radiations. Table 1.1 lists the parameters used for the basic cases of the 15-level and 17-level models, and the range in parameters used in the sensitivity tests. The computing time step of both ice model and ocean model is 1200 seconds for the 15-level model, and 600 seconds for the 17-level model.

## 2. Model simulations and sensitivity tests

Model simulations will cover a 180-day ice season period starting with day 1 on December 1. The model simulations will mainly be compared to ice observations documented on ice charts published by the Canadian Ice Service (CIS) for the 1991/92 ice season; some limited oceanographic and ice beacon data are also available to check the model performance for the 1993/94 ice season. Comparison between model simulations and ice charts will consist of the ice extent: the total surface area within the ice edge; ice area: the total area of the ice itself; and ice volume. The weekly composite ice charts are yearly digitized at the Bedford Institute and are described for the period from 1963 to 1988 in Peterson and Prinsenberg (1990). Prior to the early 1970's, the charts were based on visual observations from aircraft, while after the early 1970's satellite imagery data was also incorporated. The ice charts of the Canadian Ice Service thus have evolved with the advent of satellite imagery during the early 1970's and the side-looking airborne radar (SLAR) in the late 1970's.

The digitized ice data set consists of concentration of five ice categories (new, grey, grey-white, first-year, and old) on a  $0.5^\circ$  latitude by  $1.0^\circ$  longitude grid. These data can be used to compute (1) ice extent, (2) ice area, and (3) ice volume by assigning a mean ice thickness to each of the ice thickness range of the ice type categories as shown in the following table:

	<u>Ice Chart Range</u>	<u>Mean thickness</u>
(1) New ice	0-10 cm	5cm
(2) Grey ice	10-15 cm	12.5cm
(3) Grey-white ice	15-30 cm	22.5cm
(4) First-year ice	> 30 cm	100cm
(5) Old ice*		150cm

\*(ice which has survived at least one melt season)

The equivalent ice thickness ( $H_{ice}$ ) for both ice chart observations and model simulations is the sum of the products of ice thickness and ice concentrations of all the ice types used in the ice chart data or model simulations.

It should be noted that first-year ice includes all ice (except multiyear) thicker than 30cm. Its mean thickness is assumed to be 100cm and thus ice volume estimates are subject to large errors. In addition, the ice thickness only represents the level, undeformed ice so that any extra ice volume in ice rubble field are ignored in the ice chart data. Also ice thickness are not based on direct observed ice thickness but are indirectly inferred from ice colour and texture which also could lead to large errors in ice volume computations. Thus, although ice extent and ice areas are well represented by the ice chart data, the ice volume may not be. This should be kept in mind when comparing ice chart "observations" and model simulations.

Ikeda et al. (1996) described simulation results using the 15-level model for the ice seasons of 1968/69, 1970/71, and 1971/72. This manuscript will only present simulations from the 1971/72 ice season in section 2.6 to discuss early test results on ice strength.

## 2.1 The 15-level model

Fig. 2.1 shows time series plots derived from weekly ice charts of the ice extent, ice area and ice thickness (volume) for the Labrador and Newfoundland shelf area for the period of December 1, 1991 (model day 1) to May 28, 1992 (model day 180). The data shown is for the southern Labrador and Newfoundland shelf area south of 55°N that is contained within the analysis domain of the model (Fig. 1.1) and thus does not include Gulf of St. Lawrence. For comparison with the 2-category ice model, ice thickness of the ice charts is grouped into two ice categories: thin ice (new, grey, and grey-white ice) with a 0.15m average ice thickness and thick ice (first-year and old ice) with a 1.25m average thickness. The ice chart data indicates that the ice concentration is high within the analysis domain area; thus the ice extent and ice area are similar (Fig. 2.1). Thin and thick ice contributions to the ice area are shown by symbols.

The ice chart data shows a rapid increase in ice area after day 10, reaching a peak at day 60 made up of mostly thin ice. Northeasterly onshore winds compressed the pack ice against the shore between days 65 and 70 as indicated by the minimum in ice area on day 67. The contribution to the ice area by thin ice decreased after this day. Starting with the second maximum in ice area (day 96), thick ice made up the larger fraction of the pack ice. After April 9 (day 131), no young ice appears to be present in the ice chart data. Although the thin ice makes up a large fraction of the ice cover during the first part of the ice season, it does not contribute much to the overall ice volume. According to the ice chart data, all the variation in the ice volume after day 60 is controlled by the thick ice fraction of the ice cover. Since the decrease in ice volume due to thinning of the ice as ice melts during the later part of the ice season are not reflected in the ice chart data, the ice volume "observations" should not be used as a standard to validate ice models results.

The 1991/92 model simulated time series of the same ice properties of Fig. 2.1 are shown in Fig 2.2. The model results show the ice extent as being the total area of all the grids south of 55°N latitude containing the ice. Compared to ice chart observations, ice forms 5 days earlier in the model. This may be a result of the cold mixed layer temperature which at December 1 is below -1.5°C along the northern part of the coast allowing ice to form quickly after the start of the model run. Ice extent maxima in observed ice chart data occurred around day 60 and day 96 (broad peak), whereas in the model maxima were simulated 3 days later on days 63 and 99. The second simulated maximum has a secondary peak at day 113; no such secondary peak is present in the ice chart observations. The model does show the 1-3 day variations in ice extent in response to atmospheric forcing which are averaged out in the plot of the weekly averaged ice chart data. On the other hand, the response to the onshore winds (day 67) is larger in the ice chart data than the model simulation. The model results also show the ice volume time

series. It shows a gradual increase to a single maximum centred at day 100, whereas the ice chart data indicated two maxima; one at day 88 and one at day 103 separated by a minimum. However, due to the uncertainty of ice thickness data in ice charts no definite conclusion about the ice volume results of the model can be drawn.

One of the shortcomings of the 2-category ice type model is its inability to simulate the high ice concentration as indicated by the ice chart data. For the area south of 55°N, the ice extent simulated by the model (Fig.2.2) has an ice concentration of 25% to 40% (ratio of ice area to ice extent) in February and March, whereas ice chart data for the same area shows concentrations greater than 90%. As seen later, this shortcoming can be corrected in part by going to a 10-category ice model.

In addition to verification of the simulated ice extent, area and volume, the ice and ocean velocities simulated by the model can be compared to observations. Since the ice drifts and ocean currents respond to atmospheric forcing at time scales greater than half a day, only daily vector means are needed for model-observation comparison. Fig. 2.3 shows maps of simulated ice and ocean surface velocities for three different parts of the 1991/92 ice season: day 60 or Jan. 29; day 87 or Feb. 25; and day 120 or Mar. 29. These three examples were chosen to represent ice conditions of three different periods of ice season when in addition different wind conditions occurred. Offshore winds (SE) occurred through the centre of the domain on day 60. Predominant NW along shore winds occurred throughout the domain on day 87; while on day 120 southerly winds occurred in the southern part of the domain and turning counter-clockwise to NE onshore winds in the northern part of the domain. The wind conditions for the three days are shown in Fig 2.4 for a select few grid points of the analysis domain. The offshore SE winds and along shore NW winds occurred throughout the analysis domain whereas the southerly winds occurred on day 120 in the southern part of the domain, reduced in strength in the middle of the domain and became onshore (NE) in the northern part of the domain.

The Fig. 2.3 results show that winds are responsible for the large spatial as well as temporal variability in the ice velocity. In comparison, the first level ocean velocities are in general weaker and directed to the right of the ice velocities. They contain a low frequency current component in addition to the high frequency wind component. This low frequency current component represents a southeastward ocean drift over the shelf break called the Labrador Current (offshore branch). A weaker current, usually referred to as the inshore branch of the Labrador Current, is located over the inner shelf region. The ocean velocities respond to bottom topography as seen by the circulation pattern around offshore banks. Since the NW winds of day 87 are the predominant wind condition for the winter months, the ocean currents of day 87 represent the winter ocean surface circulation simulated by the model.

## 2.2 The 17-level model

As stated before, the 17-level ocean model separates the first level of the 15-level into three equal depth levels. This was done to investigate the effect of the ice stress on the ocean surface layer's velocity by distributing the ice stress differently to the ocean surface layer. Levels 1, 2, and 3 of the 17-level model kept the same initial temperature and salinity conditions as level 1 of the 15-level model. The initial temperature and salinity values of layers deeper than 30m remained the same for both models. To keep the 17-level model stable, the computing time step for all cases was reduced to 600 seconds, half of the time step for the 15-level model (1200 seconds). This meant that the CPU time of the 17-level doubled relative to that of the 15-level model.

The dynamic coupling between the ice and surface water layer is controlled by the ice-water drag coefficient. In the 17-level model its magnitude is  $10 \times 10^{-3}$ , twice as large as the value used in the 15-level model. In addition, the vertical mixing coefficient of momentum ( $K_v$ ) is also larger (50 times) in 3 surface layers of the 17-level than the first layer of the 15-level model (Table 2.1).

15-level ocean model		17-level ocean model	
level #	$K_v$	level #	$K_v$
1	$2 \times 10^{-4} \text{ m}^2 \text{ s}^{-1}$	1 to 3	$100 \times 10^{-4} \text{ m}^2 \text{ s}^{-1}$
2 to 15	$2 \times 10^{-4} \text{ m}^2 \text{ s}^{-1}$	4 to 17	$2 \times 10^{-4} \text{ m}^2 \text{ s}^{-1}$

Table 2.1 Comparison of the vertical mixing coefficients of momentum used in basic cases of the 15-level and the 17-level ocean model.

Ice extent and area results of the 17-level model (Fig. 2.5) can be compared with the 15-level results (Fig. 2.2) and the ice chart data (Fig. 2.1). The curves show the same general features: number, location and magnitude of major peaks as well as the overall ice cover build-up and decay. However, the magnitude of the 5-10 day variability simulated by the 17-level model is larger than the 15-level model or the weekly averaged ice chart data. The 17-level model concentrates the wind stress into a shallower oceanic surface layer and appears to cause a response of the wind forcing on ice formation and ice melting. It simulates the maximum at day 63 and the minimum at day 71 between the two major peaks better than the 15-level model. Both models however prolonged the duration of the second peak (i.e. a secondary peak on day 113) which is not seen in the ice chart observations. The time series plot of the ice volume did not alter much from of the 15-level model; the single maximum is broader (earlier), more ice was present in the early winter (days 60-70) and less ice later on in the winter (days 120-140). Due to the uncertainty in ice volume data of the ice charts; no conclusion can be made on the volume results of the two models.

Examples of daily mean ice velocities and the mean ocean velocities of the three surface levels are shown in Fig. 2.6 for 3 days: Jan. 29, Feb. 25 and Mar. 29, 1992 when strong W and NW winds occurred. The results show as expected that the strongest

oceanographic response to the wind forcing is in the thin 10m surface layer. The 10m surface layer currents are stronger than those in the two lower layers and the mean over the top 30m. The currents in the lowest layer (4<sup>th</sup> layer with depth between 30 to 80m) have the largest direction variability as the circulation at this depth already appears to be influenced by the bottom topography. Compared to the 15-level model shown in Fig. 2.3 which show the results for the same three days, the mean currents over the surface 30m of the 17-level model for these specific examples are stronger for both the offshore and inshore branches of the Labrador Current.

### 2.3 Vertical mixing coefficient of momentum

The strength of the vertical mixing in the ocean models depends on the value of the vertical mixing coefficient of momentum  $K_v$  and on the depths of the ocean layer levels. For the 17-level model  $K_v(k)$  is equal to  $10^{-2} \text{ m}^2\text{s}^{-1}$  for levels (k) 1 to 3 and is equal  $2 \times 10^{-4} \text{ m}^2\text{s}^{-1}$  for levels 4 to 17. The contribution from vertical diffusion of momentum was examined by varying  $K_v(k)$ . For test case 1, the vertical mixing in the surface layers was increased by taken  $K_v(k)$  as  $2 \times 10^{-2}$  for levels 1 to 3 which is double the value of the basic case while keeping the mixing (and  $K_v(k)$ ) the same in the other levels.

Date	ice speed (m/s)	ocean speed, level 1 (m/s)	ocean speed, level 2 (m/s)	ocean speed, level 3 (m/s)
Feb. 8, 1992	0.18	0.10	0.07	0.06
Feb. 18, 1992	0.43	0.22	0.11	0.06
Feb. 28, 1992	0.15	0.09	0.08	0.07
Mar. 9, 1992	0.16	0.10	0.06	0.05
Mar. 19, 1992	0.15	0.09	0.06	0.05
Mar. 29, 1992	0.14	0.03	0.03	0.05

Table 2.2 Ice and ocean speeds of basic case at station #40, Hamilton Bank slope.

Date	ice speed (m/s)	ocean speed, level 1 (m/s)	ocean speed, level 2 (m/s)	ocean speed, level 3 (m/s)
Feb. 8, 1992	0.18	0.10	0.07	0.06
Feb. 18, 1992	0.49	0.29	0.17	0.13
Feb. 28, 1992	0.16	0.09	0.08	0.08
Mar. 9, 1992	0.17	0.11	0.08	0.07
Mar. 19, 1992	0.16	0.09	0.07	0.06
Mar. 29, 1992	0.17	0.06	0.01	0.02

Table 2.3 Ice and ocean speeds of test case 1 at station #40, Hamilton Bank slope.

Tables 2.2 and 2.3 show daily ice and ocean surface layer speeds at station #40 located on the southern Labrador shelf slope off the Hamilton Bank (Fig. 2.7a). The tables list 6 specific days from the 180-day simulation run for test case 1 (Table 2.3) as compared to the basic case (Table 2.2). The results show that there is only a weak response in speeds to a large change in the mixing coefficient of momentum.

As seen later in section (3.2), the simulated model currents are much weaker than current meter observations. Since current meter data were usually from subsurface levels (levels 4-6), a test case (#2) was run to check if simulated currents could be increased at these depths by increasing the vertical mixing to level 6. For test case 2 the vertical diffusion in level 4, 5, and 6 was increased by increasing their  $K_v$  values to those used in the three surface levels ( $K_v(k) = 10^{-2}$ ). The  $K_v$  values for the deeper levels were kept the same.

Fig. 2.7a shows the map of current meter locations from Narayanan et al.(1996) whose data is used to compare to daily mean model simulated current speeds (Fig. 2.7b). Comparison were done for seven selected grids for which current meter data was available for 1991/1992 ice season. The results indicated that when the energy provided to the ocean by the ice cover and atmosphere is distributed to deeper levels, the speeds at these levels can be increased but the increase is relatively small. A much larger increase is required to the simulated currents of the same magnitude as current meter observations. It appears that a much finer grid ocean model is required to simulate the stronger site specific ocean current observations. It should be noted however that ice drift data is the main calibration data set for the coupled ice-ocean model followed by the ice extent and ice thickness.

Fig. 2.8a shows the time series of the ice extent, ice area and ice volume for test case 2. The plots show that the pack ice properties in the analysis area are reduced from 30% to 50% relative to the basic case (Fig. 2.5). Fig. 2.8b shows the equivalent ice thickness distributions for March 16, 1992 and Fig. 2.8c the ocean temperature and salinity profiles from the surface to 250 m for 3 site along a Hamilton Bank transect whose locations are shown on Fig. 2.8b. Location #2 is covered by 0.4m ice in basic case but was ice free in test case 2. The ocean temperature in level 1 (from the surface to 10 m) of test case 2 was  $+1.3^{\circ}\text{C}$  while in the basic it was at freezing point  $-1.8^{\circ}\text{C}$  as ice was present. The difference is that the surface layer oceanic heat is comparable to the heat provided to the atmosphere by the growth of 0.4m of ice. So not only did the surface layer in the test case receive oceanic flux to heat the water, it also received heat to melt the ice. Both these heat fluxes are provided by the increase in vertical mixing so that the area stayed ice free and surface oceanic layer was warmer. Changing the magnitude of the vertical mixing coefficient of momentum  $K_v(k)$  thus greatly affects the ice properties while only marginally affects the ocean currents, the reason for the test. Changing the vertical mixing coefficient of momentum is thus a means to fine-tune the ice properties in the numerical simulations, not ocean currents. For future simulations, the values of  $K_v(k)$  are shown in the column of basic case of Table 1.1.

## 2.4 Horizontal mixing coefficient

Model sensitivity to horizontal mixing coefficients was studied in test cases 3 and 4. In test case 3 the horizontal coefficient of momentum was reduced to 20% of its original value of the basic case and in test case 4, in addition, the horizontal mixing coefficient of T and S was reduced by 50% (Table 2.4). Both test cases 3 and 4 use the same initial conditions and atmospheric forcing as the basic case.

Test case #	horizontal mixing coeff. of momentum	horizontal mixing coeff. of T/S
basic	$1.0 \times 10^3 \text{ m}^2/\text{s}$	$0.2 \times 10^3 \text{ m}^2/\text{s}$
3	$0.2 \times 10^3 \text{ m}^2/\text{s}$	$0.2 \times 10^3 \text{ m}^2/\text{s}$
4	$0.2 \times 10^3 \text{ m}^2/\text{s}$	$0.1 \times 10^3 \text{ m}^2/\text{s}$

Table 2.4 Horizontal mixing coefficients of test cases 3 and 4.

Fig. 2.9 shows the comparison of the ice extent and ice area due to variations in horizontal mixing for the 17-level ice-ocean model; no ice volume results are shown. The plots show that the sensitivity to horizontal mixing is small but accumulates throughout the time series so that the larger changes appear in the spring period. The basic shape of the seasonal variations is the same, just the total magnitudes varies reaching a 10% increase in the spring (day 140 to 180), closer to observed properties (Fig. 2.1). As mixing is reduced in both the momentum and T/S, the ice extent and ice area increase as less ice is lost in the offshore direction where it melts and less warm water is imported from offshore which again results in reduction of ice melt.

Figs. 2.10 and 2.11 show time series plots of daily mean simulated current speeds for seven selected grids for which the current meter data was available (see the map of Fig. 2.7a) for test cases 3 and 4, respectively. The ocean speeds of offshore stations of both test cases are larger than basic case. But speeds of the two inshore stations (21 and 24) located on or between banks of both test cases are reduced. The figures also show that as mixing coefficients are reduced in both the momentum and T/S (case 4) even larger speeds than test case 3 in offshore stations than when just the momentum coefficient was decreased (case 3). Reducing the horizontal mixing coefficient thus reduces the diffusion of the energy of the Labrador Current to the shelf area without greatly affecting the pack ice properties on the shelf.

## 2.5 Albedos of water and ice

The ice-ocean model uses water and ice albedo parameters to calculate the flux from short wave radiation. When ice is present a high albedo is used as most of the radiation is reflected, whereas a low value is used in open water condition when most of the radiation is absorbed. The basic case assumes constant albedo values for both water and ice. The main difference between simulated and ice chart ice extents is in the springtime (day 130 to 180). Using these constant albedo values, the model does not simulate through accumulation over time enough ice during this period. By increasing the albedos of ice and water to 0.75 after March 1, much larger than those used by the basic case (Table 2.5), it was found that the spring ice extent increased unrealistically to winter values of  $24 \times 10^4 \text{ km}^2$  for day 180. Too much ice thus remained as the radiation flux into the ocean and ice was now reduced too much. Other simulations were done with variations in albedo values (Table 2.5) to reflect better the possible variations in albedos throughout the year due to melting of the reflective snow layer and due to increased wave activity during the winter storm season.

# of day	Basic case		Test case 5		Test case 6		Test case 7	
	ice	water	ice	water	ice	water	ice	water
1 - 40	0.5	0.1	0.5	0.1	0.5	0.25	0.5	0.25
41 - 54	0.5	0.1	0.7	0.4	0.9	0.45	0.5	0.25
55 - 90	0.5	0.1	0.8	0.8	0.9	0.45	0.9	0.90
91 - 100	0.5	0.1	0.8	0.8	0.9	0.45	0.9	0.90
101 - 110	0.5	0.1	0.7	0.4	0.9	0.45	0.9	0.90
111 - 120	0.5	0.1	0.5	0.1	0.9	0.45	0.6	0.15
121 - 180	0.5	0.1	0.5	0.1	0.6	0.30	0.6	0.15

Table 2.5 Water and ice albedo values for simulation tests 5 through 7.

In test #6 too much ice was produced for the winter/spring period when the ice and water albedos were increased to simulate the increased reflectivity due to the white snow layer and increased wave activity (Fig 2.13). When the albedos were changed to reduce the reflection of the radiation in the spring for both the ice and water (test #7, Fig. 2.14), the ice extent reduced for day 160-180 period to the observed level. However the ice extent in the late winter (day 100 to 160) was still too high. Test case #5 (Fig. 2.12) reduced the albedos further so that the ice extent did follow the observed pattern for the period Day 100 to 160 but it underestimated the late spring ice extent. Although the basic case using constant albedo values simulates reasonable time series plots of ice extent, ice area and ice volume (Fig. 2.5), they can be readily modified in the later part of the simulation runs by varying albedos. Albedo values should seasonally vary due to the high reflectivity of the snow layer and the ocean wave activity such as shown by test case #5 (Fig. 2.12).

## 2.6 Ice strength (P\*)

In Hibler's ice model, the ice pressure P is formulated as:

$$P = P^* \times H_{ice} \times \exp[-C(1-A)]$$

where P\* and C are fixed empirical constants, A is ice concentration and H<sub>ice</sub> is equivalent thickness in meters within the model's grid. This formulation makes the ice to strengthen as it becomes thicker.

Simulations of the heavy ice year 1971/72 were described by Ikeda et al. (1996). The sensitivity tests of the pack ice properties due to variations in P\* done then and again here using the 17-layer ice model are shown in this section using the 1971/72 ice season. Simulations cases 15.1 and 17.1 are basic cases for 15-level and 17-level models respectively. For the 15-layer ocean model P\* was increased by 400% (15.2) relative to its basic case (15.1) to reduce the ice thickness along the shore line. For the 17-layer ocean model test (17.2) the increase in ice pressure P relative the basic case (17.1) was achieved by increasing its dependency on the equivalent thickness to a weak quadratic term to reflect the increase in ice strength to horizontal confinement as ice thickens.

Case	Ice strength (P*), Pa
15.1	$5 \times 10^3$
15.2	$20 \times 10^3$
17.1	$5 \times 10^3$
17.2	$5 \times 10^3 \times (1 + 0.25 \times H_{ice})$

Table 2.6 Values of ice strength (P\*) for test cases using 15- and 17-level ocean model.

Fig. 2.15 shows the time series of the ice extent, and ice thickness (volume) for the period of December 1, 1971 to May 28, 1972 as derived from ice charts. Similar to the 1991/92 winter, the 1971/72 winter was severe. The ice extent rapidly increased to a broad maximum value of  $30 \times 10^4 \text{ km}^2$  for day 70 to 100 at which time it decreased towards a minimum at day 135. The spring melt was delayed until day 180 when a large ice extent still existed (larger than 1991/92). The ice volume was larger than that estimated from ice charts for the 1971/72 season. Ice chart data indicates an increase in ice thickness after day 145; this may be thick ice imported from higher latitudes.

The simulated time series for two 15-level cases are shown in Fig. 2.16. The model simulation for the low ice-strength case (15.1) agrees well with the ice extent. The maximum is not as high as observations indicate; also the maximum is broader, extending from day 60 to 120. Ice volume time series shows the short-coming of a model using a constant, low value for the ice strength. The ice continues to deform, increasing the ice volume into the area near the coast. Using a larger P\* (stronger ice), the ice extent time series is not altered but the ice volume plot starts to look more realistic.

Even though the larger  $P^*$  provided what is considered a better ice volume time series plot, using a constant value for  $P^*$  may not be suitable when both thin and thick ice are present. For the 17-level ocean model (Table 2.6), the ice strength  $P^*$  was varied from the constant case (17.1) according to the mean ice thickness  $H_{ice}$  within each grid cell to:

$$P^* = 5 \times 10^3 \times (1 + 0.25 \times H_{ice})$$

where the mean ice thickness in each grid cell  $H_{ice}$  is in units of meters. Using this  $P^*$  formulation, thin ice will now deform easily just as the basic case (17.1), but as ice thickens deformation will require an increasingly larger compression force. Comparison of the two cases is shown in Fig. 2.17 using again 1971/72 ice season but using the 17-level ocean model. The constant ice-strength case (17.1) simulates too much ice volume even though the ice extent agrees with the observations. For the variable ice-strength case (17.2), both ice extent and ice volume agree well with observations shown in Fig 2.15.

Since the variable ice strength formulation reflects better the expected ice property and simulates closer the observed ice volume even if these are uncertain; it will be applied in later simulations but with a smaller constant of 0.1 rather than 0.25.

## 2.7 Wind and air temperature forcing

The atmospheric circulation mainly controls the seasonal ice forming and melting along the Canadian east coast. In the winter, northwesterly winds along the Labrador coast brings in the cold Arctic air which cools the sea surface to the freezing point at which time ice starts to grow. The wind forces the ice and ocean waters southwards along the coast. Ocean currents beneath the pack ice contribute to ice distribution as it transports ice and cold low salinity water from higher latitudes.

Regression analysis, trying to determine the reasons for the interannual variability in ice extent, is hampered by the fact that the two major forcing parameters, the northwesterly winds and air temperatures, are in phase thus making it impossible to determine the contribution due to wind and air temperature separately on the ice extent (Prinsenberget al.,1997). Numerical simulations on the other hand can independently vary the northwesterly wind strength and the air temperature to determine the contribution of these forcing parameters on the variability of the ice extent. Several tests will examine the affects of wind and air temperature on the pack ice properties relative to conditions attained by the base case for the ice season of 1991/92. The cases tested are:

1. Increased wind strength
  - Wind strength increased by 20% in all directions for the entire region.
2. Increase NW winds and decrease SE winds
  - Increased wind speed by 20% if from north-west and decrease by 20% if from south-east, and interpolated linearly for winds with other directions.

### 3. Colder but normal winds

- Reduced air temperature by 50% if they are below 0°.

### 4. Colder and increased NW winds

- Increased NW winds and decreased SE winds in addition to colder air temperatures (-50%) when these are negative.

Fig. 2.18 shows the comparison of ice extent and ice volume between the basic case and the two wind cases: tests 1 and 2. Both test cases show a small increase in ice extent area when the pack ice is advancing southwards but a small decrease when the ice is retreating in the spring or being compressed against the coast in mid-winter as occurred around day 70. Variations due to wind forcing are thus amplified as the wind strength is increased. The changes in total ice extents south of 55°N latitude are less than expected from just considering the ice fluxes across 55°N. The ice flux across 55°N is linearly dependent on the wind speeds; the ice extent south of 55°N is not. So although southwards ice fluxes may increase across 55°N, the ice extent south of 55°N increase is smaller as ice melted faster at the southern ice edge. The total ice volume south of 55°N were 20% higher than the value of basic case as thicker ice from the north entered the region while the thinner ice melted faster at the southern ice edge. The increase in NW wind forcing thus altered the ice volume while only affecting the ice extent very little.

Fig. 2.19 shows ice extent and ice volume of test cases 3 and 4 when the air temperature below 0°C is decreased while the NW winds are unaltered (test 3) or increased by 20% (test 4). When the cooling is increased, the maximum ice extent is increased by 20% and the maximum ice volume by 60% as the ice growth is larger and the ice melt smaller. The change from the basic case is a much larger than that seen when the winds were increased (tests 1 and 2). However the two effects, colder temperatures and stronger NW winds usually occur at the same time (test case 4) and their effects on ice properties are thus hard to separate in regression analysis of pack ice observations. One should thus expect that if the northwesterly wind strength increases as simulated in test 2, the air temperatures should also be cooler as simulated in test 3. Both these departures from the norm increase the ice extent due to the increase in the southward ice flux, and the reduction in ice melt. The effects on the ice extent and ice volume accumulate throughout the ice season so that it retards the ice retreat in spring as the ice is thicker and air temperatures are colder. This then results in high ice extent and high ice volume in the spring months of April and May. During the sharp decreases in the ice extent of Fig. 2.19 on day 60 in winter and on day 120 in the spring, the stronger winds decrease the ice extent. This can be seen on day 60 during a northerly wind event, which compressed the pack ice against the coast thereby reducing the ice area extent. In contrast, around day 138, the increase in winds pushed the ice in the southern region of the analysis area faster offshore where the ice melted faster than in the normal observed wind case (Fig. 2.20), thus opposing the affect of the colder air temperatures. The daily wind condition for the analysis area for April 16 (day 138) is shown in Fig. 2.21.

Daily ice transports averaged from Hamilton Bank grids between 54.75°N to 55°N are shown as time series plots for the along-shore (135°) and offshore (45°) in Figs. 2.22 and 2.23 for wind test cases 1 and 2 and in Figs. 2.24 and 2.25 for the wind/temperature test cases 3 and 4. As in the ice extent plots, the deviations from the basic case are larger for the temperature effects than for the wind effects. Combining the two effects as shown by case 4 produced the largest deviations from the basic case and simulates conditions when severe winter conditions are occurring in the region. The along-shore plots show that the flux in the Hamilton Bank area is nearly always southwards and reaches maximum values in the winter months when the winds are the strongest and pack ice extent and ice thickness across the shelf are large. The across-shelf ice transport in the Hamilton Bank area varies from being positive (offshore) to being negative (onshore). More offshore transports occur in winter while more onshore transports occur in the spring. The seasonal variation of these fluxes are listed in Tables 2.7 and 2.8 for the basic and four test cases as monthly mean values.

day	normal wind and air temp	120% wind and normal air temp	increased NW wind; normal air temp	normal wind; -50% air temp	increased NW wind; -50% air temp
1 - 30	0.050	0.063	0.059	0.069	0.077
31 - 60	0.063	0.086	0.076	0.079	0.093
61 - 90	0.098	0.135	0.132	0.139	0.159
91 - 120	0.123	0.133	0.125	0.146	0.148
121 - 150	0.066	0.078	0.068	0.096	0.121
151 - 180	0.052	0.057	0.056	0.099	0.110

Table 2.7 1991/92 monthly mean ice transports (along-shore), averaged across Hamilton Bank for the basic and four test cases (unit: km<sup>3</sup>/day/km).

day	normal wind and air temp	120% wind and normal air temp	Increased NW wind; normal air temp	normal wind; -50% air temp	increased NW wind; -50% air temp
1 - 30	0.015	0.020	0.016	0.021	0.020
31 - 60	0.015	0.020	0.014	0.018	0.015
61 - 90	-0.006	-0.016	-0.015	-0.011	-0.024
91 - 120	-0.012	-0.008	-0.010	-0.012	-0.011
121 - 150	-0.019	-0.021	-0.019	-0.025	-0.034
151 - 180	-0.003	-0.004	-0.004	-0.004	-0.007

Table 2.8 1991/92 monthly mean ice transports (offshore), averaged across Hamilton Bank for the basic and four test cases (unit: km<sup>3</sup>/day/km).

## 2.8 Multiple category ice-ocean model

The ice model of the coupled ice-ocean model discussed so far uses the two category ice model by Hibler (1979), i.e. only the mean ice thickness and concentration for each grid is calculated providing one category for open water and one for ice. Model simulation results with the 2-category model have shown that ice concentrations are not well reproduced. In order to improve the representation of thin ice, the 2-category ice model was changed to a 10-category ice model. This then will provide a better means to represent the mechanical deformation and thermodynamics of the different ice thickness of the pack ice. The theoretical background for multiple ice categories was derived from Thorndike et al. (1975) and Hibler (1980). The numerical implementation was done by Hibler in 1980. Ice thickness categories in the 10-category model (Table 2.9) has 9 different ice thickness categories and one open-water category.

Category	Thickness range (m)
1 (open water)	-0.1 to 0.1
2	0.1 to 0.2
3	0.2 to 0.3
4	0.3 to 0.5
5	0.5 to 1
6	1 to 2
7	2 to 3
8	3 to 4.5
9	4.5 to 6
10	6 to 8

Table 2.9 Ice thickness categories of the 10-category ice model.

To compare the results of the 10-category model with the 2-category model, the same initial conditions and atmospheric forcing of the 1991/92 ice season are used for both coupled ice-ocean models each using the 17-level ocean model. The biggest difference resulting in using the two ice models is that the 10-category model has larger ice concentration than the 2-category model (Figs. 2.26 and 2.27). This of course was the reason for changing to a more complex ice model. Fig. 2.27 shows the higher ice concentration along the Labrador coast simulated by the 10-category ice model in comparison to the 2-category ice model for February 26, 1992. The ice extent on the other hand did not alter much until mid-winter when the ice extent of the 10-category ice model increased relative to that of the 2-category ice model as a large fraction of ice remained in the thinner ice categories. Compared to observation (Fig. 2.1), the total ice area south of 55°N (Fig. 2.26) reaches the same mid-winter maximum, however the ice area is too large during the early winter as was also found with the 2-category ice model. It is assumed that this is related to the oceanic heat flux, which is dependent on the initial stability of the ocean and vertical diffusion. In contrast the spring ice area, although bigger than the 2-category ice model, is still too small relative to observed distributions.

### 3. Comparison of model ice and ocean velocity simulations with observations

So far the comparison of model simulations to observations has concentrated on the ice extent and ice area. Now model simulations of ice drifts and ocean currents will be compared to available ice drift and ocean current observations. Comparison will concentrate on the 1991/92 ice season when the CASP II (the Canadian Atlantic Storms Program II) program made atmospheric, ice and oceanographic observations over the shelves off the east coast of Newfoundland and southern Labrador.

#### 3.1 Ice velocities

The image-derived ice velocities and the beacon-derived ice velocities collected during CASP II are summarised by Fissel et al., 1994. They are used by modellers of the Canadian Ice-Ocean Model Working Group as a calibration data set. Tables 3.1 and 3.2 list the ice velocity that is available when the image- and beacon-derived ice drift data are re-mapped to the model grids.

Date	number of velocities						
Feb 12	3	Feb 13	2	Feb 14	2	Feb 15	3
Feb 16	2	Feb 17	4	Feb 18	4	Feb 19	4
Feb 20	3	Feb 21	4	Feb 22	4	Feb 23	4
Feb 24	5	Feb 25	5	Feb 26	4	Feb 27	4
Feb 28	4	Feb 29	3	Mar 1	2	Mar 2	4
Mar 3	4	Mar 4	4	Mar 5	3	Mar 6	3
Mar 7	6	Mar 8	7	Mar 9	7	Mar 10	7
Mar 11	7	Mar 12	7	Mar 13	7	Mar 14	7
Mar 15	6	Mar 16	7	Mar 17	7	Mar 18	11
Mar 19	10	Mar 20	9	Mar 21	10	Mar 22	12
Mar 23	11	Mar 24	13	Mar 25	12	Mar 26	12
Mar 27	11	Mar 28	11	Mar 29	11	Mar 30	11
Mar 31	10	Apr 1	9	Apr 2	8	Apr 3	10
Apr 4	10	Apr 5	9	Apr 6	9	Apr 7	8
Apr 8	9	Apr 9	8	Apr 10	8	Apr 11	8
Apr 12	6	Apr 13	6	Apr 14	4	Apr 15	7
Apr 16	6	Apr 17	5	Apr 18	5	Apr 19	3
Apr 20	3	Apr 21	3	Apr 22	3	Apr 23	3
Apr 24	3	Apr 25	2	Apr 26	2	Apr 27	2
Apr 28	2	Apr 29	2	Apr 30	2		

Table 3.1 Number of grid's daily ice velocities for each day available from beacon-derived velocity observations.

The image-derived ice velocities represent the displacement of individual ice floes or identifiable ice features over a period of one day. The original data were collected at approximately daily intervals, with each interval starting and ending at approximately 18:00 UTC. The image-derived ice velocities were available for six days on Feb. 22, Mar. 7, Apr. 6, 9, 16 and 17. The beacon-derived ice velocities were available for 79 consecutive days from Feb. 12 to Apr. 30.

Date	number of velocities	Date	number of velocities	Date	number of velocities
Feb 22	140	Mar 7	148	Apr 6	50
Apr 9	108	Apr 16	75	Apr 17	104

Table 3.2 Number of grid's daily ice velocities for each day available from image-derived velocity data sets.

Figs. 3.1 to 3.4 show four examples of daily ice velocities of the beacon-derived data and model simulations for the same model grids. Strong north-westerly winds from March 7 to March 8 (Fig. 3.1) moved the pack ice southwards parallel to the coastline. As the winds died and turned offshore, the ice drifts in both beacon-derived and model simulation plots indicate that the ice drift reduces in magnitude (Fig. 3.2) and turns offshore (Figs. 3.3 and 3.4), closely following the changes in the wind pattern.

Figs. 3.5 to 3.8 show four examples of ice velocity plots available from the image-derived data and model simulations for the same model grids. The four plots, two for February and March, and two for April, show that although more grid data is available per plot, it does not provide many independent data points due to the high degree of homogeneity of the data. In addition, most image-derived data are restricted to westerly winds when cloud-free conditions occur, further reducing the variability in direction and magnitude of the image-derived data set.

Correlation analysis between the observed and model simulated ice velocities were done using the following definitions:

$n$ : number of ice velocities;

$U$  mod and  $V$  mod: east and north components of model ice velocity;

$\bar{U}$  mod and  $\bar{V}$  mod: average east and north components of model ice velocity;

$U$  ob and  $V$  ob: east and north components of observed ice velocity;

$\bar{U}$  ob and  $\bar{V}$  ob: average of east and north components of observed ice velocity.

$$\text{Variance}(U \text{ mod}): \sqrt{\frac{\sum (U \text{ mod} - \bar{U} \text{ mod})^2}{n}}$$

$$\text{BIAS}(U): \sum (U \text{ ob} - U \text{ mod}) / n$$

$$\text{BIAS}: \sqrt{(\text{BIAS}^2(U) + \text{BIAS}^2(V))}$$

$$RMSE(U): \sqrt{\frac{\sum (U_{ob} - U_{mod})^2}{n}}$$

$$RMSE: \sqrt{\frac{\sum [(U_{ob} - U_{mod})^2 + (V_{ob} - V_{mod})^2]}{n}}$$

$$r^2(U): \frac{[\sum (U_{ob} - \bar{U}_{ob})(U_{mod} - \bar{U}_{mod})]^2}{\sum (U_{ob} - \bar{U}_{ob})^2 \sum (U_{mod} - \bar{U}_{mod})^2}$$

$$r^2: \frac{[\sum \{(U_{ob} - \bar{U}_{ob})(U_{mod} - \bar{U}_{mod}) + (V_{ob} - \bar{V}_{ob})(V_{mod} - \bar{V}_{mod})\}]^2}{\sum \{(U_{ob} - \bar{U}_{ob})^2 + (V_{ob} - \bar{V}_{ob})^2\} \sum \{(U_{mod} - \bar{U}_{mod})^2 + (V_{mod} - \bar{V}_{mod})^2\}}$$

The correlation analysis results for the total ice season and three separate months are listed in Tables 3.3a to 3.3d for the beacon-derived ice drift data and in Tables 3.4a to 3.4d for the image-derived data. For the three months, the observed mean south-easterly ice drift is well simulated by the model (Table 3.3a). The observations do have a larger variance about the mean than that simulated by the model. The correlation coefficient ( $r^2$ ) shows that the model simulates 55% of the observed variance. Similar results are listed for each month (Tables 3.3b to 3.3d). During February (Table 3.3b), strong winds produce a large and persistent mean ice drift. Although the model mean ice drift is also larger; it did not increase as much as the observed value and causes a large bias in the easterly ice drift component which in turn causes the correlation coefficient to reduce to .45 from its mean value of .55. As the winds reduced in March, the mean ice drift reduced and is closely simulated by the model (Table 3.3c). The bias is smaller relative to the February value and the correlation coefficient increases to .49, indicating that the model simulated 49% of the observed variance. During April (Table 3.3d), most of the beacon data is from the Newfoundland shelf area where the pack ice diverges under the predominant north-westerly to westerly winds. The model simulates the mean ice drift well, the bias is small but the variance simulated is still smaller than the observed variance. The correlation coefficient is .66, indicating that the model simulated 66% of the observed variance in the beacon-derived ice drift.

Table 3.4a shows the correlation results for the total ice season when the image-derived ice drift is compared to the model simulations. Again the mean ice drift is well duplicated by the model. However the correlation coefficient is very low (.22). As stated earlier this is mainly caused by the narrow range in magnitude and direction of the observed ice drift as can be seen in the scatter plots of observed versus model ice drift components (Figures 3.9 to 3.11). The same poorer results for each separate month are shown in Tables 3.4b to 3.4d.

	<b>model</b>	<b>observed</b>
<b>Mean velocity</b>	0.15 m/s, 131.7°T	0.15 m/s, 140.9°T
<b>Mean east component</b>	0.11 m/s	0.09 m/s
<b>Mean north component</b>	-0.10 m/s	-0.12 m/s
<b>Variance ( east component )</b>	0.13 m/s	0.16 m/s
<b>Variance ( north component )</b>	0.13 m/s	0.19 m/s
<b>BIAS</b>	0.02 m/s, 217.0°T	
<b>BIAS ( east component )</b>	-0.01 m/s	
<b>BIAS ( north component )</b>	-0.02 m/s	
<b>RMSE</b>	0.17 m/s	
<b>RMSE ( east component )</b>	0.10 m/s	
<b>RMSE (north component )</b>	0.13 m/s	
<b>r<sup>2</sup></b>	0.55	
<b>r<sup>2</sup> ( east component )</b>	0.60	
<b>r<sup>2</sup> ( north component )</b>	0.51	

Table 3.3a Correlation results of model versus observed ice beacon velocities for the total ice season covering 79 days (478 samples) between February and April, 1992.

	<b>Model</b>	<b>observed</b>
<b>mean velocity</b>	0.26 m/s, 135.4°T	0.23 m/s, 149.9°T
<b>mean east component</b>	0.18 m/s	0.12 m/s
<b>mean north component</b>	-0.18 m/s	-0.20 m/s
<b>Variance ( east component )</b>	0.08 m/s	0.09 m/s
<b>Variance ( north component )</b>	0.10 m/s	0.12 m/s
<b>BIAS</b>	0.07 m/s, 254.3°T	
<b>BIAS ( east component )</b>	-0.06 m/s	
<b>BIAS ( north component )</b>	0.02 m/s	
<b>RMSE</b>	0.13 m/s	
<b>RMSE ( east component )</b>	0.10 m/s	
<b>RMSE (north component )</b>	0.09 m/s	
<b>r<sup>2</sup></b>	0.45	
<b>r<sup>2</sup> ( east component )</b>	0.34	
<b>r<sup>2</sup> ( north component )</b>	0.52	

Table 3.3b Correlation results of model versus observed ice beacon velocities for February, 1992 covering 18 days (64 samples).

	<b>model</b>	<b>observed</b>
<b>Mean velocity</b>	0.14 m/s, 117.1°T	0.13 m/s, 128.0°T
<b>Mean east component</b>	0.12 m/s	0.11 m/s
<b>Mean north component</b>	-0.06 m/s	-0.08 m/s
<b>Variance ( east component )</b>	0.12 m/s	0.15 m/s
<b>Variance ( north component )</b>	0.14 m/s	0.20 m/s
<b>BIAS</b>	0.03 m/s, 221.8°T	
<b>BIAS ( east component )</b>	-0.02 m/s	
<b>BIAS ( north component )</b>	-0.02 m/s	
<b>RMSE</b>	0.18 m/s	
<b>RMSE ( east component )</b>	0.10 m/s	
<b>RMSE ( north component )</b>	0.15 m/s	
<b>r<sup>2</sup></b>	0.49	
<b>r<sup>2</sup> ( east component )</b>	0.55	
<b>r<sup>2</sup> ( north component )</b>	0.45	

Table 3.3c Correlation results of model versus observed ice beacon velocities for March, 1992 covering 31 days (249 samples).

	<b>model</b>	<b>observed</b>
<b>Mean velocity</b>	0.13 m/s, 152.9°T	0.15 m/s, 152.9°T
<b>Mean east component</b>	0.06 m/s	0.07 m/s
<b>Mean north component</b>	-0.11 m/s	-0.13 m/s
<b>Variance ( east component )</b>	0.14 m/s	0.20 m/s
<b>Variance ( north component )</b>	0.11 m/s	0.18 m/s
<b>BIAS</b>	0.02 m/s, 155.1°T	
<b>BIAS ( east component )</b>	0.01 m/s	
<b>BIAS ( north component )</b>	-0.02 m/s	
<b>RMSE</b>	0.16 m/s	
<b>RMSE ( east component )</b>	0.11 m/s	
<b>RMSE ( north component )</b>	0.12 m/s	
<b>r<sup>2</sup></b>	0.66	
<b>r<sup>2</sup> ( east component )</b>	0.73	
<b>r<sup>2</sup> ( north component )</b>	0.57	

Table 3.3d Correlation results of model versus observed ice beacon velocities for April, 1992 covering 30 days (165 samples).

	<b>model</b>	<b>observed</b>
<b>Mean velocity</b>	0.19 m/s, 127.8°T	0.18 m/s, 132.1°T
<b>Mean east component</b>	0.15 m/s	0.13 m/s
<b>Mean north component</b>	-0.12 m/s	-0.12 m/s
<b>Variance ( east component )</b>	0.08 m/s	0.10 m/s
<b>Variance ( north component )</b>	0.09 m/s	0.13 m/s
<b>BIAS</b>	0.02 m/s, 247.6°T	
<b>BIAS ( east component )</b>	-0.01 m/s	
<b>BIAS ( north component )</b>	-0.01 m/s	
<b>RMSE</b>	0.15 m/s	
<b>RMSE ( east component )</b>	0.11 m/s	
<b>RMSE ( north component )</b>	0.11 m/s	
<b>r<sup>2</sup></b>	0.22	
<b>r<sup>2</sup> ( east component )</b>	0.06	
<b>r<sup>2</sup> ( north component )</b>	0.37	

Table 3.4a Correlation results of model versus image-derived ice velocities for February to April, 1992 covering 6 days (625 samples).

	<b>model</b>	<b>observed</b>
<b>Mean velocity</b>	0.22 m/s, 122.3°T	0.18 m/s, 109.4°T
<b>Mean east component</b>	0.19 m/s	0.17 m/s
<b>Mean north component</b>	-0.12 m/s	-0.06 m/s
<b>Variance ( east component )</b>	0.04 m/s	0.09 m/s
<b>Variance ( north component )</b>	0.04 m/s	0.08 m/s
<b>BIAS</b>	0.06 m/s, 96.0°T	
<b>BIAS ( east component )</b>	-0.02 m/s	
<b>BIAS ( north component )</b>	0.06 m/s	
<b>RMSE</b>	0.14 m/s	
<b>RMSE ( east component )</b>	0.10 m/s	
<b>RMSE ( north component )</b>	0.10 m/s	
<b>r<sup>2</sup></b>	0.027	
<b>r<sup>2</sup> ( east component )</b>	0.004	
<b>r<sup>2</sup> ( north component )</b>	0.145	

Table 3.4b Correlation results of model versus image-derived ice velocities for February, 1992 covering 1 day (140 samples).

	<b>model</b>	<b>observed</b>
<b>mean velocity</b>	0.32 m/s, 136.6°T	0.30 m/s, 151.1°T
<b>mean east component</b>	0.22 m/s	0.14 m/s
<b>mean north component</b>	-0.23 m/s	-0.26 m/s
<b>variance ( east component )</b>	0.07 m/s	0.10 m/s
<b>variance ( north component )</b>	0.07 m/s	0.13 m/s
<b>BIAS</b>	0.08 m/s, 250.0°T	
<b>BIAS ( east component )</b>	-0.08 m/s	
<b>BIAS ( north component )</b>	-0.03 m/s	
<b>RMSE</b>	0.19 m/s	
<b>RMSE ( east component )</b>	0.13 m/s	
<b>RMSE ( north component )</b>	0.13 m/s	
<b>r<sup>2</sup></b>	0.04	
<b>r<sup>2</sup> ( east component )</b>	0.02	
<b>r<sup>2</sup> ( north component )</b>	0.07	

Table 3.4c Correlation results of model versus image-derived ice velocities for March, 1992 covering 1-day period (148 samples).

	<b>model</b>	<b>observed</b>
<b>Mean velocity</b>	0.12 m/s, 121.6°T	0.14 m/s, 126.5°T
<b>Mean east component</b>	0.10 m/s	0.11 m/s
<b>Mean north component</b>	-0.06 m/s	-0.09 m/s
<b>Variance (east component)</b>	0.05 m/s	0.10 m/s
<b>Variance (north component)</b>	0.07 m/s	0.11 m/s
<b>BIAS</b>	0.03 m/s, 148.1°T	
<b>BIAS ( east component )</b>	0.01 m/s	
<b>BIAS ( north component )</b>	-0.02 m/s	
<b>RMSE</b>	0.14 m/s	
<b>RMSE ( east component )</b>	0.10 m/s	
<b>RMSE ( north component )</b>	0.10 m/s	
<b>r<sup>2</sup></b>	0.15	
<b>R<sup>2</sup> ( east component )</b>	0.06	
<b>r<sup>2</sup> ( north component )</b>	0.24	

Table 3.4d Correlation results of model versus image-derived ice velocities for April, 1992 covering 4 days (337 samples).

A second set of ice drift data derived from ice beacons is available from 1993/94 to test the ice-ocean model in addition to those done above for the 1991/92 ice season. During the winter of 1993/94, the Bedford Institute of Oceanography deployed 20 satellite-tracked ice beacons off the Labrador coast on land-fast and drifting ice (Peterson et al., 1995). Several different types of ice beacons were used, all of which telemeter their environmental data via the ARGOS satellite system in addition to their location data. The beacons generally drifted from 10 to 20 cm/sec towards to south or south-east, parallel to the coast. The 1993/94 data set provided 170 sets of 3-day ice drifts over a 68-day period for model to observation comparison. The analysis did not provide any more insight into the ocean-ice-atmosphere interactions than provided by the 1991/92 data analysis. The regression results are presented in Table 3.5 while Fig. 3.12 displays the model and observed ice drift data.

	<b>model</b>	<b>observed</b>
<b>Mean velocity</b>	0.10 m/s, 133.5°T	0.12 m/s, 146.8°T
<b>Mean east component</b>	0.08 m/s	0.07 m/s
<b>Mean north component</b>	-0.07 m/s	-0.10 m/s
<b>Variance ( east component )</b>	0.09 m/s	0.09 m/s
<b>Variance ( north component )</b>	0.10 m/s	0.12 m/s
<b>BIAS</b>	0.03 m/s, 194.8°T	
<b>BIAS ( east component )</b>	-0.01 m/s	
<b>BIAS ( north component )</b>	-0.03 m/s	
<b>RMSE</b>	0.12 m/s	
<b>RMSE ( east component )</b>	0.07 m/s	
<b>RMSE ( north component )</b>	0.10 m/s	
<b>r<sup>2</sup></b>	0.47	
<b>r<sup>2</sup> ( east component )</b>	0.47	
<b>r<sup>2</sup> ( north component )</b>	0.47	

Table 3.5 Correlation results of model versus observed ice beacon velocities (3-day mean) for March to May, 1994 covering 68 days (170 samples).

### 3.2 Ocean parameters

The ocean data required for comparison with model simulations were available from moored current meters (MCM) which provided in addition to ocean velocities, the salinity and temperature of the ocean at the depth of the current meter. The hourly MCM data was averaged to provide daily time series for the Jan. 30 to Apr. 28, 1992 period. For the model analysis area, current meter data was available for a variety of depths ranging between 50 and 1,000m. Model simulations, however, are for specific depths layers (Table 3.6) whose layer's centre may not coincide with the depths of the current meters so that at times averages of two layers are used (Table 3.7). The location of the MCM data was previously shown in section 2 (Fig. 2.7a).

Number of level	depth (m)	depth (m) of the centre
1	10	5
2	20	15
3	30	25
4	80	55
5	150	115
6	250	165
7	380	315
8	540	460
9	770	655
10	1050	910
11	1400	1085

Table 3.6 Model depth levels.

Comparison of ocean parameter simulations and observations were as expected disappointing, possible due that model simulations represent a large grid size averages where as the observations represent site-specific values. Figs. 3.13a to 3.13c show the comparison for the Newfoundland shelf with station 15 on the inner region of the shelf and stations 18 and 19 on the outer region of the shelf. Although the model does simulate the mean speed of the currents, it does not simulate the large observed variability about the mean at the depths of the current meter even though it simulates large variability at the surface. The mean velocity increases from station 15 to station 18 (75m depth) where the offshore Labrador Current appears to be located along the section of the shelf break. Offshore from there at Station 19 (400m depth), the mean current decreases again. Farther north along the southern Labrador Shelf, similar results are found. On the inner shelf (Station 30), the mean simulated current speed near the bottom (195m) does not show any of the variability seen in the observations and simulated by the model at the surface. The steeper shelf break at this latitude (Station 40) narrows the spatial extent of the Labrador Current that the large grid of the model can not duplicate. The result is that the observed variability of the Labrador Current is larger at a specific location than that simulated by the

model. The mean current simulated by the model is also smaller at depth and at the surface than that observed at the station at 400m.

number of stations	Latitude (°N)	longitude (°W)	depth (m)	Matched Levels	Data available
18	49.5943	50.2525	75	4, 5	UVTS
17	49.2873	51.2628	310	6, 7	UVT
15	48.8245	52.6802	215	6, 7	UV
19	49.7467	49.7388	400	7, 8	UVTS
19	49.7467	49.7388	900	9, 10	UVT
20	49.9537	52.7837	455	7, 8	UVT
20	49.9537	52.7837	325	7, 8	UVT
21	50.2485	51.9213	245	6, 7	UVT
21	50.2485	51.9213	75	4, 5	UVTS
22	50.5268	51.0590	275	6, 7	UVTS
22	50.5268	51.0590	80	4, 5	UVTS
40	55.0477	53.9423	990	10, 11	UVT
40	55.0477	53.9423	400	7, 8	UVT
30	53.7472	55.4763	195	6, 7	UVT
28	52.4928	51.1905	202	6, 7	UVTS
28	52.4928	51.1905	302	6, 7	UVT
28	52.4928	51.1905	502	7, 8	UVT
27	51.9040	50.5610	305	6, 7	UVT
27	51.9040	50.5610	205	6, 7	UVTS
27	51.9040	50.5610	505	8, 9	UVT*
26	51.9027	51.1192	325	7, 8	UVT
23	50.8617	54.3075	235	6, 7	UV
24	51.3902	52.7335	75	4, 5	UVTS

Table 3.7. Location and depth of MCM data and model layers used for comparison with the available east and north components of ocean velocity, U and V, and ocean temperatures and salinities, T and S. (\* data period is to March 29 only; locations of stations were shown on Fig. 2.7a)

Winter salinity and temperature profiles of the water column are only available from the Hamilton Bank area, where profiles were collected during the deployment of ice beacons. Six set of profiles are shown in Fig. 3.14. Profiles 1, 2 and 3 are from the Hamilton Bank area and show intrusion of warm salty bottom from the Labrador Sea entering the shelf. Profiles 4,5 and 6 are from a deeper channel (Cartwright Saddle) north of Hamilton Bank where more homogeneous conditions were observed with the temperatures near the freezing point throughout the water column. Figs. 3.15 and 3.16 show the initial (December 1, 1991) and the winter (March 16 and 17, 1992) condition of the model grids representing the locations of the observations. Although the same initial conditions are used, the water column properties of the two regions (Bank versus Saddle) evolve differently and result in

distinct water column stabilities, similar but not as extreme as those observed in the middle of the winter. Over the Bank (Stns 1, 2 and 3), offshore water intrusion (or remnants of the initial conditions) are still present while in the Saddle area the water column is more homogeneous than either the initial condition and those occurring over the Bank area.

#### 4. Conclusions

Sensitivity analysis showed that when the number of ocean surface layers was increased from 15 to 17 in the ocean model, the ice extent and ice area short-term variability increased as more of the wind stress was concentrated in the shallower surface layers. However, it did not increase the simulated ocean currents at the depth of the moorings (~200m). The same low ocean sensitivity results were found by changing the vertical coefficient of mixing; changes in  $K_v$  only altered the ocean currents slightly while affecting the ice properties greatly. The surface layer ocean properties are more affected than the deeper layers where currents were monitored by current meters. Changing the value of  $K_v$  thus tunes the model more effectively for ice properties than the ocean currents. Since ice and water albedo values are scarce, most model simulations used constant values throughout simulations. Simulation tests however show that the ice extent and ice area are strongly affected by albedo values thus suggesting that seasonal variable albedo values reflecting the high reflectivity due to snow cover and high ocean wave activity should be used. Most models use a constant ice strength ( $P^*$ ). In our sensitivity analysis the ice strength ( $P^*$ ) was made dependent on ice thickness so that thinner ice deformed before the thicker ice. The ice strength may also be made to vary seasonally as the ice strength will change when the ice warms up in the spring and the ice strength decreases.

Parameter	Basic case of 10-category model
number of levels	17
ice strength ( $P^*$ )	$5 \times 10^3 (1 + 0.1 \times H_{ice})$
ice-water drag coefficient	$10 \times 10^{-3}$
turning angle, wind	$10^\circ$
turning angle, water	$10^\circ$
ice albedo	climatic norm variable
water albedo	climatic norm variable
precipitation	0
clouds	climatic norm variable
coefficient of horizontal mixing of U, V	$1 \times 10^3 \text{ m}^2 \text{ s}^{-1}$
coefficient of horizontal mixing of T, S	$0.2 \times 10^3 \text{ m}^2 \text{ s}^{-1}$
coefficient of vertical mixing of U, V	$100 \times 10^{-4} \text{ m}^2 \text{ s}^{-1}$ levels 1-3, $2 \times 10^{-4} \text{ m}^2 \text{ s}^{-1}$ for others
coefficient of vertical mixing of T, S	$10 \times 10^{-4} \text{ m}^2 \text{ s}^{-1}$ levels 1-3, $1 \times 10^{-4} \text{ m}^2 \text{ s}^{-1}$ for others
time step	600 s

Table 3.8 Model parameters used in the final version of the 10-category ice-ocean coupled model whose simulation results are shown in Figs. 3.17 and 3.18.

The turning angles of wind and water are taken as  $25^\circ$  in 2-category model's simulations that use 30m surface oceanic layers and are forced by 10m surface winds. Smaller turning angles of  $10^\circ$  are used in the 10-category model as the surface mixed layer is thinner. A constant cloud concentration of 0.9 is used for the 2-category ice model and for the 10-category model simulations of the 1991/92 ice season. However, the cloud concentration for the Labrador-Newfoundland shelf does vary through the year (deTracey and Tang, 1998); ranging between 0.5 to 0.8. When the cloud cover was reduced from 0.9 to 0.6 for the early and middle spring, the ice melt rate increased producing an extent closer to

that what is observed. A further major improvement of ice extent simulations was accomplished by initiating the 10-category model with a gridded oceanographic data set based on AFAP data (Tang and Wang, 1996). These improved simulated results of the 10-category ice model are shown in Figs. 3.17 and 3.18 and form the basis for future global warming simulations. The model was mainly run with the original parameters listed in Table 1.1 except for the parameters shown in Table 3.8. Ice with this model is restricted to the shelf region (Fig. 3.18); no ice appears in the northern Labrador Sea as was the case with the 2- and 10-category ice models initialised with the Levitus data (Fig. 2.27). The simulated time series of daily ice extent and ice area (Fig. 3.17) are shown along side the ice chart weekly observations.

Ice concentration simulated by the 10-category ice model is higher and duplicates observations closer than the 2-category ice model. When changing to a more up-to-date initial salinity and temperature field, the ice extent along the northern Labrador Sea improves further as ice is restricted to the continental shelf area as indicated by observations. It was found that although the 2-category model do simulate the ice extent and ice drift to a high degree, the 10-category model simulates the ice concentration better. Long-term means of the ocean parameters such as current and water column stability are only simulated by the coupled model not their short-term variabilities.

Simulations indicate that the southern extent of the sea-ice is mainly a function of the air temperature and not of wind strength. So although the ice comes south faster as the NW wind increases, it will also melt faster and thus will not greatly alter the ice extent. These results will be studied further when the model is used to address the effects of global warming on the sea ice properties of the Canadian east coast.

### **Acknowledgement**

The authors would like to thank Drs. Tom Yao and Moto Ikeda for their help throughout the development of the ice-ocean model and their suggestions on the manuscript. The work was funded through the Federal Panel of Energy, Research and Development.

## References

- Bryan, K., 1969. A Numerical Method for the Study of the Circulation of the World Ocean. *J. Comput. Phys.*, 4: 347-376.
- DeTracey B. M. and C. L. Tang, 1997. Monthly Climatological Atlas of Surface Atmospheric Conditions of the Northwest Atlantic. Canadian Technical Report of Hydrography and Ocean Sciences 152: iv + 63pp.
- Fissel, D., F. Welsman, R. Chave and R. Birch, 1994. Preparation of Additional Ice Model Verification Data Sets for the East Newfoundland/Labrador Region. Report prepared for Ice Center Environment Canada by ASL Environment Sciences Inc., Sidney, B.C., 15pp. + appendices.
- Hibler, W.D., 1979. A Dynamic Thermodynamic Sea Ice Model. *J. Phys. Oceanogr.*, 9: 815-846.
- Hibler, W. D., 1980. Modeling a Variable Thickness Sea Ice Cover. *Mon. Wea. Rev.*, 108: 1943-1973.
- Ikeda, M., T. Yao and G. Symonds, 1988. Simulated Fluctuation in Annual Labrador Sea-Ice Cover. *Atmos. Ocean*, 26: 16-39.
- Ikeda, M., 1991. Numerical Modelling of Ocean Circulation and Ice Cover Over the Continental Shelf. *J. Phys. Oceanogr.*, 21: 97-117.
- Ikeda, M., T. Yao and Q. Yao, 1996. Seasonal Evolution of Sea Ice Cover and Shelf Water off Labrador Simulated in a Coupled Ice-Ocean Model. *J. Geophys. Res.*, Vol 101, No. C7: 16,465-16,489.
- Levitus, S., 1982. Climatology atlas of world ocean. NOAA Prof. Rep.#13, U.S. Govt. Print. Off., Wahington, D.C., 173pp.
- Mysak, L.A., S. Peng and R.G. Wood, 1991. Application of a Coupled Ice-Ocean Model to the Labrador Sea. *Atmos. Ocean*, 29: 232-255.
- Narayanan, S., S. J. Prinsenberg and P. C. Smith, Current Meter Observations from the Labrador and Newfoundland Shelves and comparisons with Barotropic Model Predictions and IIP Surface Currents. *Atmos. Ocean*, 34 (1) 1996, 227-255
- Peterson, I. K., S. J. Prinsenberg and G.A. Fowler, 1995. Newfoundland Shelf Sea Ice Program, 1993 and 1994. Canadian Technical Report of Hydrography and Ocean Sciences 167: vi + 167pp.
- Prinsenberg, S. J., I. K. Peterson, S. Narayanan and J. U. Umoh, 1997. Interaction between atmosphere, ice cover, and ocean off Labrador and Newfoundland from 1962 to 1992. *Can. J. Fish. Aquat. Sci.* 54 (Suppl. 1): 30-39.
- Tang, C. L. and C.K. Wang, 1996. A Gridded Data Set of Temperature and Salinity for the Northwest Atlantic Ocean. Canadian Technical Report of Hydrography and Ocean Sciences 148: iv + 45pp.
- Thorndike, A. S., D. A. Rothrock, G. A. Maykut and R. Colony, 1975. The Thickness Distribution of Sea Ice. *J. Geophys. Res.*, Vol. 80: 4,501-4,513.

Yao, T. and M., Ikeda, 1990. A model of Sea Ice and the Upper Ocean Mixed Layer off Labrador. J. Geophys. Res., Vol. 95: 11,603-11,612.

THE FIELD OF THE MODEL

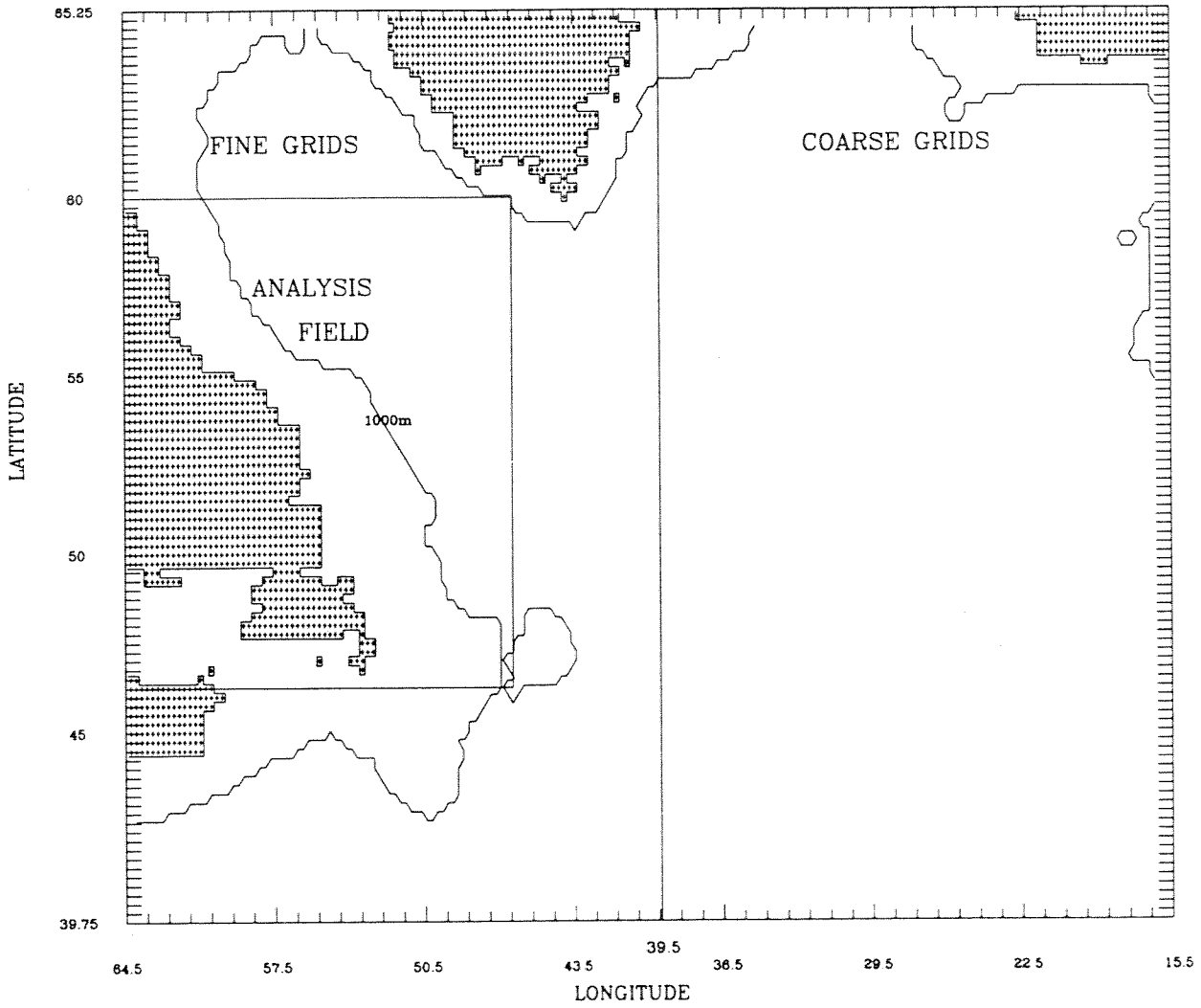


Fig. 1.1 Extent of the model domain.

TOPOGRAPHY, FOR THE 15-LEVEL MODEL

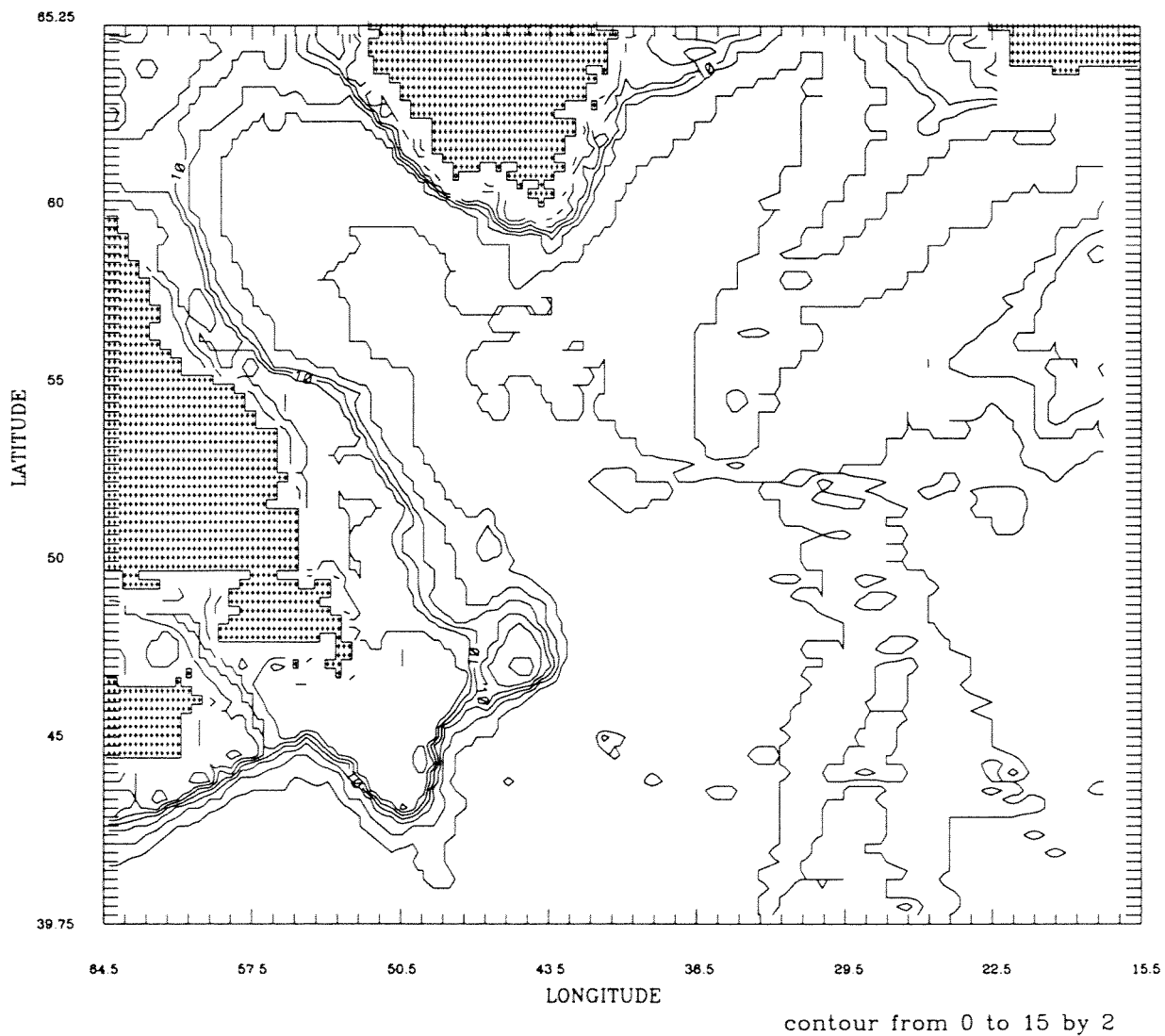
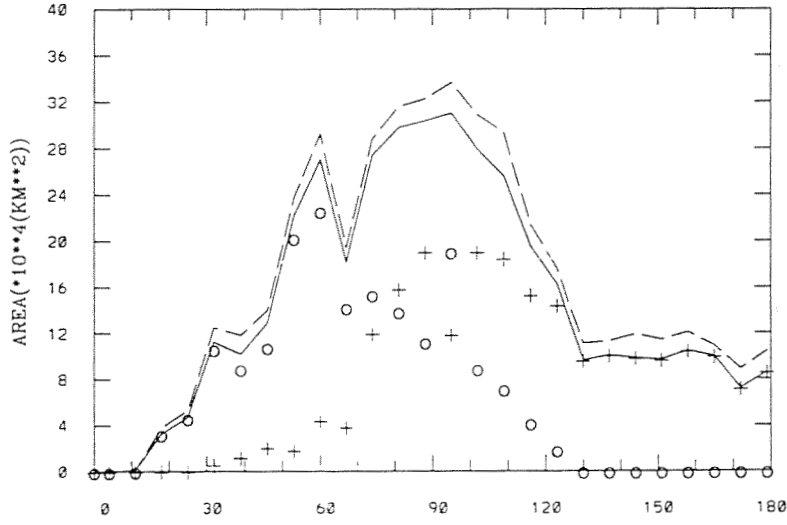


Fig. 1.2 Model's representation of bottom topography using 15 depth layers.

OBSERVED DATA 91/92 ICE SEASON

solid line - total area, dashed line - total ice extent  
 o - thin ice, gw, grey & new, + - thick ice, old & fy



solid line - total ice volume  
 o - thin ice, 0.15M, + - thick ice, 1.25M

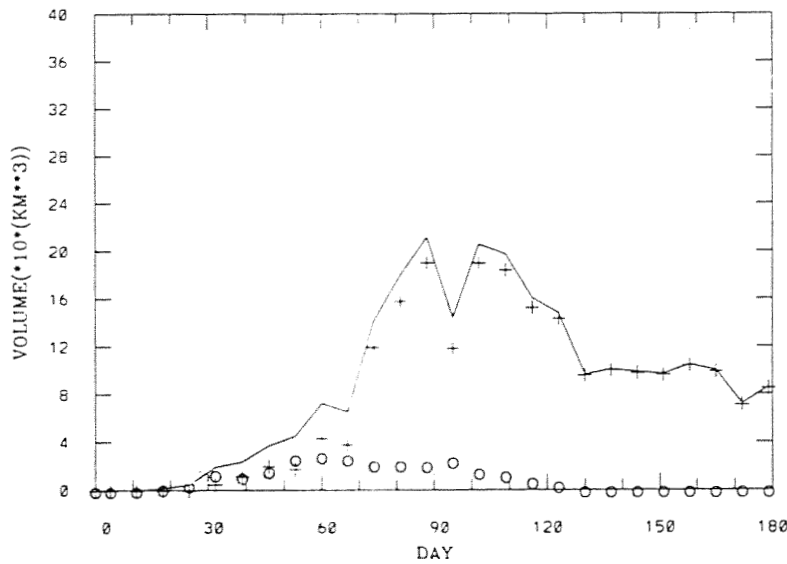


Fig. 2.1 Weekly time series data of ice extent, ice area and ice volume for the 1991/92 ice season for the Labrador and Newfoundland Shelf area.

## 2-CATEGORY MODEL, 15 LEVELS, 91/92 ICE SEASON

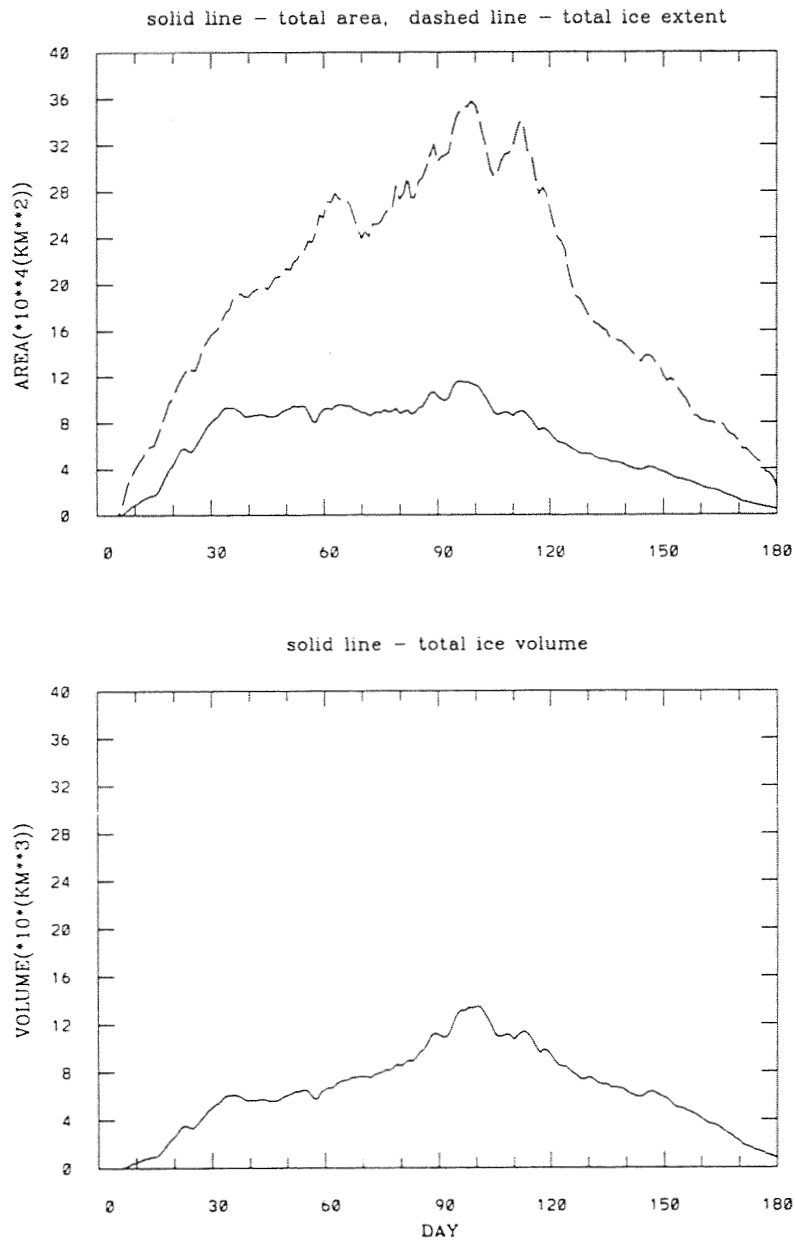


Fig. 2.2 Time series simulated by the 2-category model with 15 ocean layers for the 1991/92 ice season.

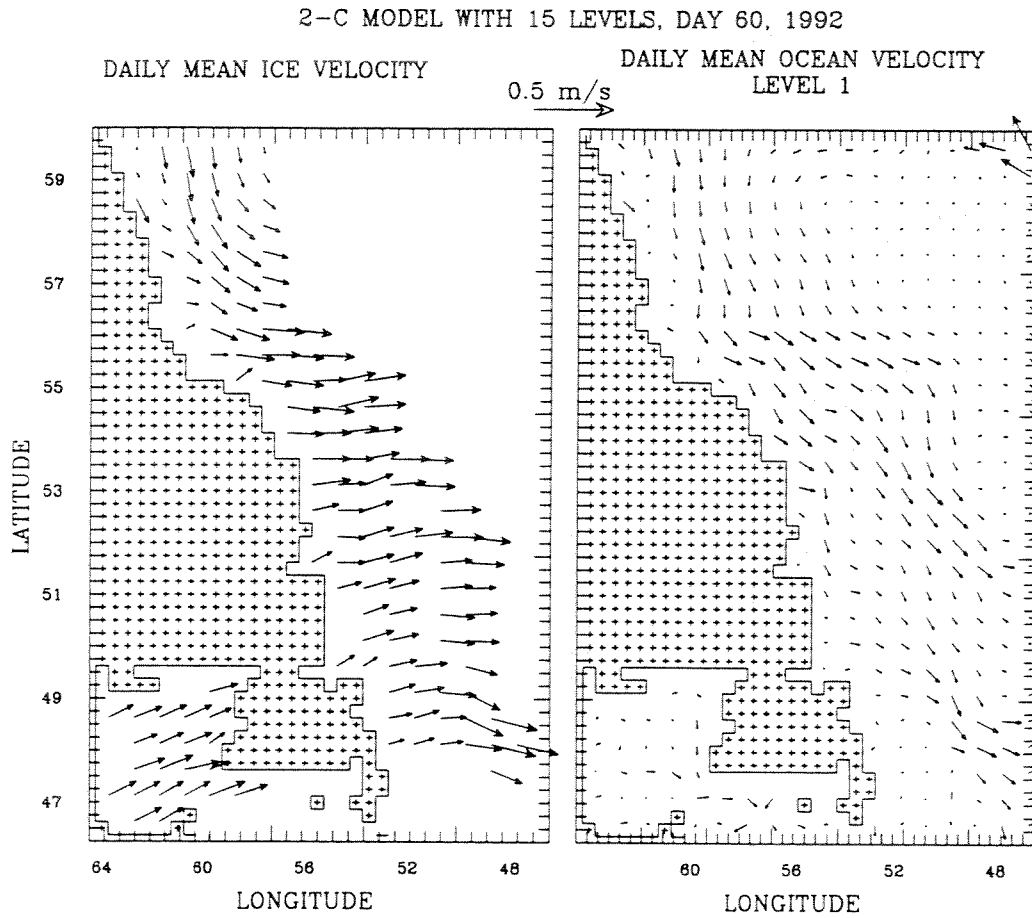


Fig. 2.3a Daily mean ice velocity and mixing layer's ocean velocity simulated by the 2-category model with 15 ocean layers for Jan. 29, 1992.

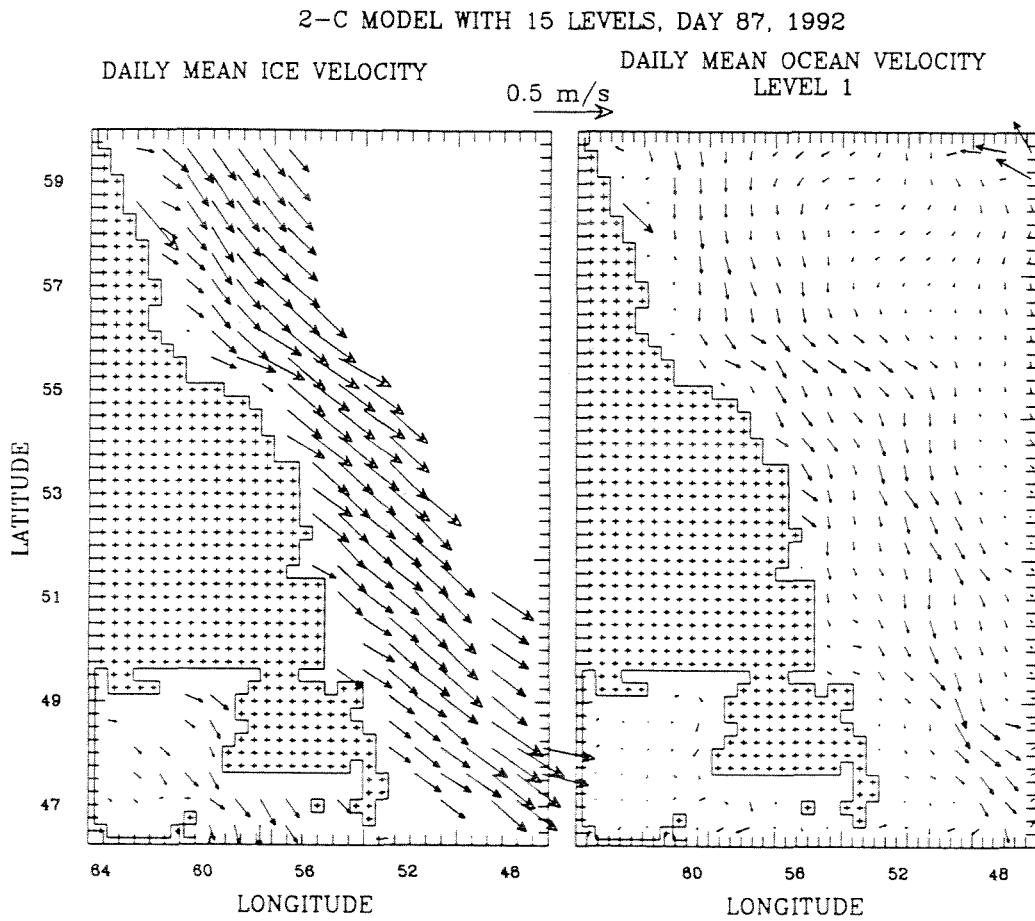


Fig. 2.3b Daily mean ice velocity and mixing layer's ocean velocity simulated by the 2-category model with 15 ocean layers for Feb. 25, 1992.

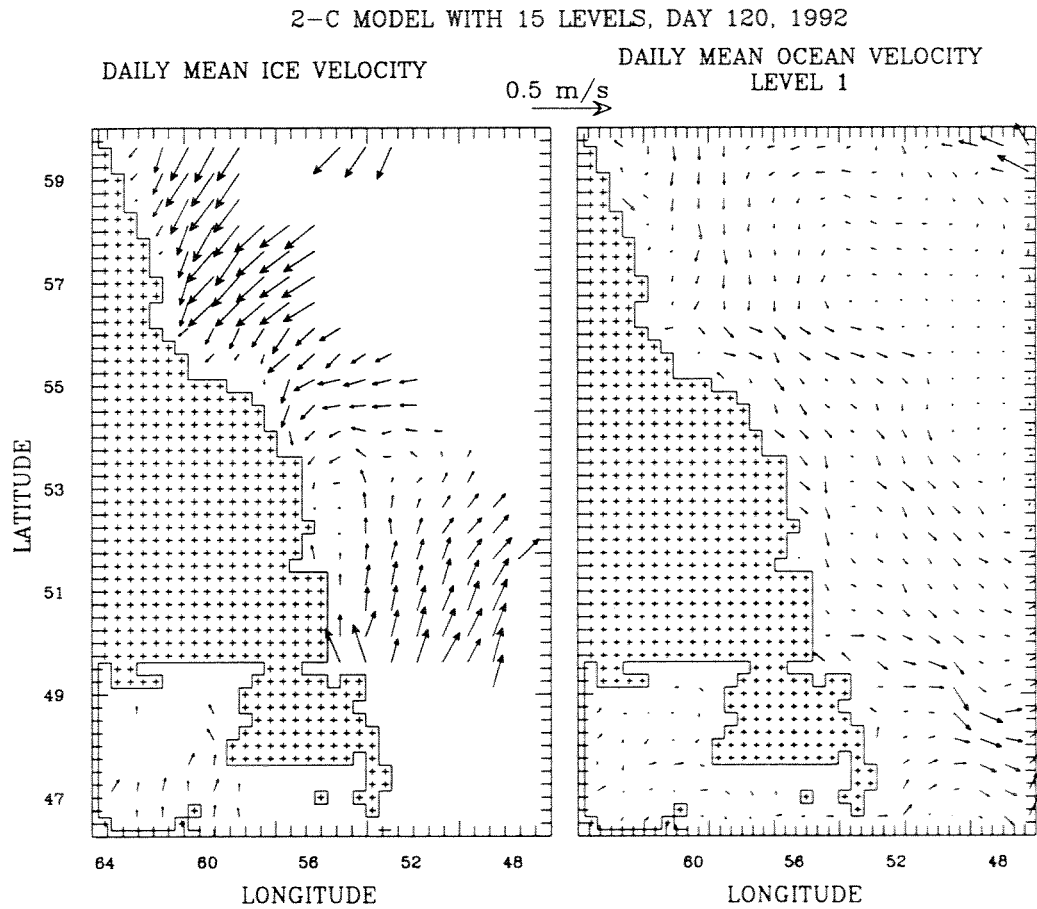


Fig. 2.3c Daily mean ice velocity and mixing layer's ocean velocity simulated by the 2-category model with 15 ocean layers for Mar. 29 1992.

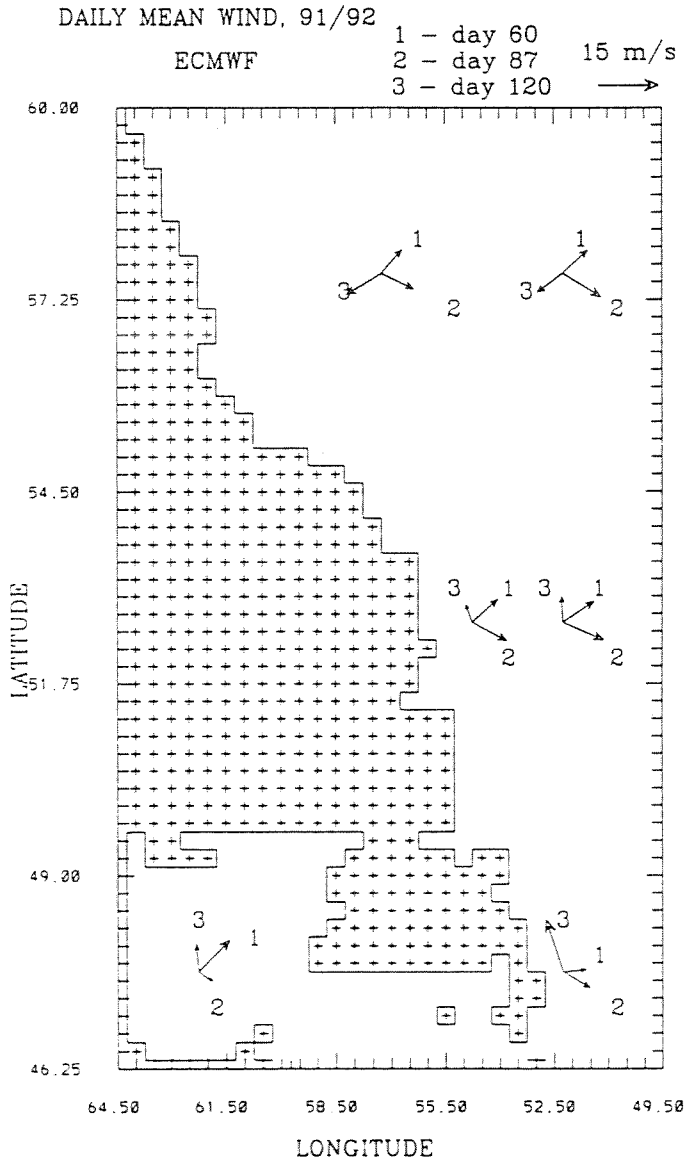


Fig. 2.4 Daily mean ECMWF winds for different 3 days at 6 locations.

## 2-CATEGORY MODEL, 17 LEVELS, 91/92 ICE SEASON

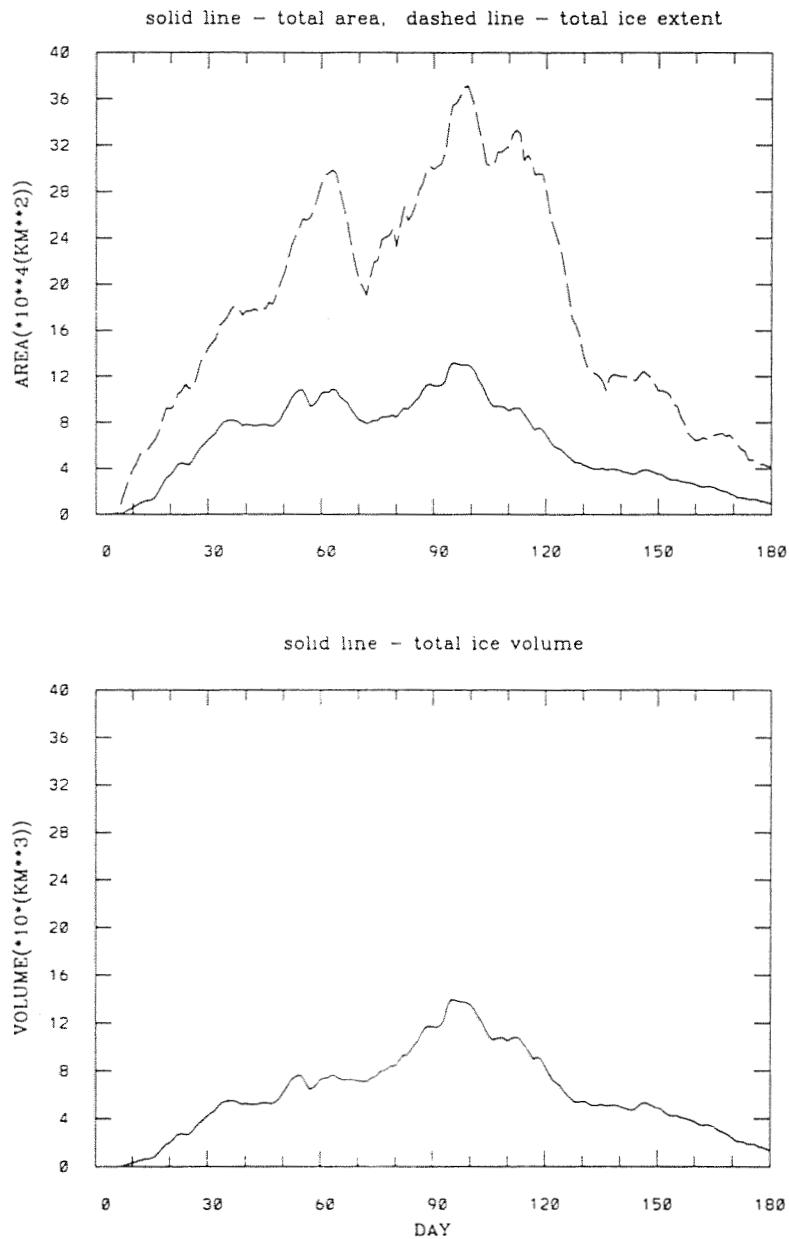


Fig. 2.5 Time series simulated by the 2-category model with 17 ocean layers for the 1991/92 ice season for Labrador and Newfoundland Shelf area.

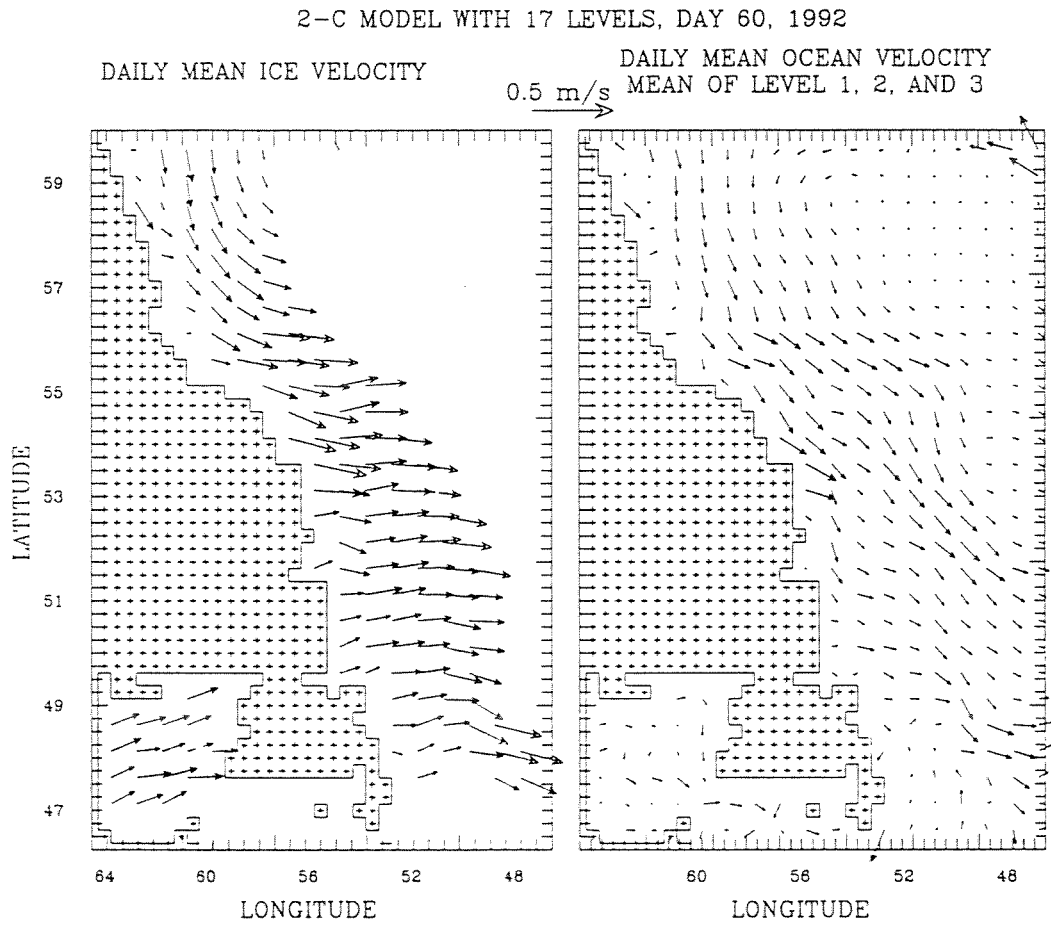


Fig. 2.6a<sub>1</sub> Daily mean ice velocity and ocean velocity averaged over layers 1, 2 and 3 simulated by the 2-category model with 17 ocean layers for Jan. 29, 1992.

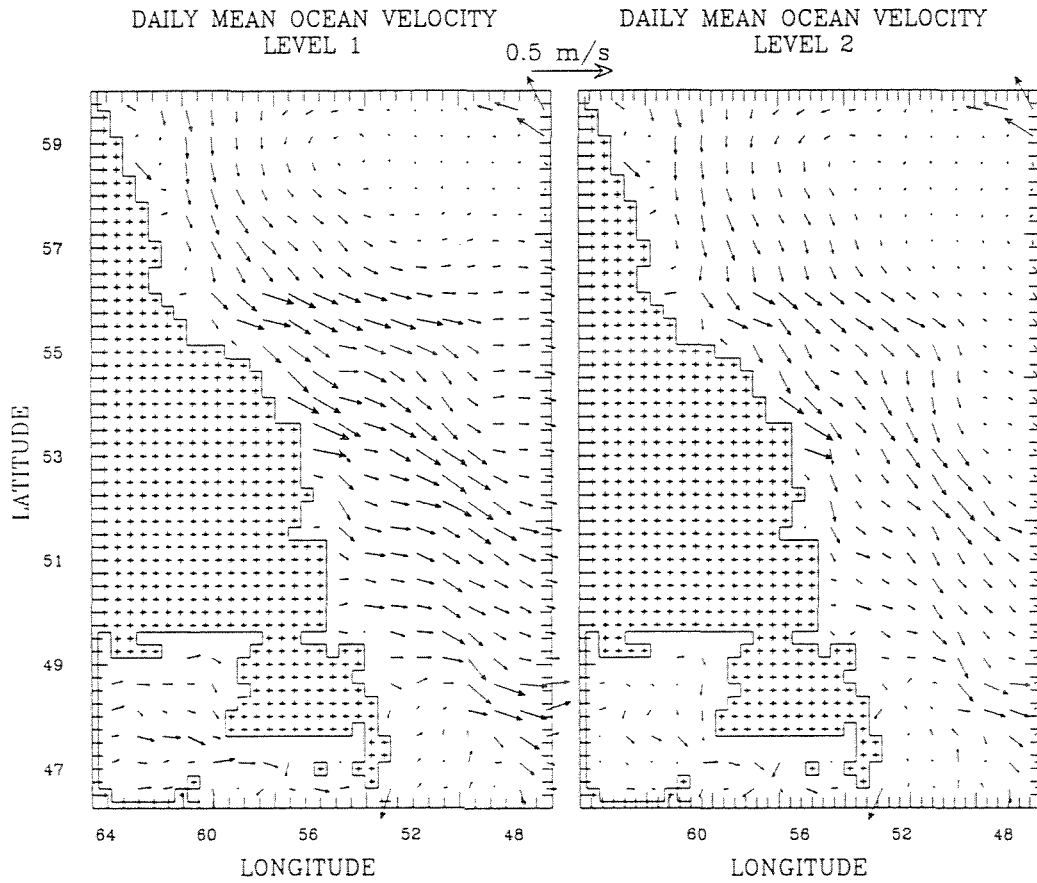


Fig. 2.6a<sub>2</sub> Daily mean ocean velocities of the surface and second layers simulated by the 2-category model with 17 ocean layers for Jan. 29, 1992.

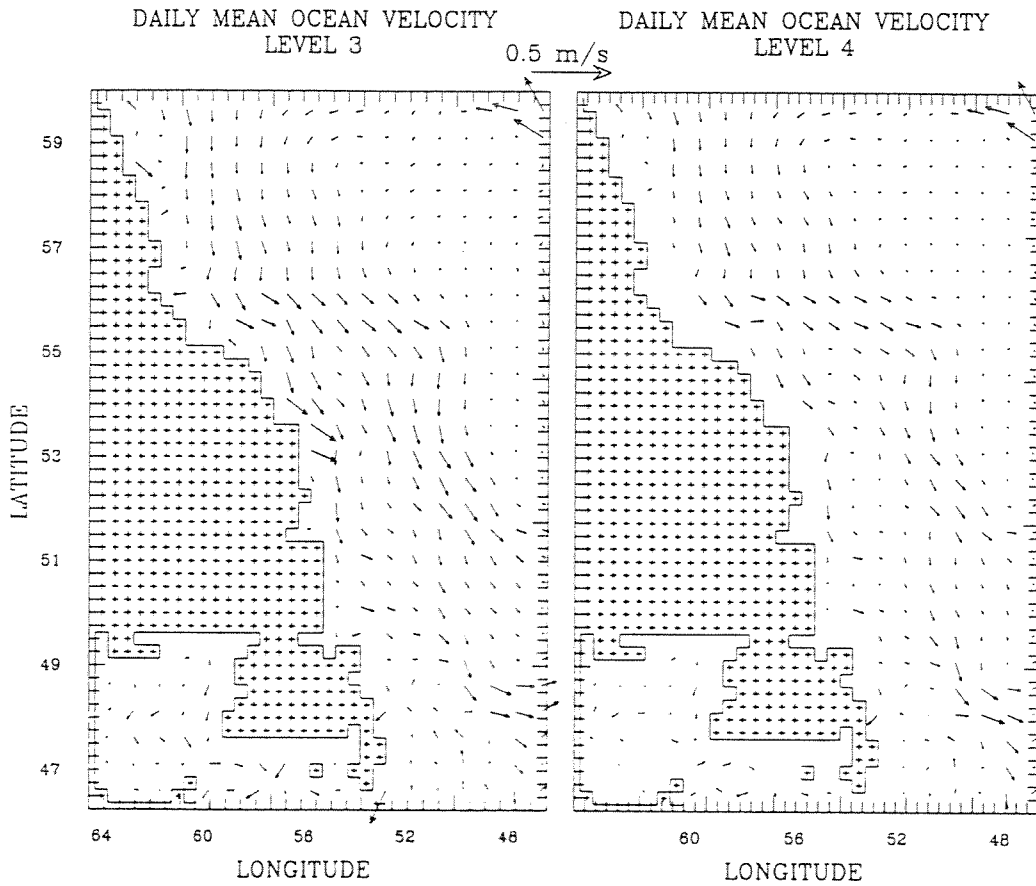


Fig. 2.6a<sub>3</sub> Daily mean ocean velocities of the third and fourth layers simulated by the 2-category model with 17 ocean layers for Jan. 29, 1992.

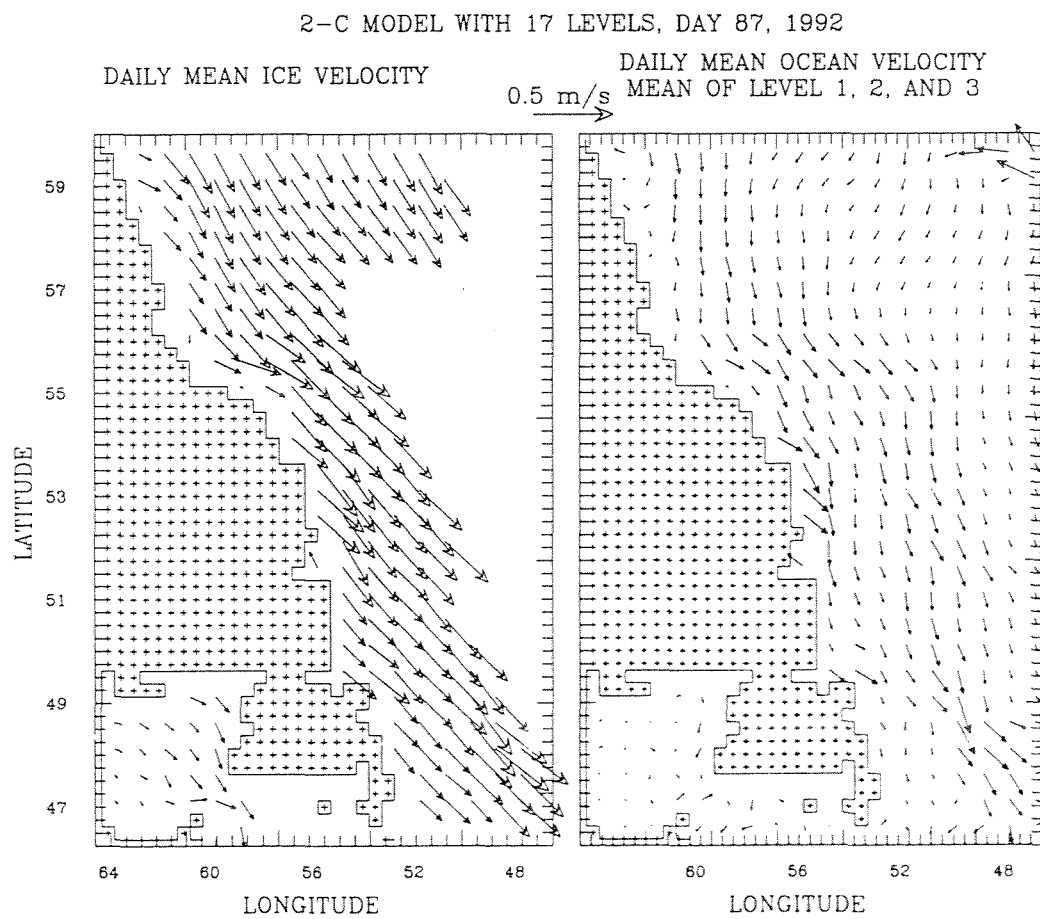


Fig. 2.6b<sub>1</sub> Daily mean ice velocity and ocean velocity averaged over layers 1, 2 and 3 simulated by the 2-category model with 17 ocean layers for Feb. 25, 1992.

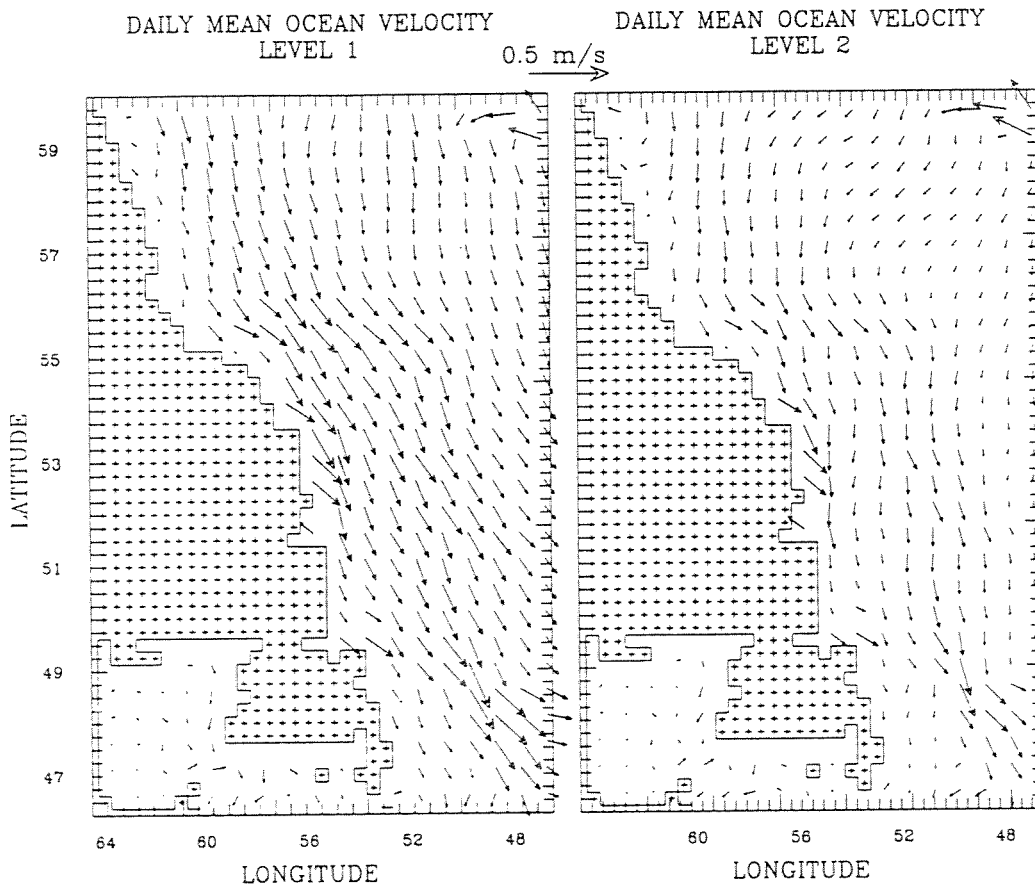


Fig. 2.6b<sub>2</sub> Daily mean ocean velocities of the surface and second layers simulated by the 2-category model with 17 ocean layers for Feb. 25, 1992.

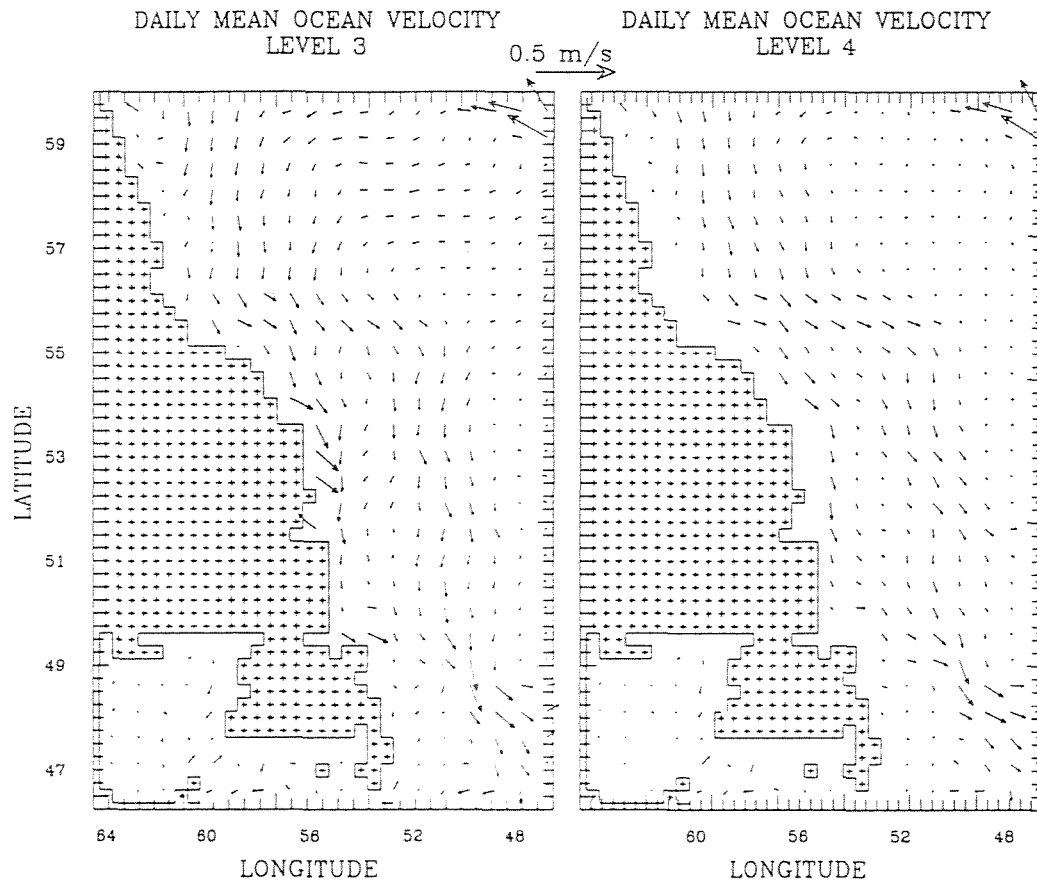


Fig. 2.6b<sub>3</sub> Daily mean ocean velocities of the third and fourth layers simulated by the 2-category model with 17 ocean layers for Feb. 25, 1992.

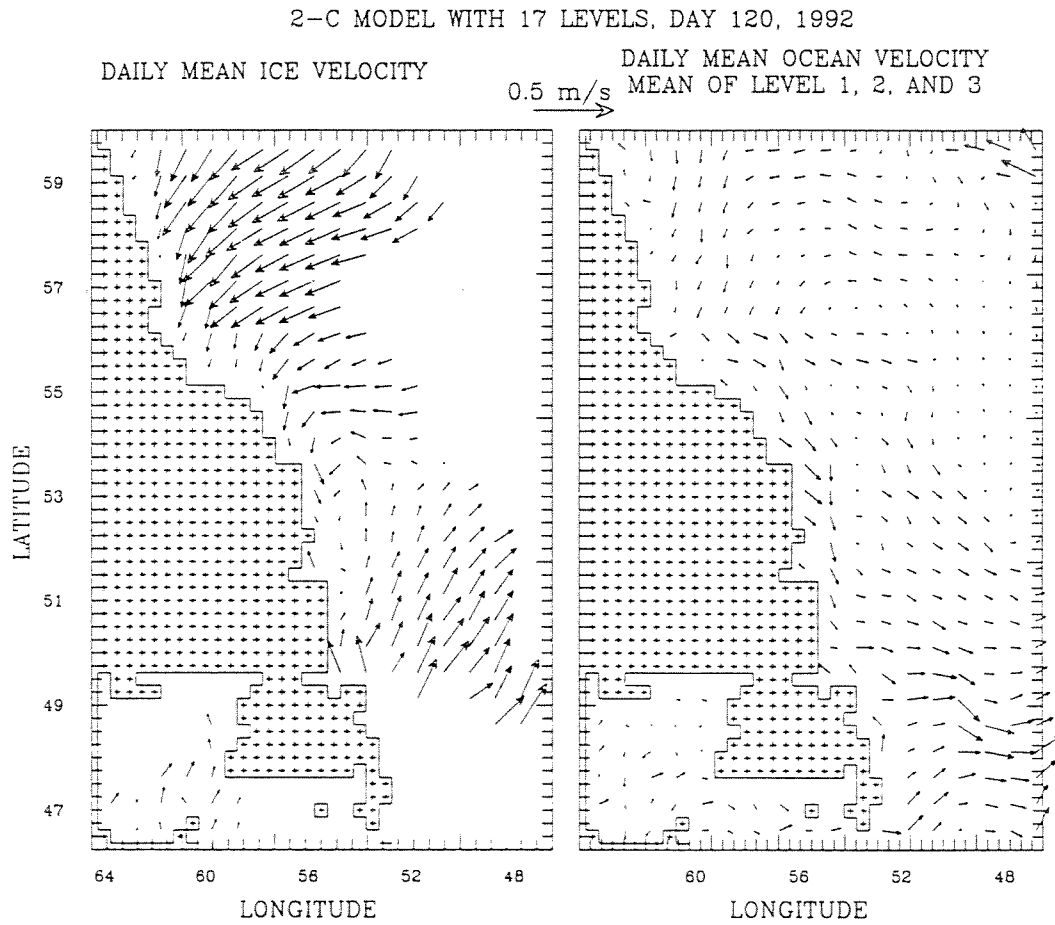


Fig. 2.6c<sub>1</sub> Daily mean ice velocity and ocean velocity averaged over layers 1, 2 and 3 simulated by the 2-category model with 17 ocean layers for Mar. 29, 1992.

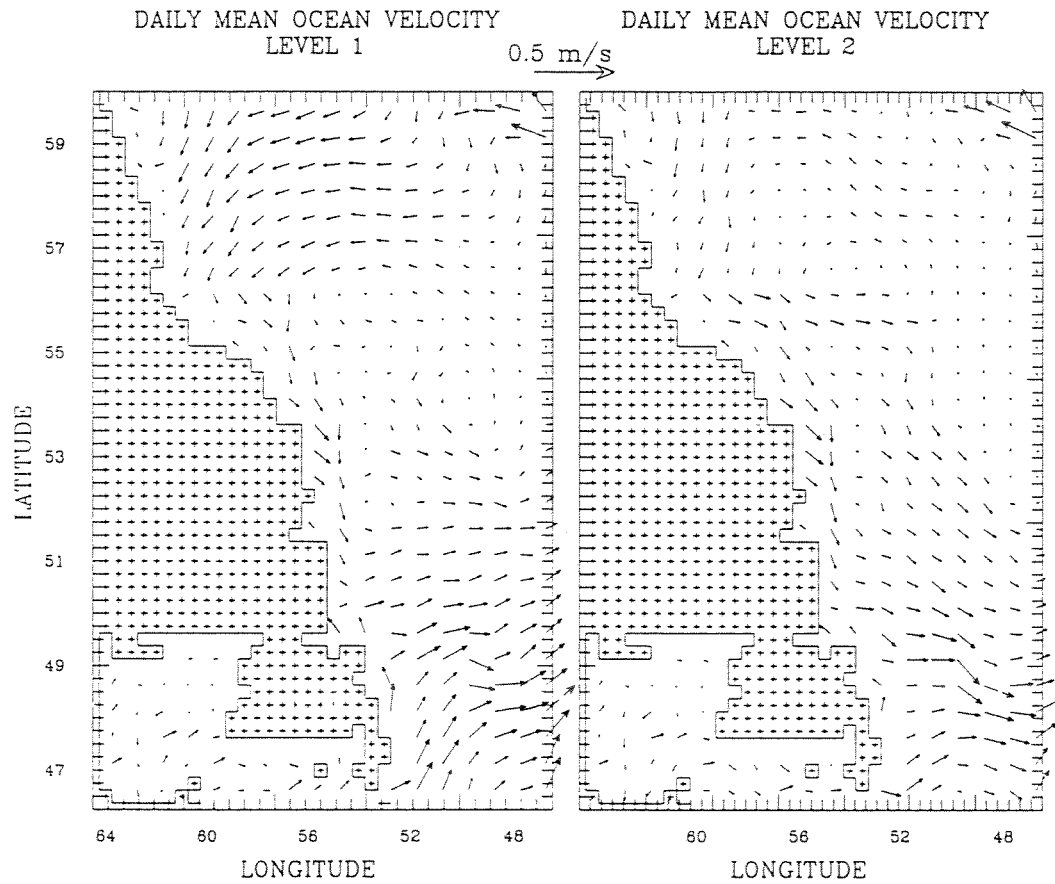


Fig. 2.6c<sub>2</sub> Daily mean ocean velocities of the surface and second layers simulated by the 2-category model with 17 ocean layers for Mar. 29, 1992.



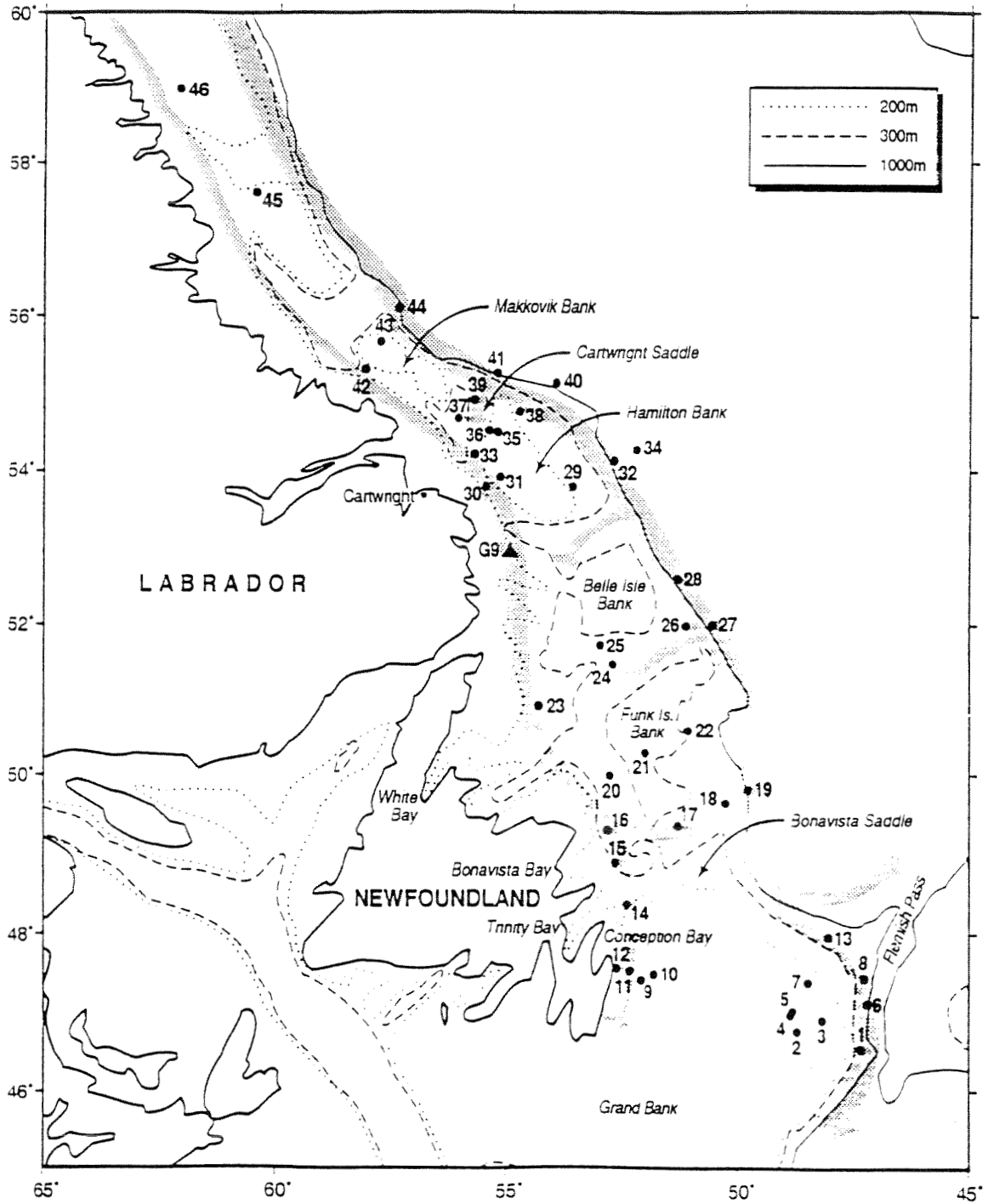


Fig. 2.7a Locations of current meter stations.

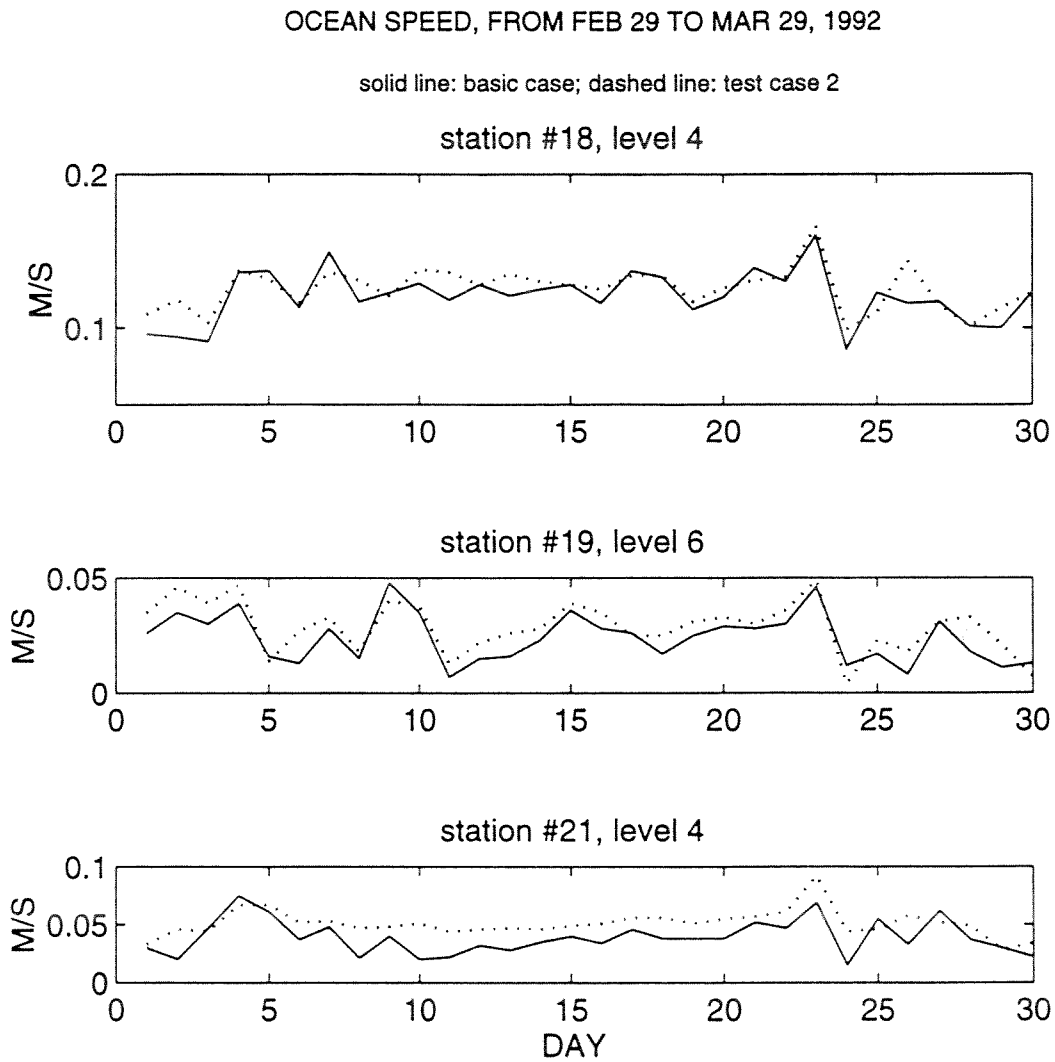


Fig. 2.7b<sub>1</sub> Model ocean speeds at stations 18, 19 and 21 of basic and test 2 for Feb. 29 to Mar. 29, 1992. Depth range of level 4 is from 30 to 80m and for level 6 from 150 to 250m.

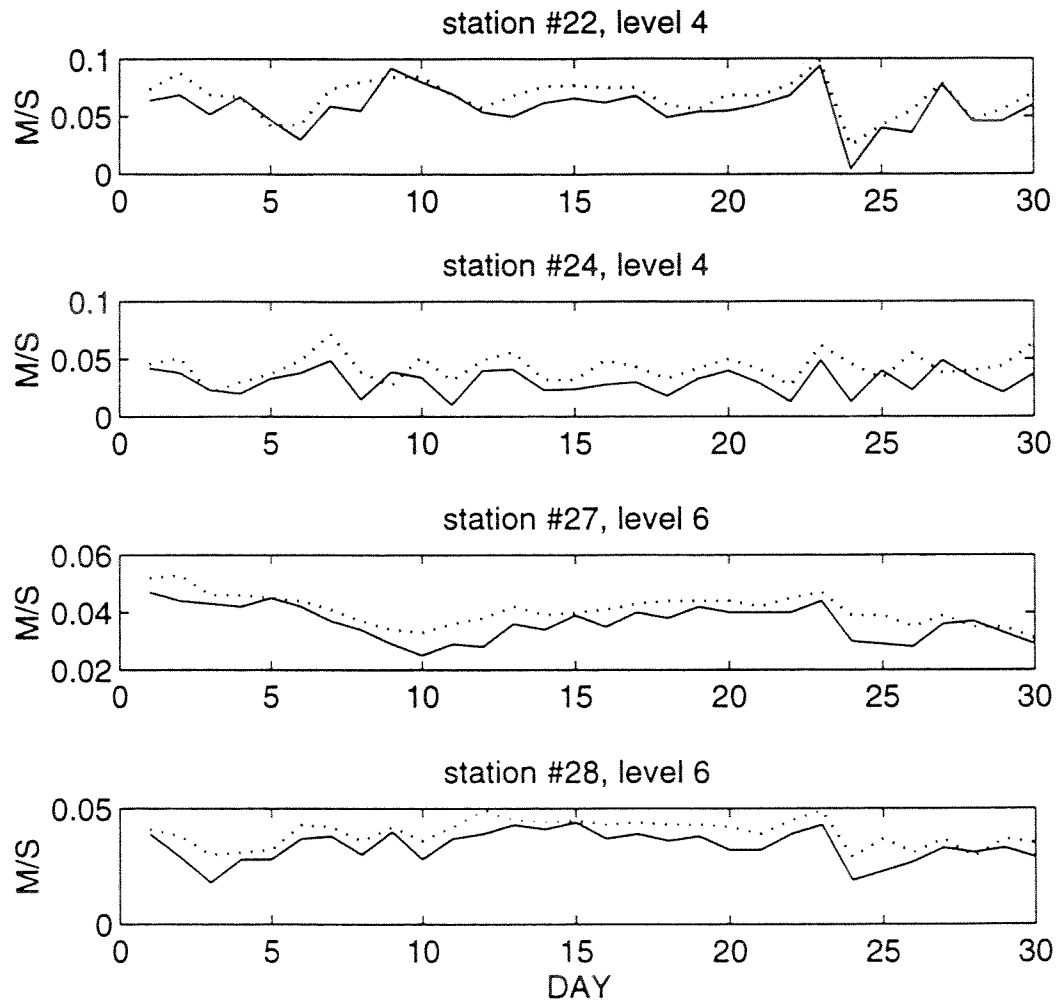


Fig. 2.7b<sub>2</sub> Model ocean speeds at stations 22, 24, 27 and 28 of basic and test 2 for Feb. 29 to Mar. 29, 1992. Depth range of level 4 is from 30 to 80m and for level 6 from 150 to 250m.

## VERTICAL MIXING COEFF. TEST CASE2, 91/92 ICE SEASON

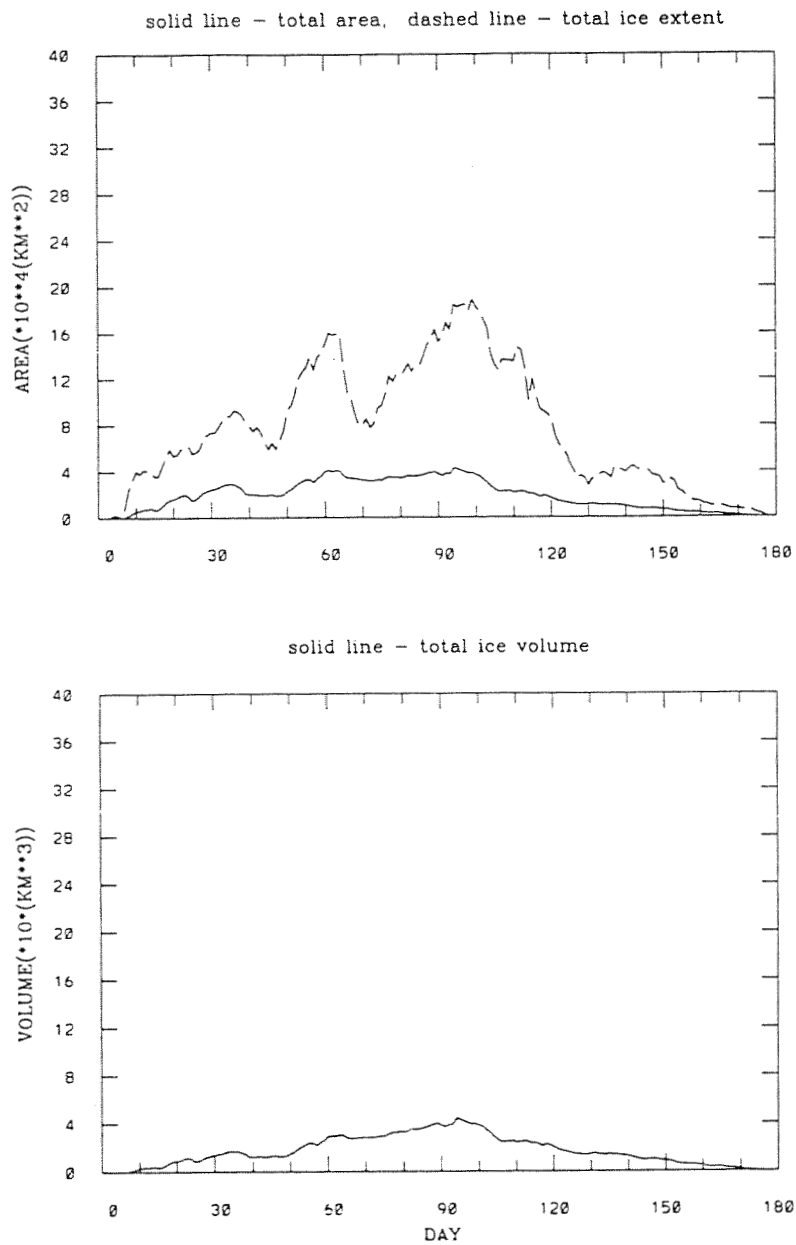


Fig. 2.8a Simulated time series of ice extent, ice area and ice volume of test case 2 for the 1991/92 ice season.

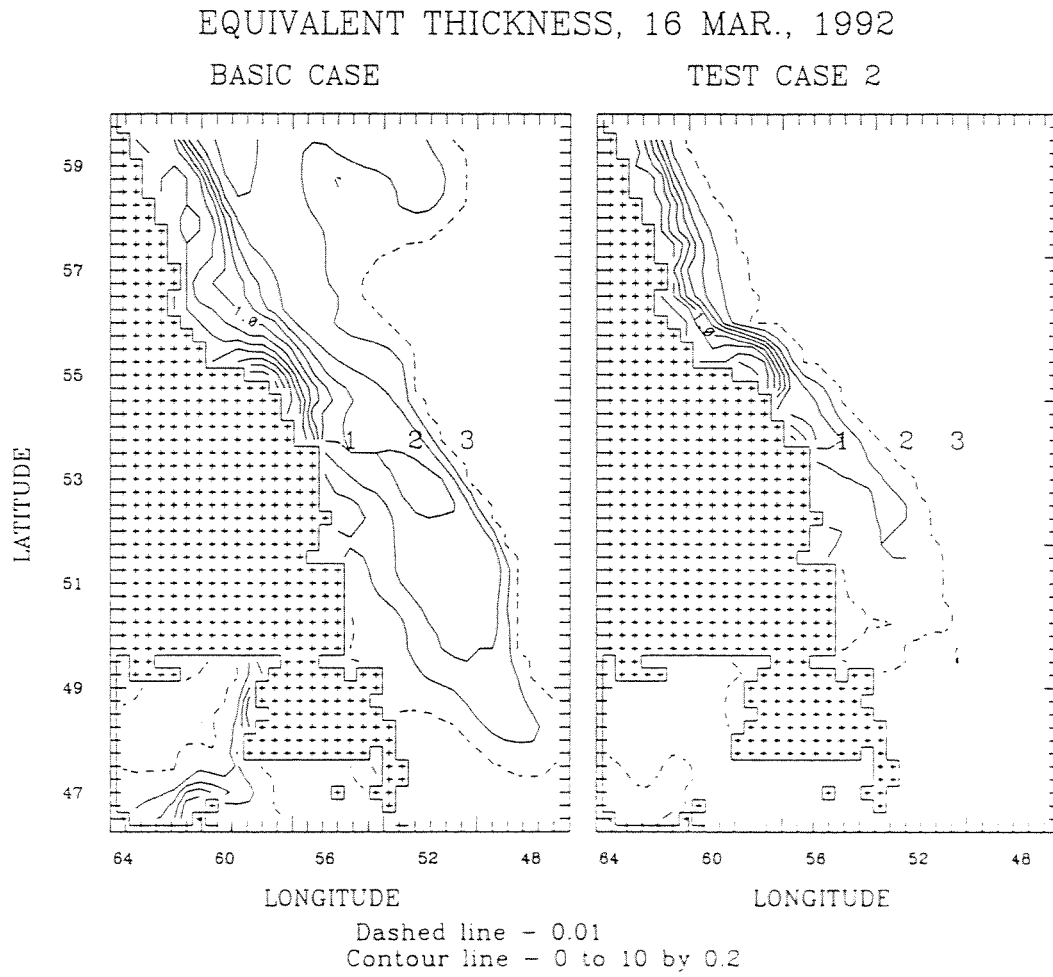


Fig. 2.8b Simulated ice equivalent thickness of basic and test case 2 for Mar. 16, 1992.

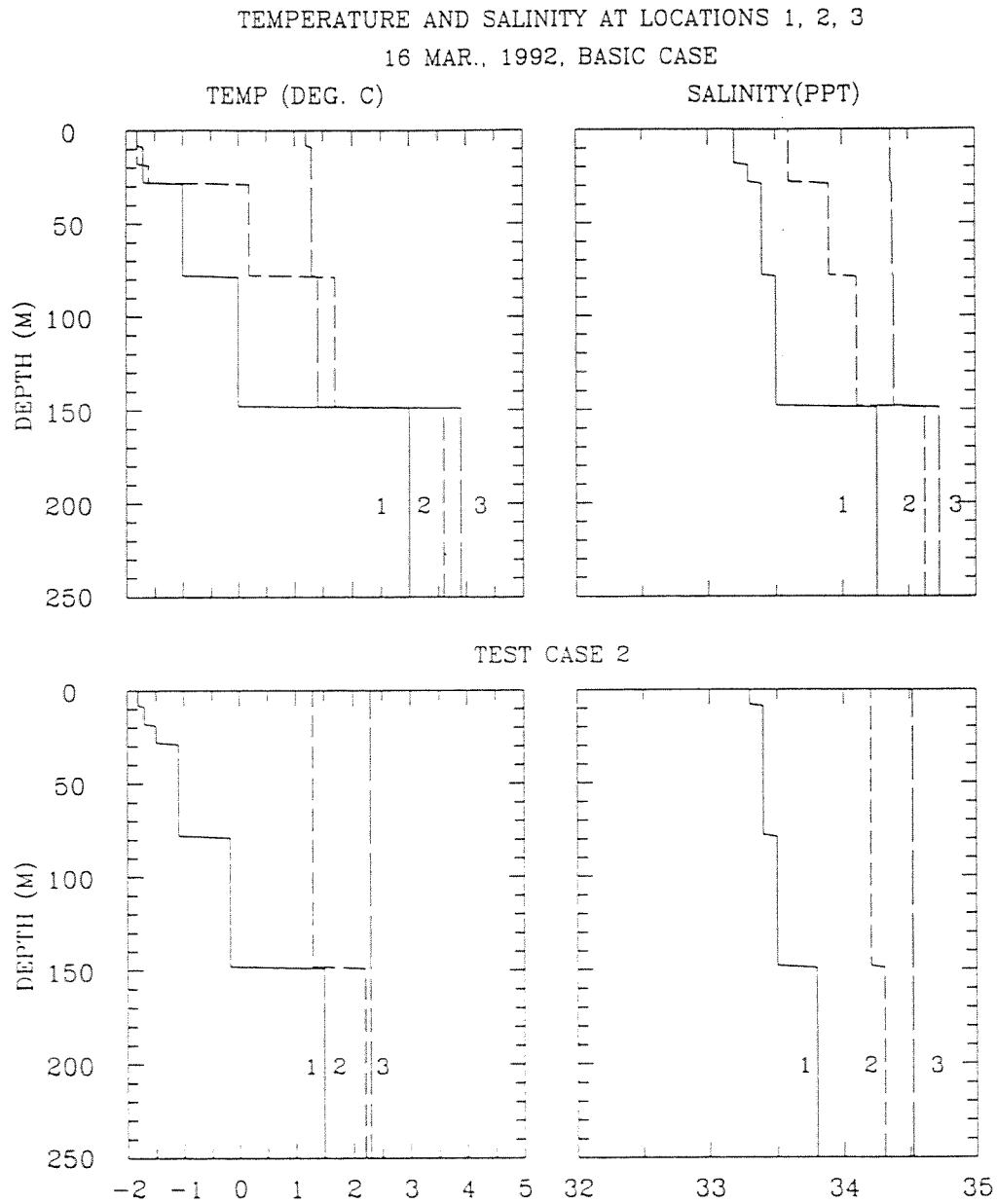


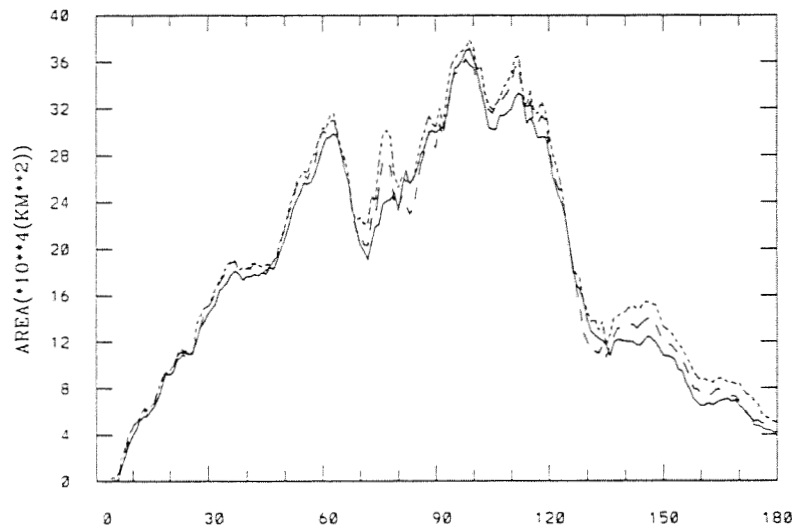
Fig. 2.8c Simulated temperature and salinity profiles at locations 1, 2, and 3 (locations shown on Fig. 2.8b) of basic and test case 2 for Mar 16, 1992.

## HORIZONTAL MIXING COEFF. TESTS, 91/92 ICE SEASON

solid line- basic case, dashed line - test case3

dotted line - test case4

TOTAL ICE EXTENT



TOTAL ICE COVERED AREA

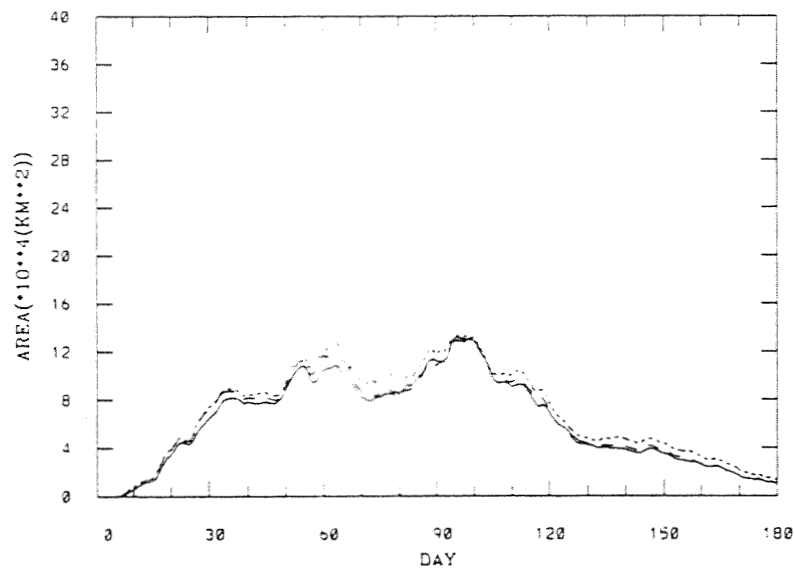


Fig. 2.9 Simulated time series of test 3, 4 and basic cases for 1991/92 ice season

## OCEAN SPEED, FROM FEB 29 TO MAR 29, 1992

solid line: basic case; dashed line: test case 3

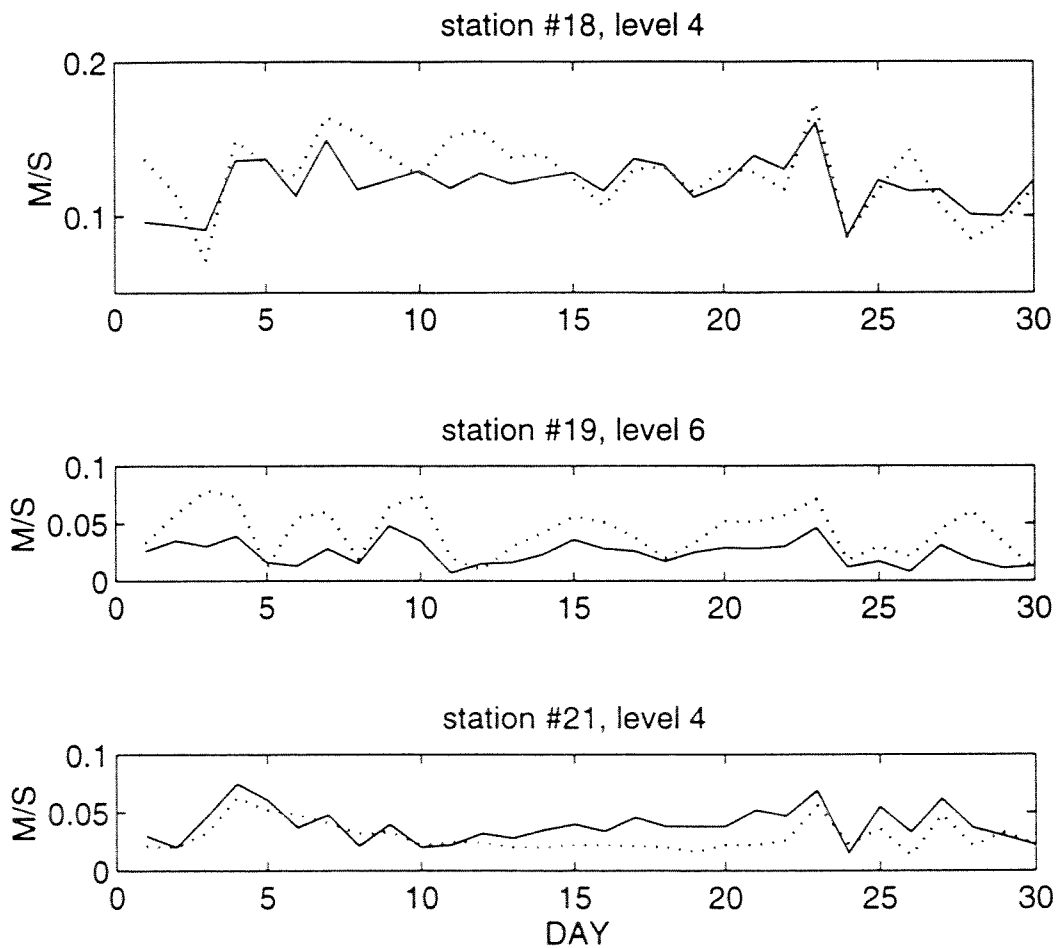


Fig. 2.10a Model ocean speeds at stations 18, 19 and 21 of basic and test 3 for Feb. 29 to Mar. 29, 1992. Depth range of level 4 is from 30 to 80m and for level 6 from 150 to 250m.

A27

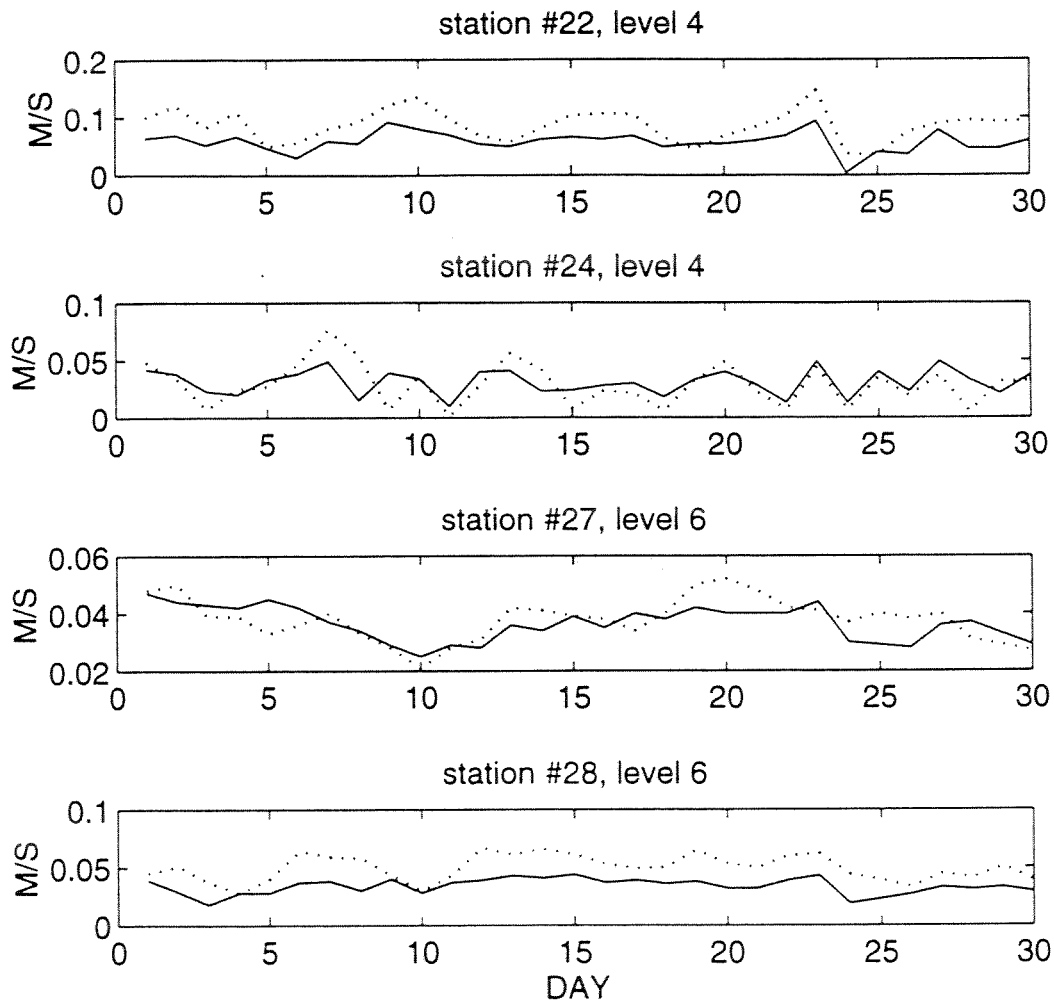


Fig. 2.10b Model ocean speeds at stations 22, 24, 27 and 28 of basic and test 3 for Feb. 29 to Mar. 29, 1992. Depth range of level 4 is from 30 to 80m and for level 6 from 150 to 250m.

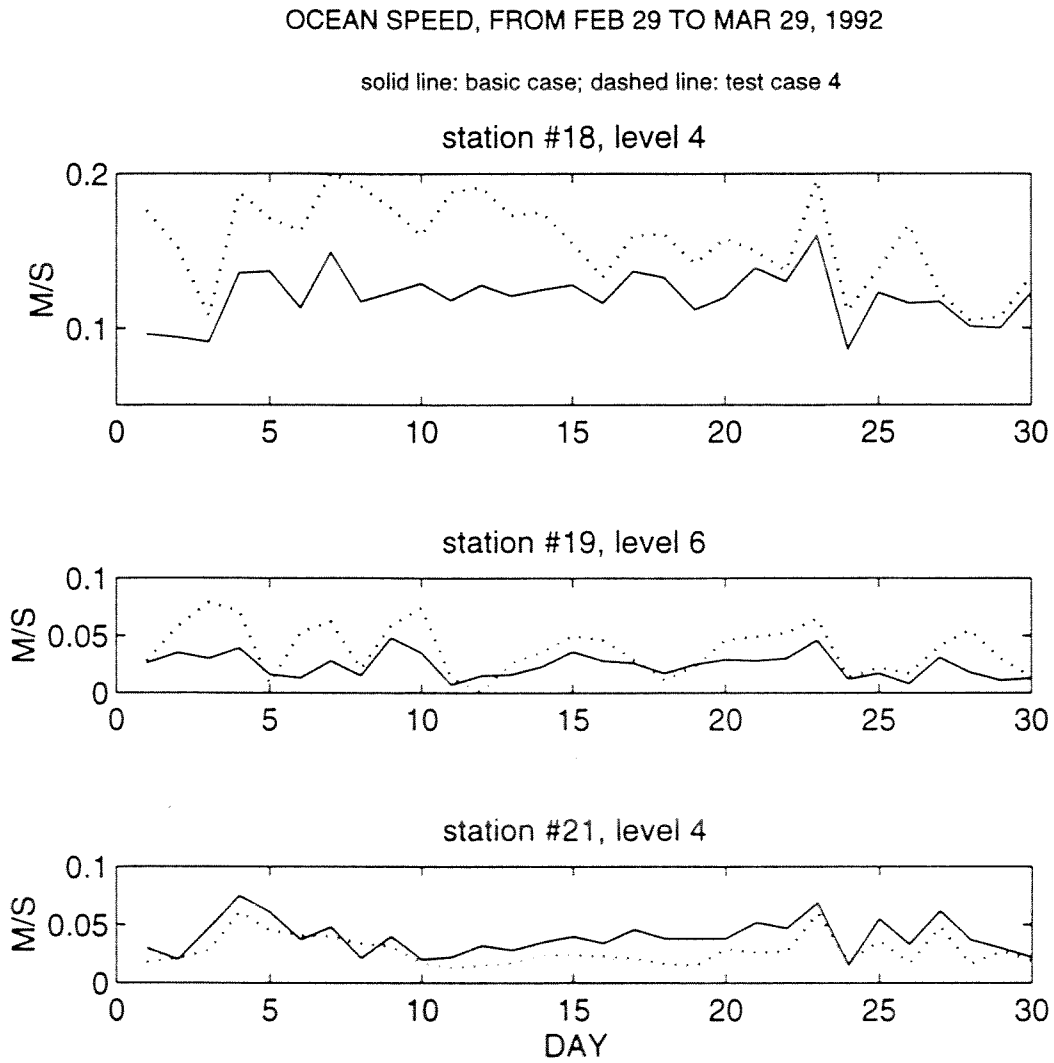


Fig. 2.11a Model ocean speeds at stations 18, 19 and 21 of basic and test 4 for Feb. 29 to Mar. 29, 1992. Depth range of level 4 is from 30 to 80m and for level 6 from 150 to 250m.

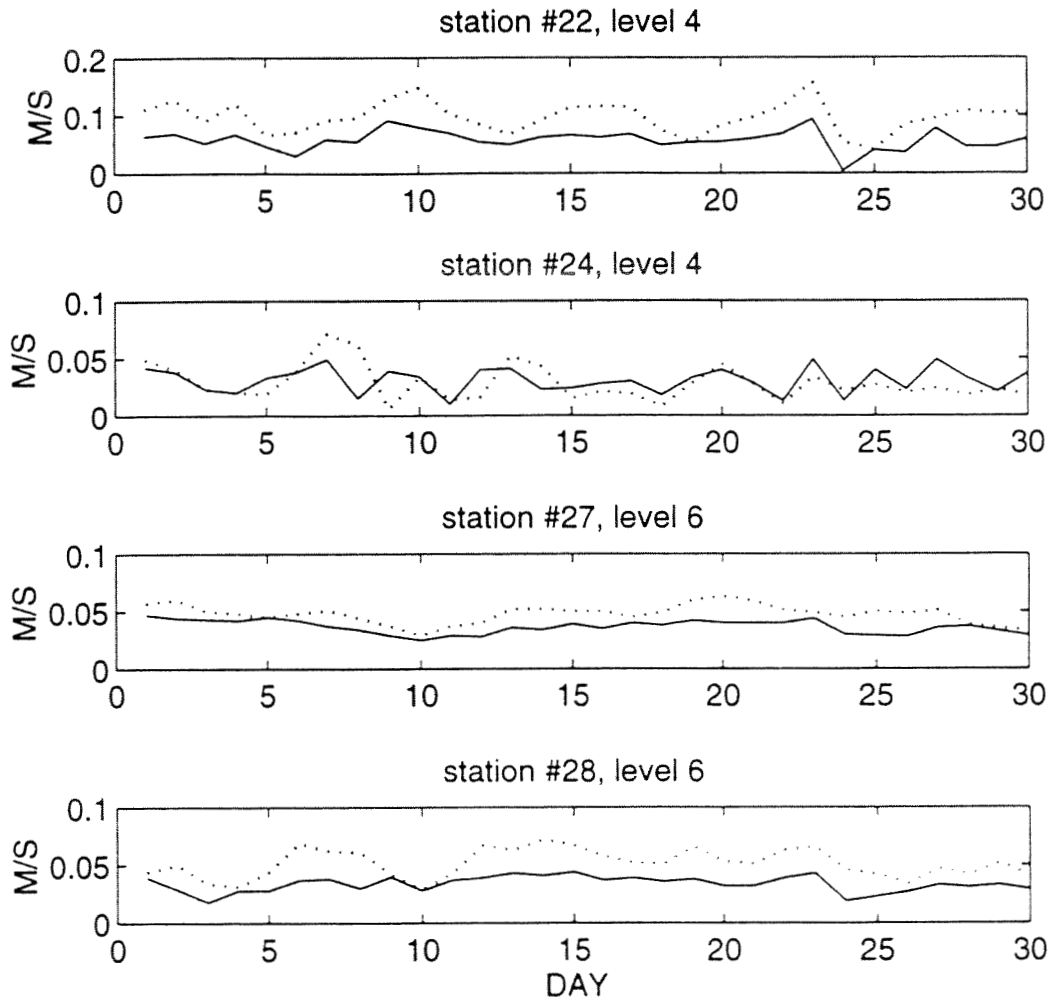


Fig. 2.11b Model ocean speeds at stations 22, 24, 27 and 28 of basic and test 4 for Feb. 29 to Mar. 29, 1992. Depth range of level 4 is from 30 to 80m and for level 6 from 150 to 250m.

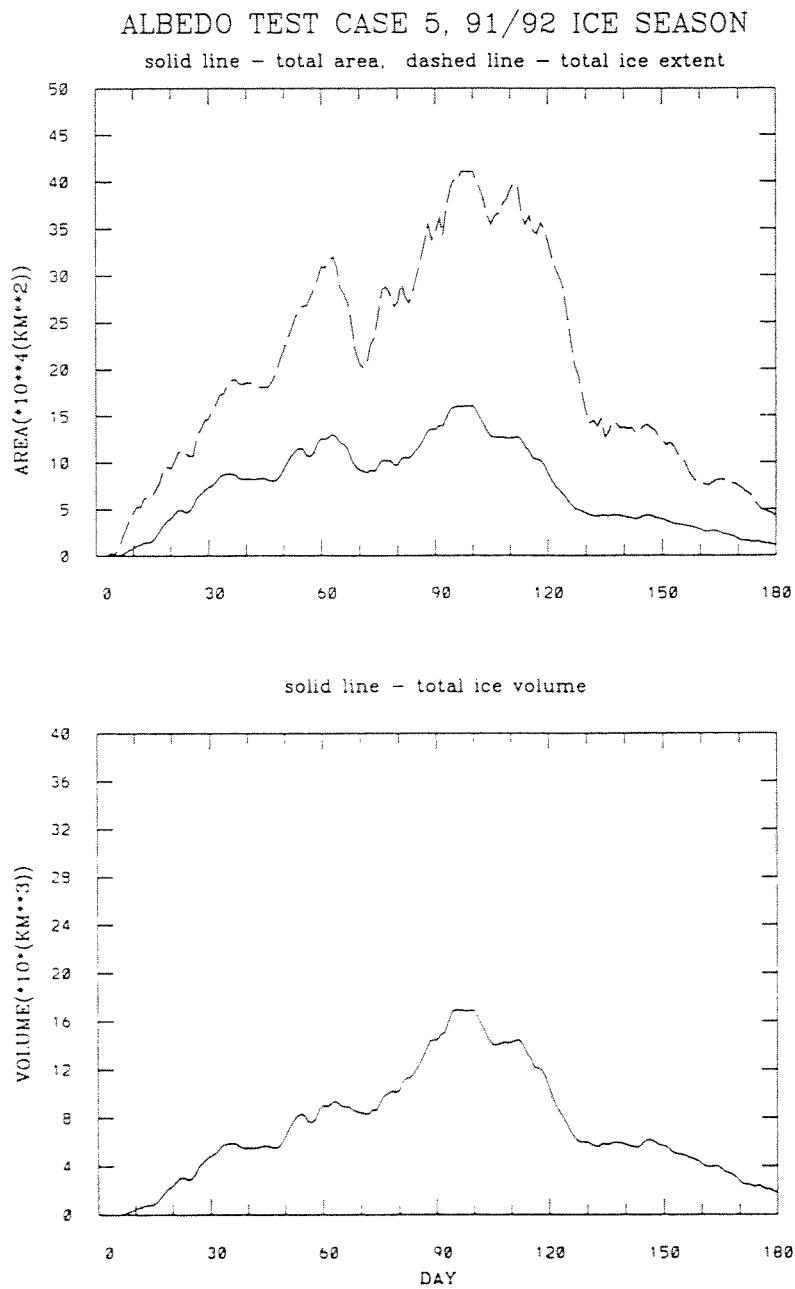


Fig. 2.12 Simulated time series of ice extent, ice area and ice volume of albedo test case 5 for the 1991/92 ice season.

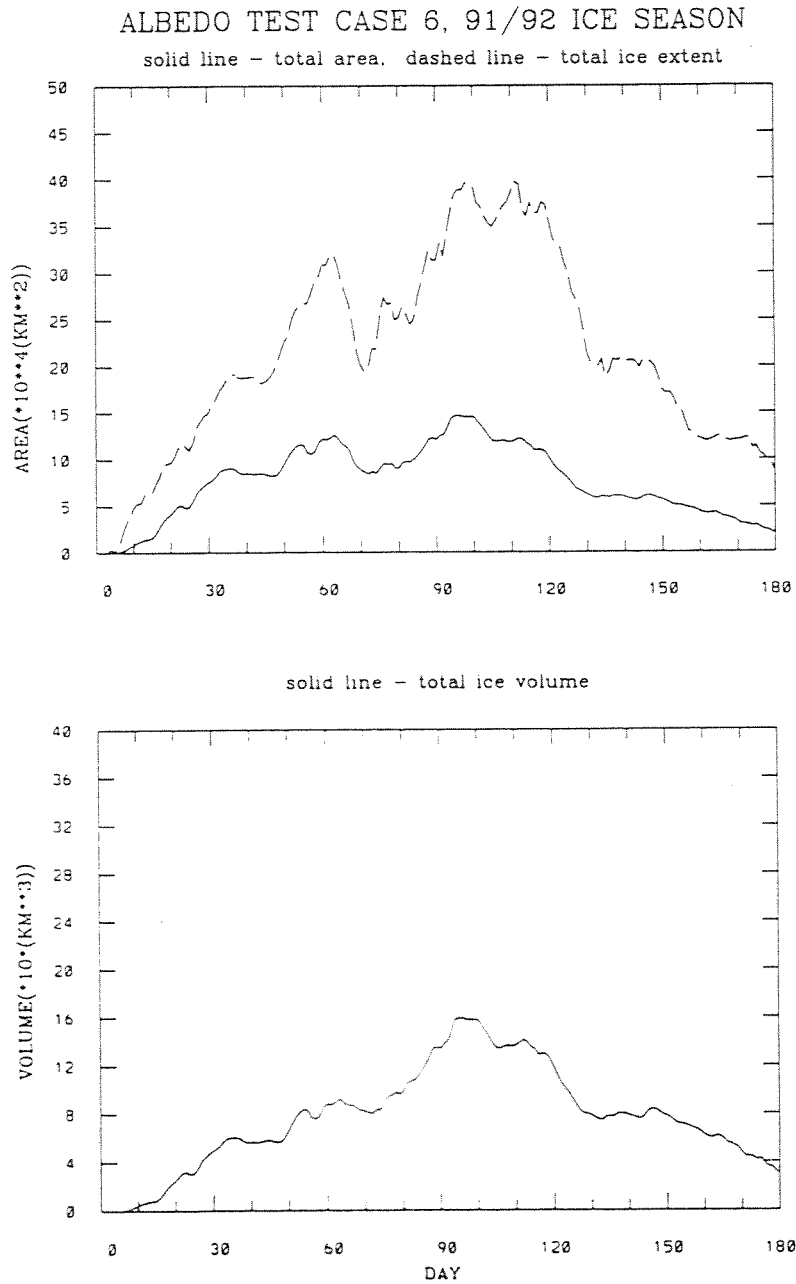


Fig. 2.13 Simulated time series of ice extent, ice area and ice volume of albedo test case 6 for the 1991/92 ice season.

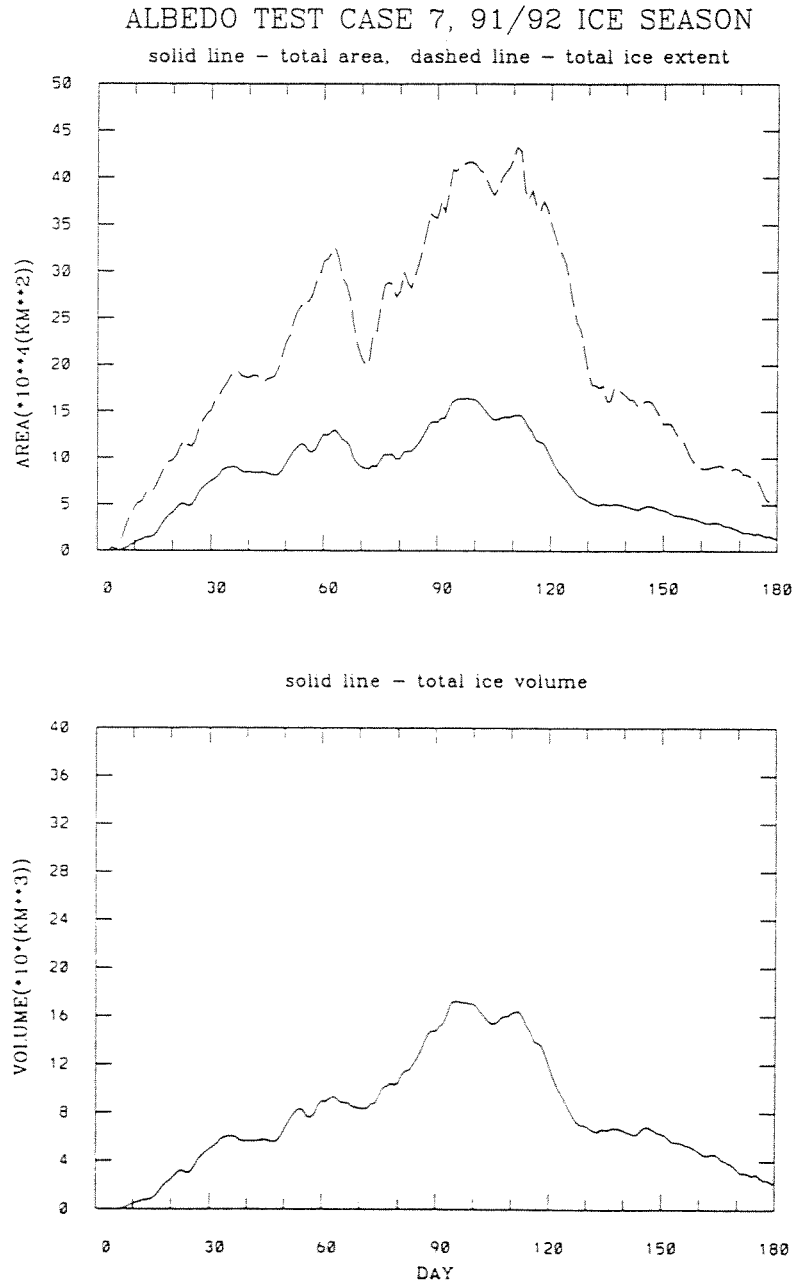
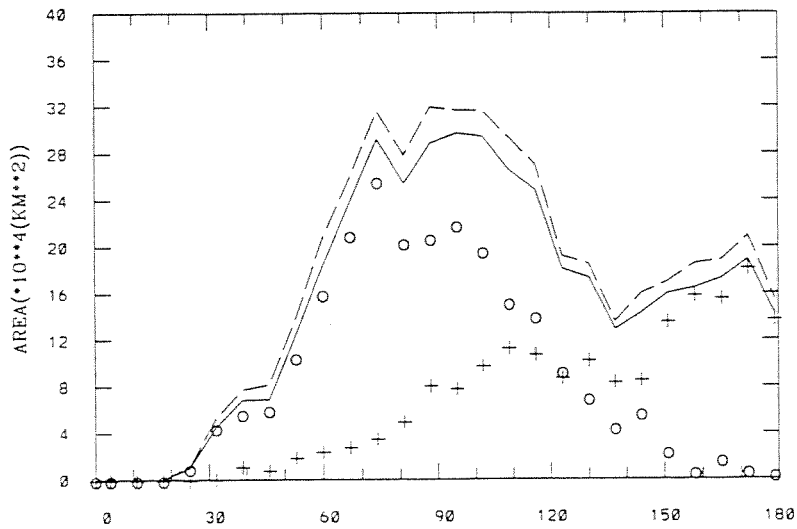


Fig. 2.14 Simulated time series of ice extent, ice area and ice volume of albedo test case 7 for the 1991/92 ice season.

OBSERVED DATA 71/72 ICE SEASON

solid line - total area, dashed line - total ice extent  
 o - thin ice, gw. grey & new, + - thick ice, old & fy



solid line - total ice volume  
 o - thin ice, 0.15M, + - thick ice, 1.25M

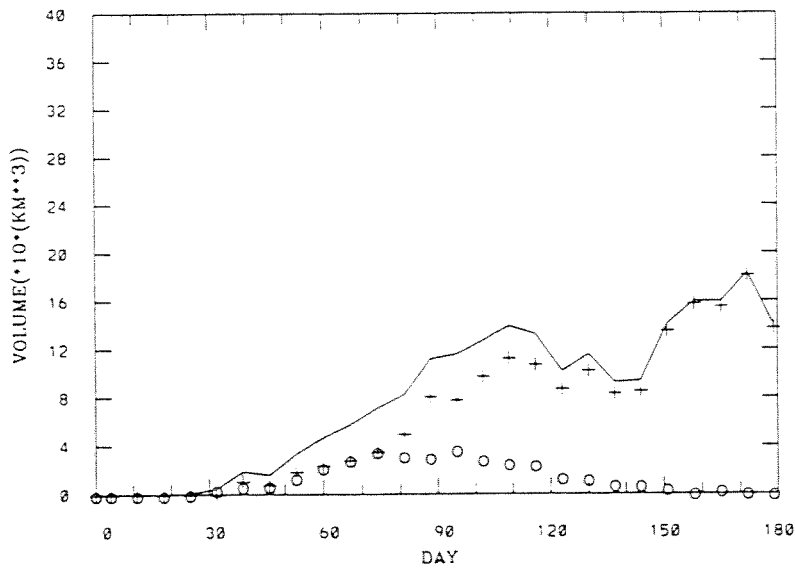


Fig. 2.15 Weekly time series data of ice extent, ice area and ice volume for the 1971/72 ice season for the Labrador and Newfoundland Shelf area.

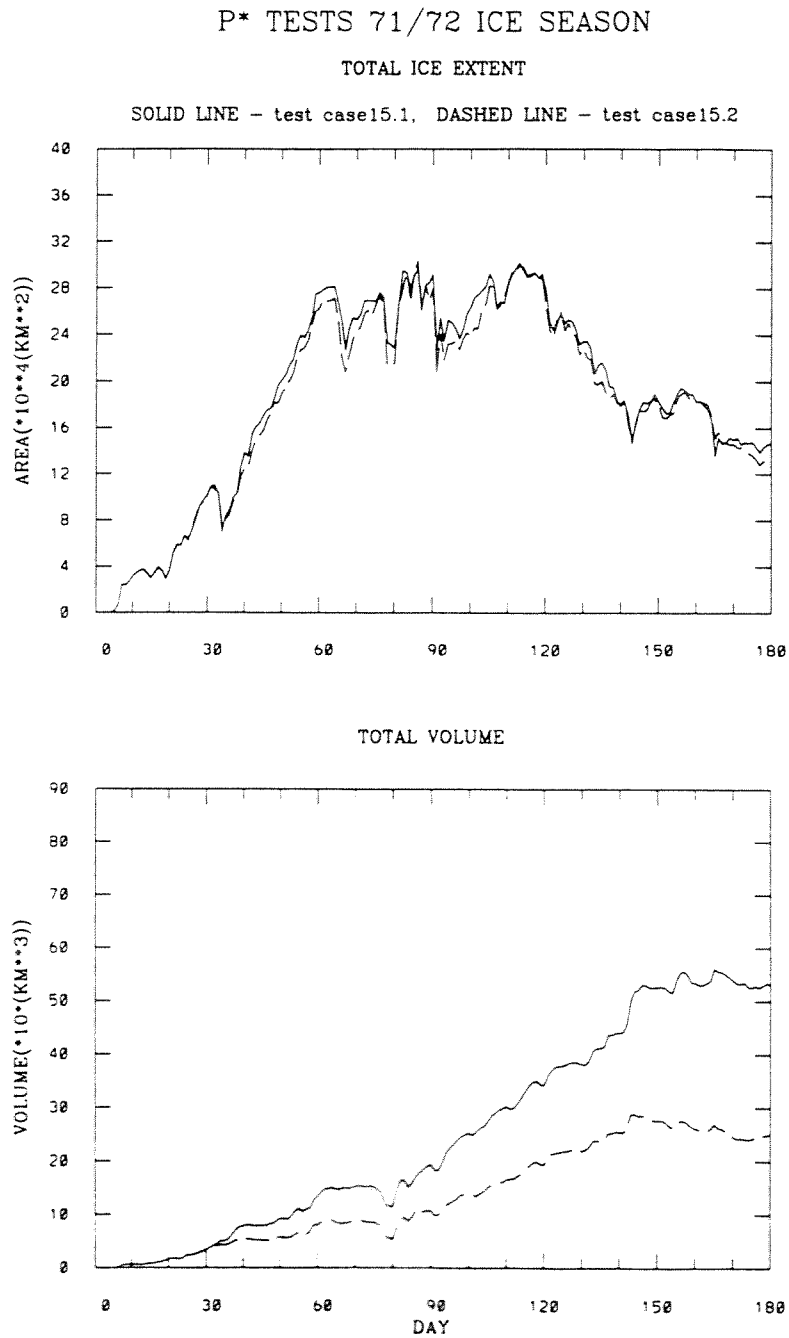


Fig. 2.16 Simulated time series of ice extent, and ice volume of P\* test case 15.1 and 15.2 for the 1971/72 ice season.

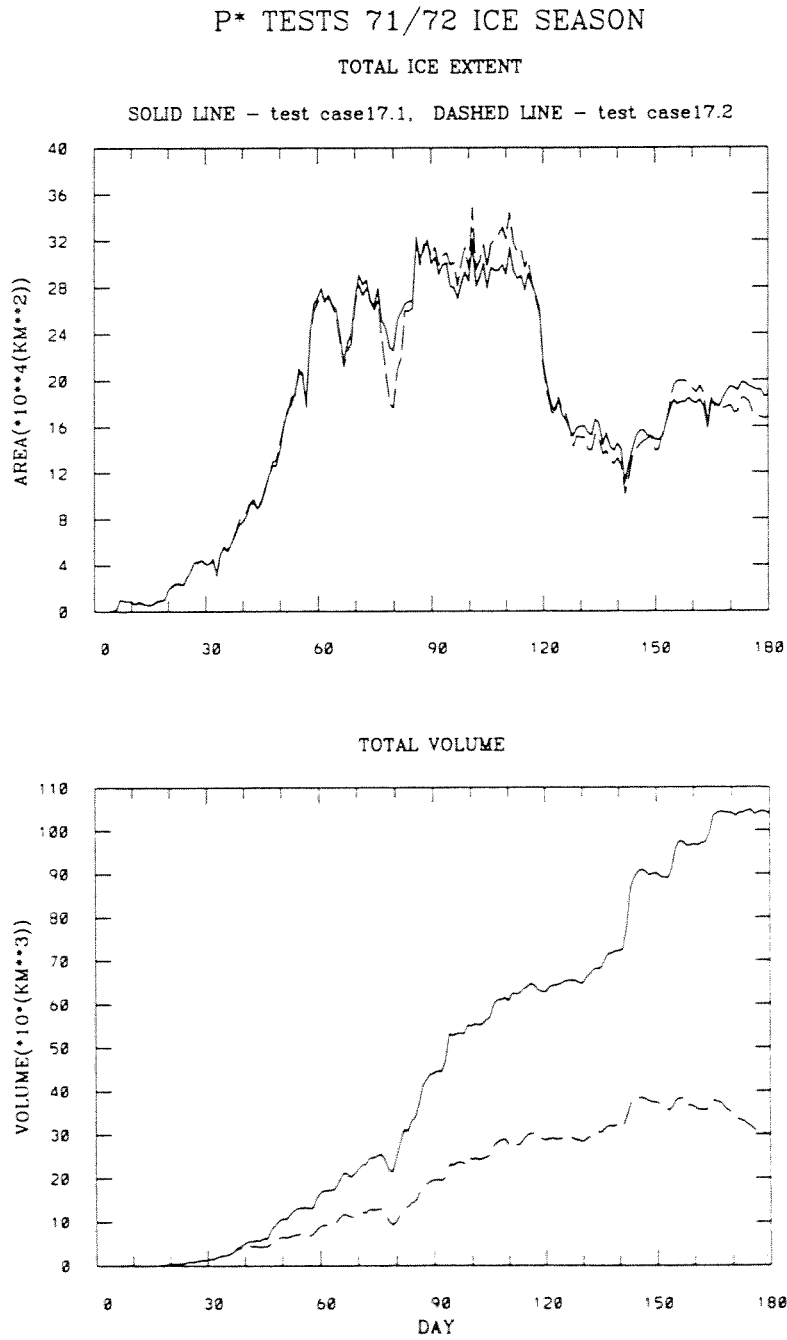
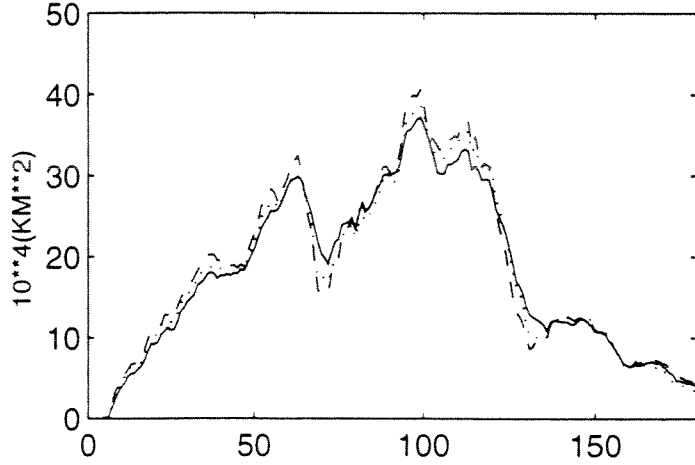
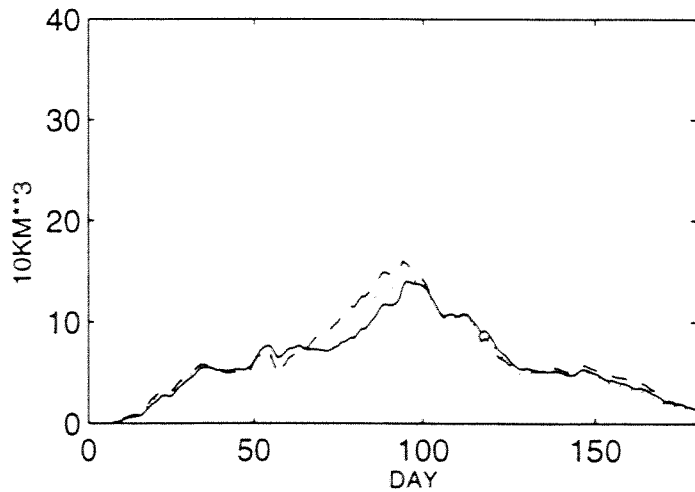


Fig. 2.17 Simulated time series of ice extent, and ice volume of P\* test case 17.1 and 17.2 for the 1971/72 ice season.

91/92, Wind/Air Temp Test, Area of Ice Covered Grids



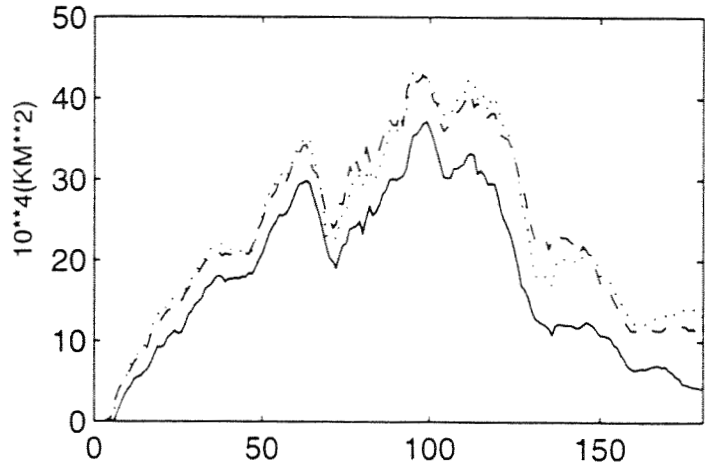
Volume



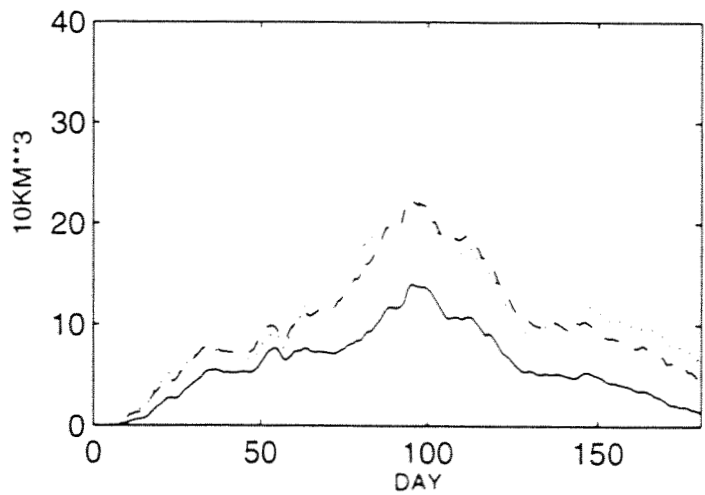
solid line: normal wind and temp  
dashed line: add 20% wind  
dotted line: increased NW winds

Fig. 2.18 Simulated time series of wind and air temperature tests for 2 wind cases compared to basic case of the 1991/92 ice season.

91/92, Wind/Air Temp Test, Area of Ice Covered Grids



Volume



solid line: normal wind and temp  
dashed line: -50% air temp if negative  
dotted line: -50% air temp if negative, and increased NW winds

Fig. 2.19 Simulated time series of wind and air temperature tests for 2 air temperature cases compared to basic case of the 1991/92 ice season.

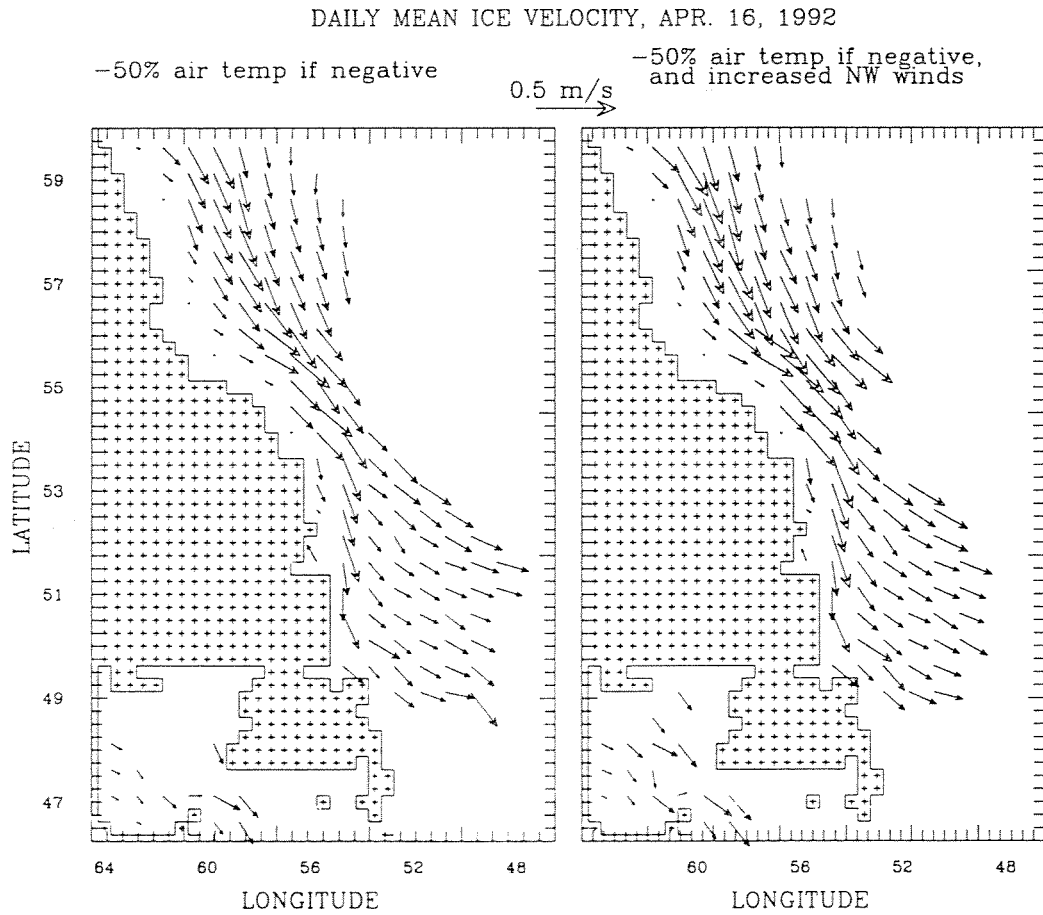


Fig. 2.20 Daily mean ice velocity examples for 2 air temperature cases on Apr 16, 1992.

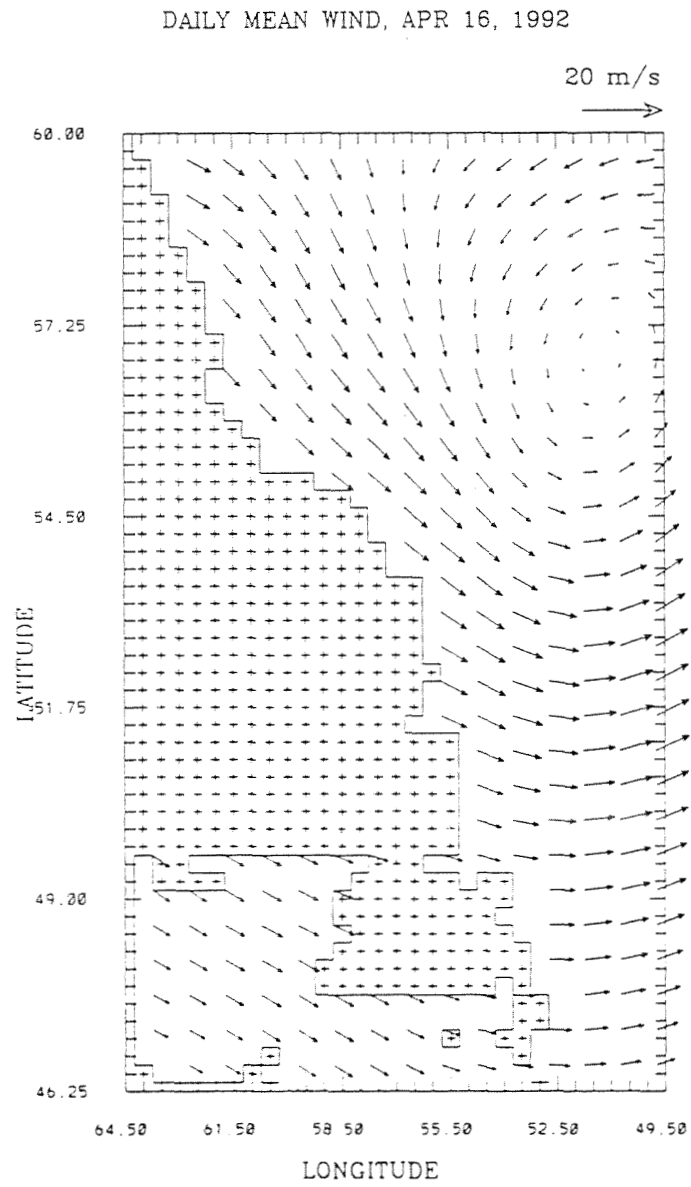


Fig. 2.21 Daily mean wind distribution for Apr 16, 1992.

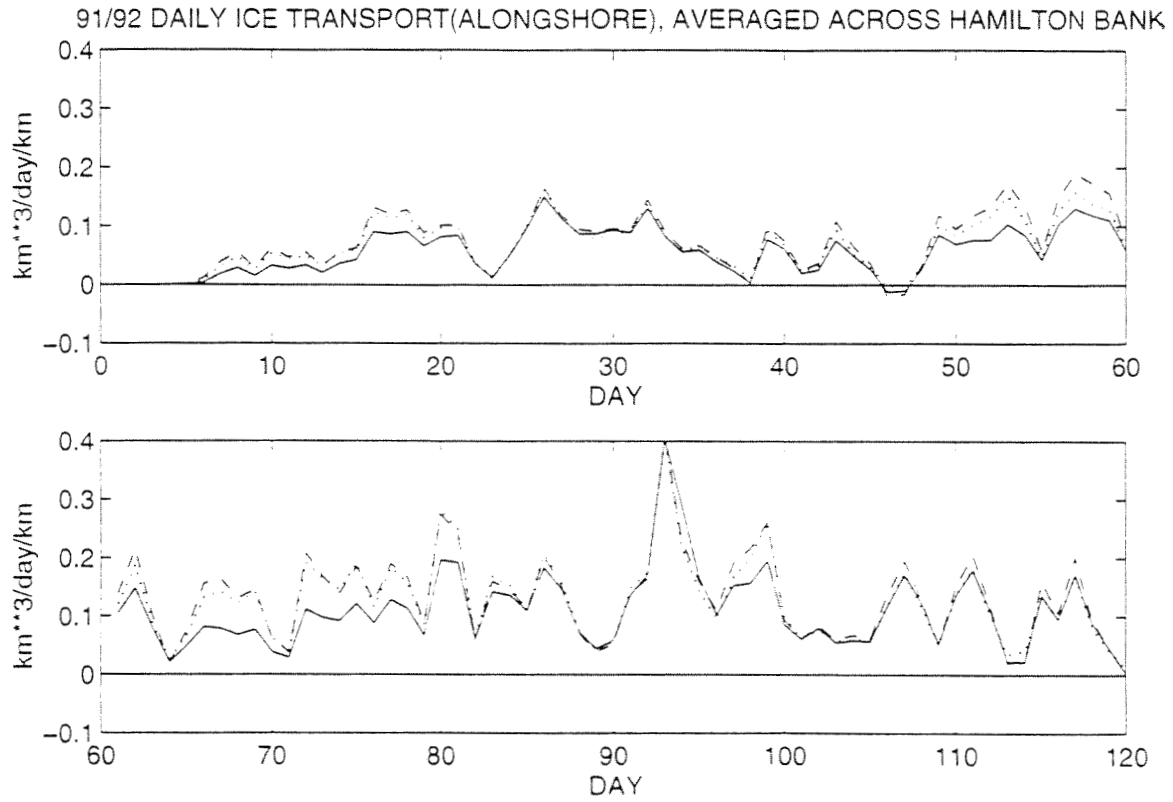


Fig. 2.22a Alongshore components of daily ice transport averaged across Hamilton Bank for wind and basic cases between Dec. 1 1991 to Mar. 29, 1992.

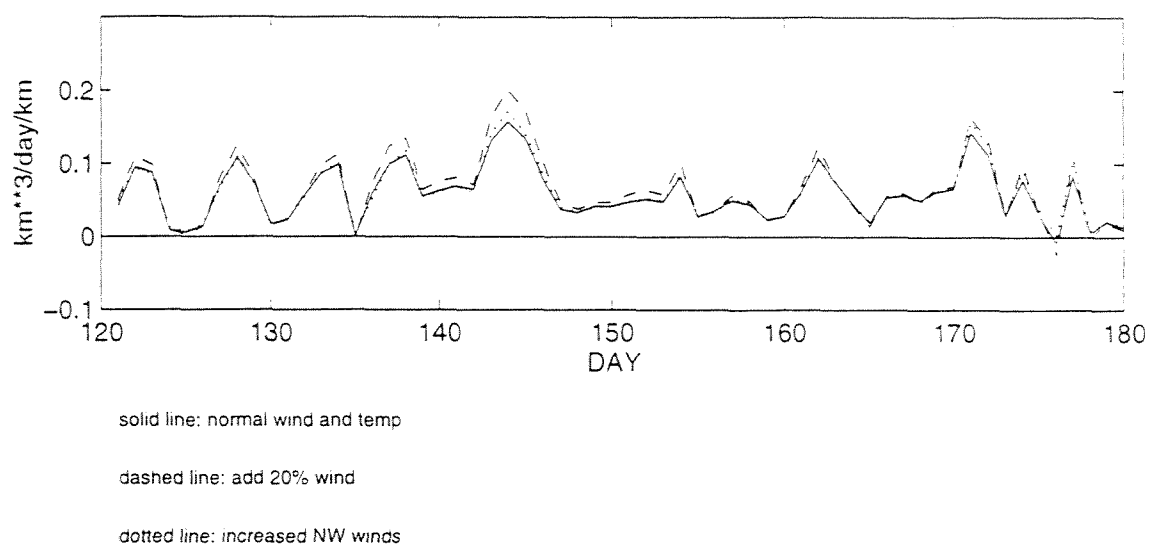


Fig. 2.22b Alongshore component of daily ice transport averaged across Hamilton Bank for wind and basic cases between Mar 30, 1992 to May 28.

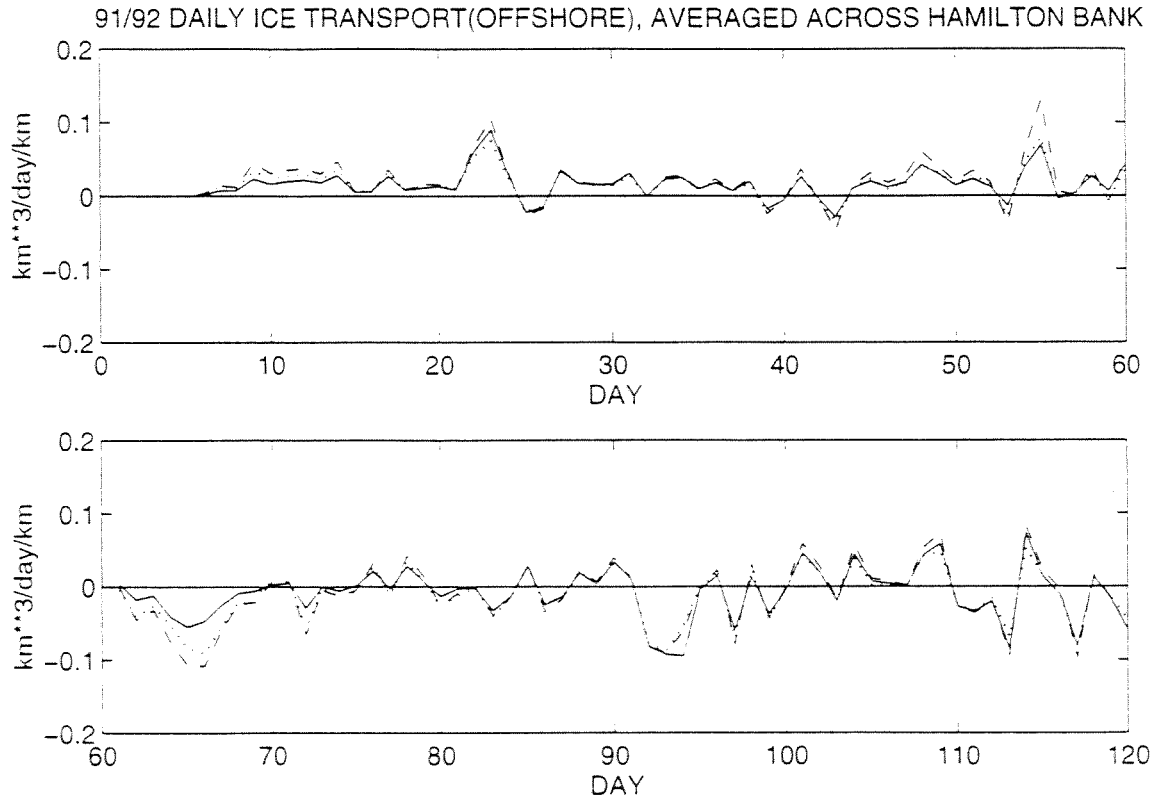


Fig. 2.23a Offshore components of daily ice transport averaged across Hamilton Bank for wind and basic cases between Dec. 1 1991 to Mar. 29, 1992.

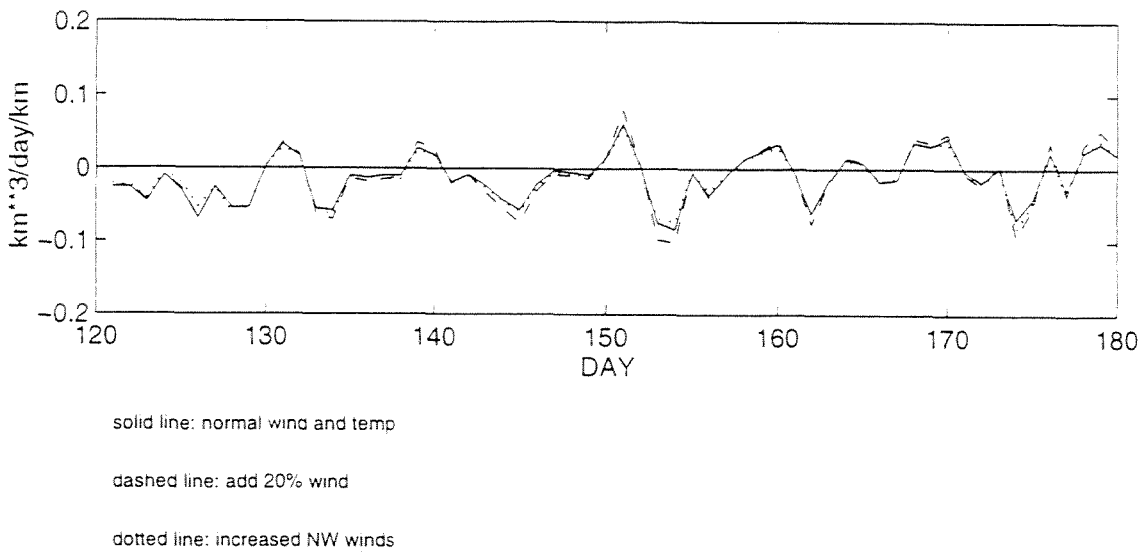


Fig. 2.23b Offshore component of daily ice transport averaged across Hamilton Bank for wind and basic cases between Mar 30, 1992 to May 28.

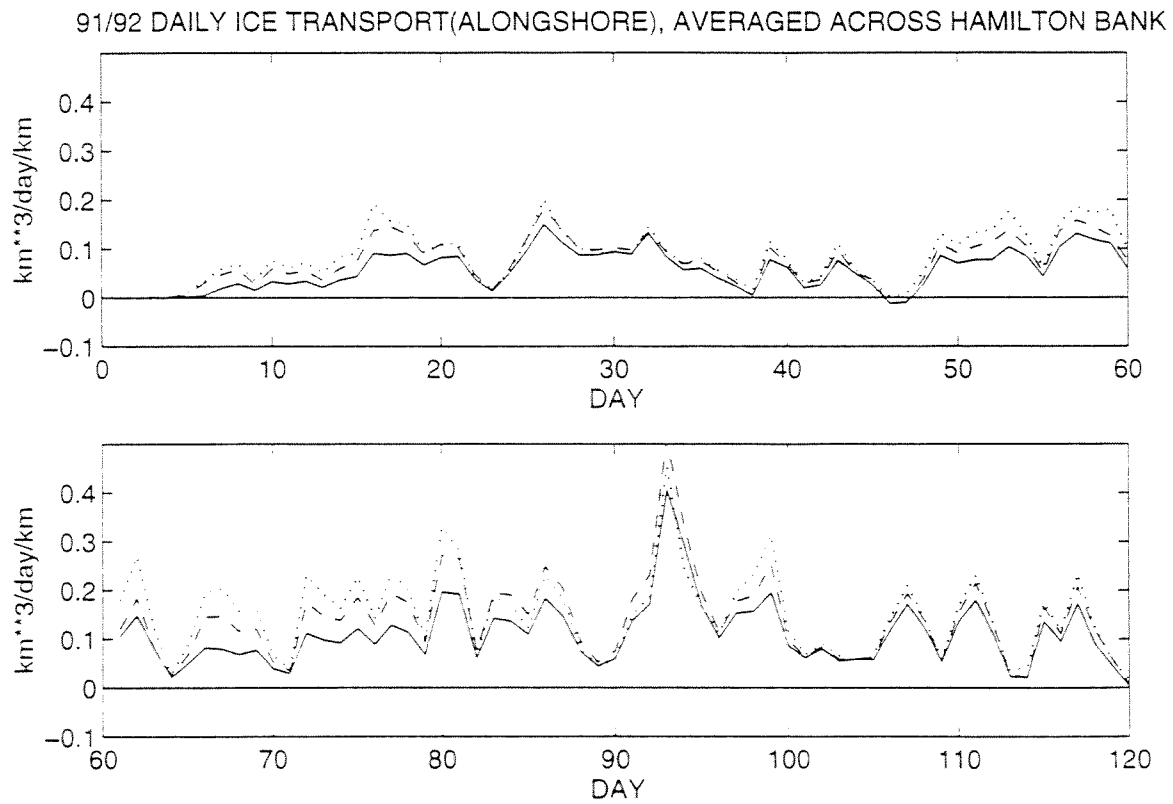


Fig. 2.24a Alongshore components of daily ice transport averaged across Hamilton Bank for air temperature and basic cases between Dec. 1 1991 to Mar. 29, 1992.

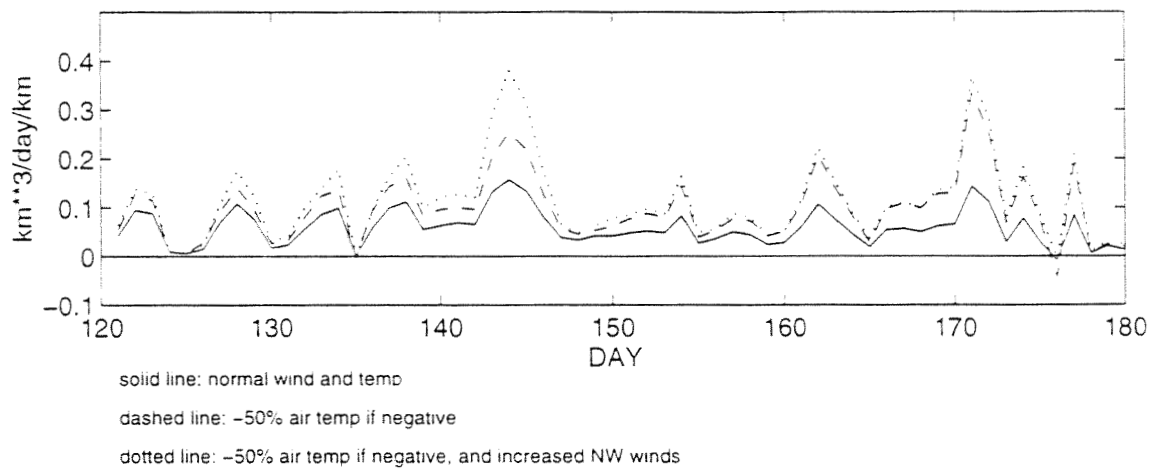


Fig. 2.24b Alongshore component of daily ice transport averaged across Hamilton Bank for air temperature and basic cases between Mar 30, 1992 to May 28.

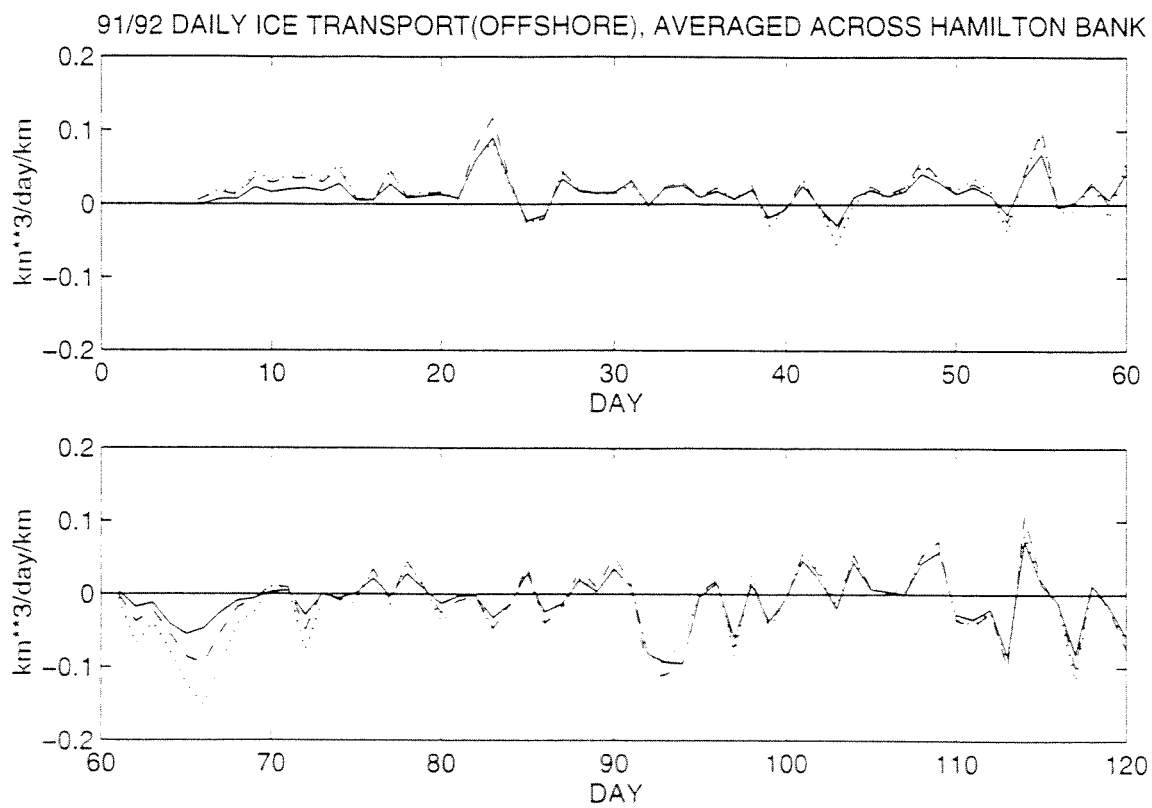


Fig. 2.25a Offshore components of daily ice transport averaged across Hamilton Bank for air temperature and basic cases between Dec. 1 1991 to Mar. 29, 1992.

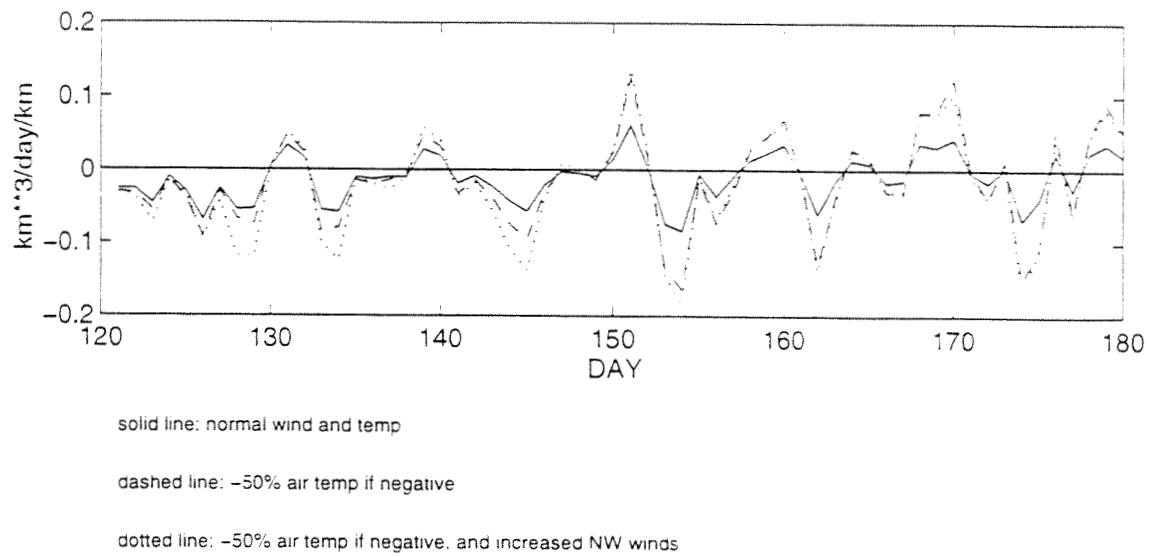


Fig. 2.25b Offshore component of daily ice transport averaged across Hamilton Bank for air temperature and basic cases between Mar 30, 1992 to May 28.

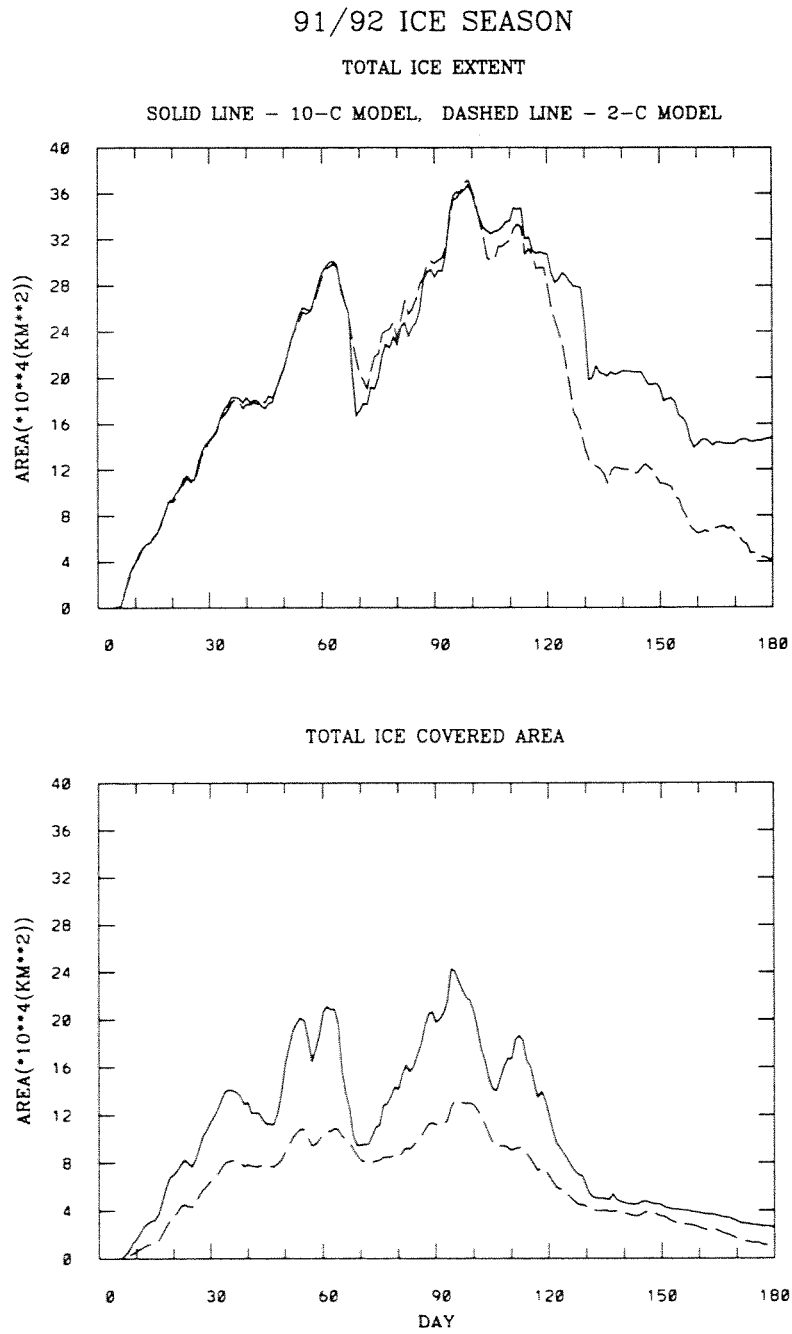


Fig. 2.26 Comparison of 2- and 10-category ice models for 1991/92 ice season.

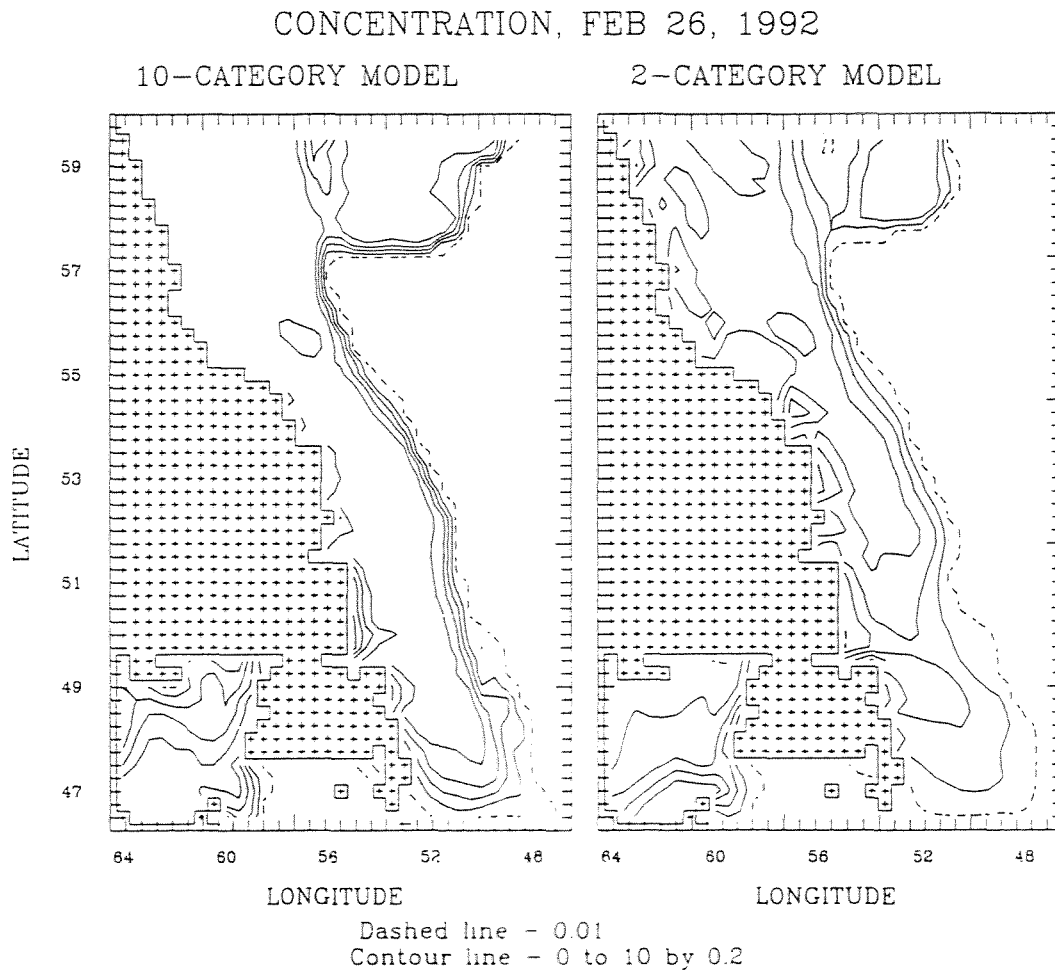


Fig. 2.27 Comparison of ice concentration by 2- and 10-category ice models for Feb. 26, 1992.

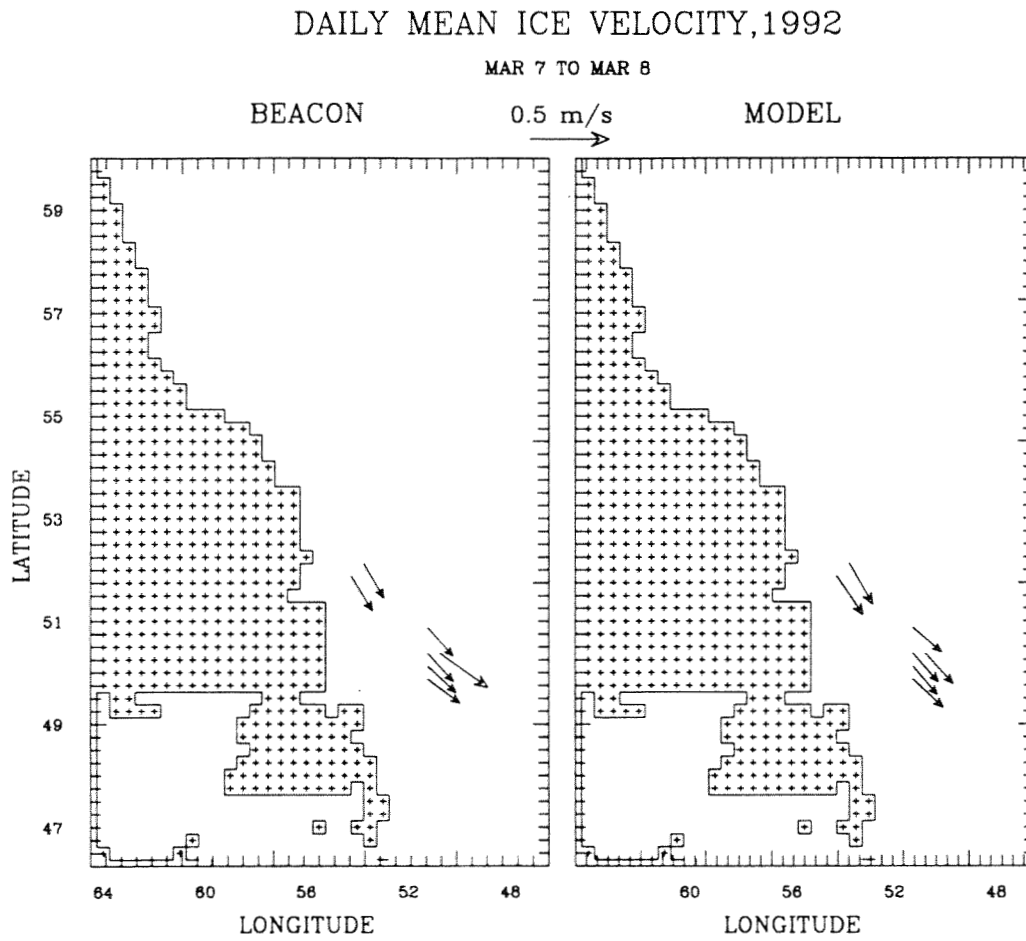


Fig. 3.1 Comparison of daily mean ice velocities of beacon data and model simulations for Mar. 8, 1992.

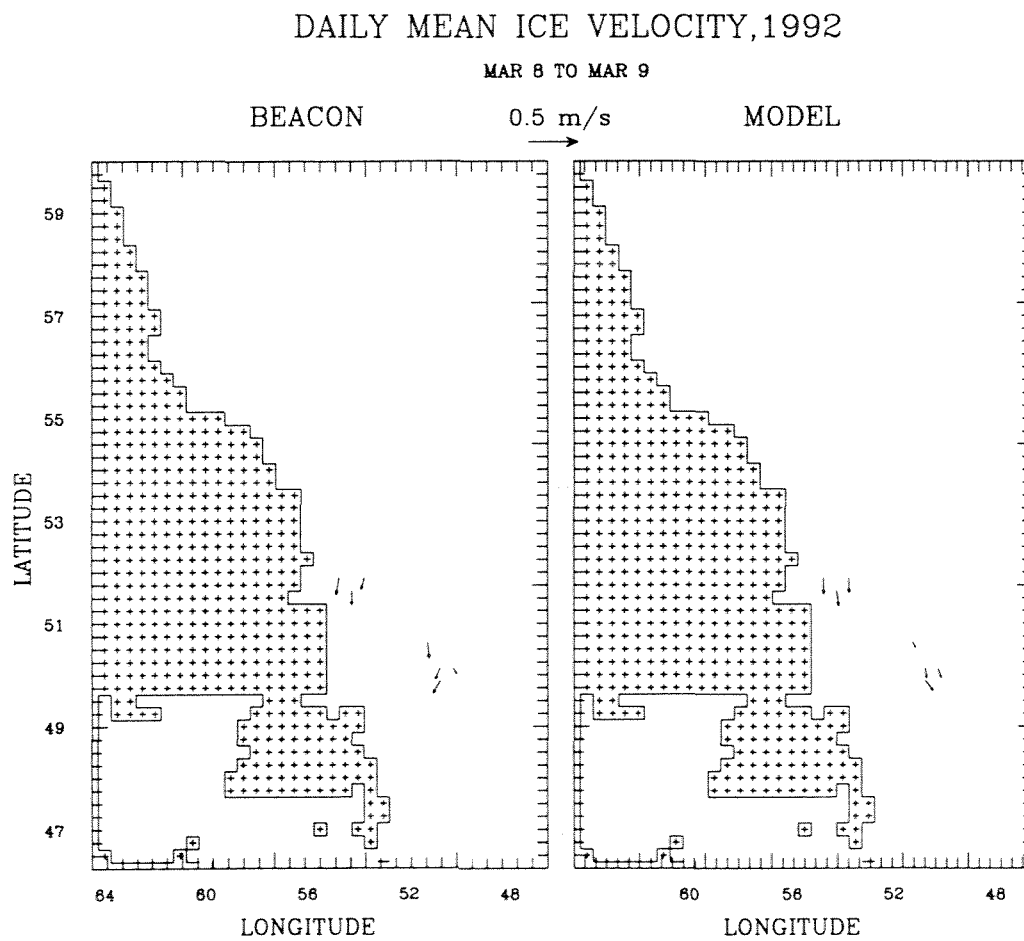


Fig. 3.2 Comparison of daily mean ice velocities of beacon data and model simulations for Mar. 9, 1992.

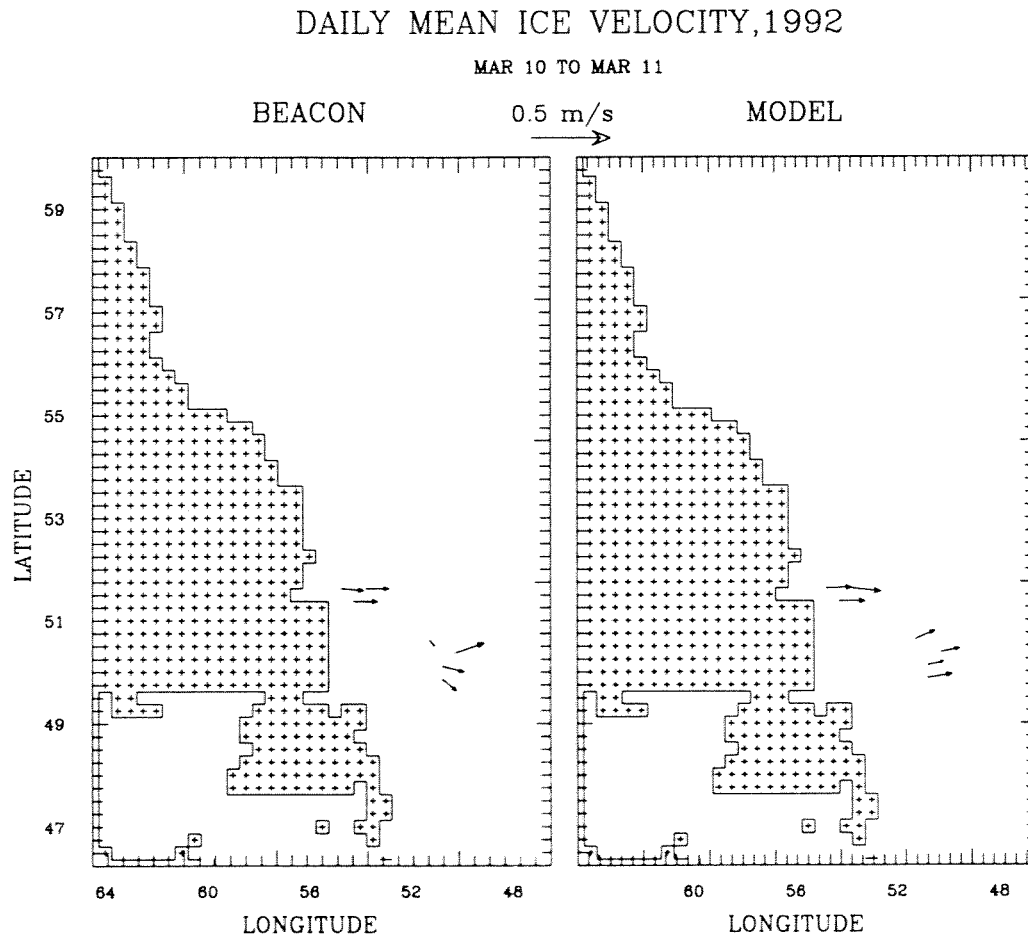


Fig. 3.3 Comparison of daily mean ice velocities of beacon data and model simulations for Mar. 11, 1992.

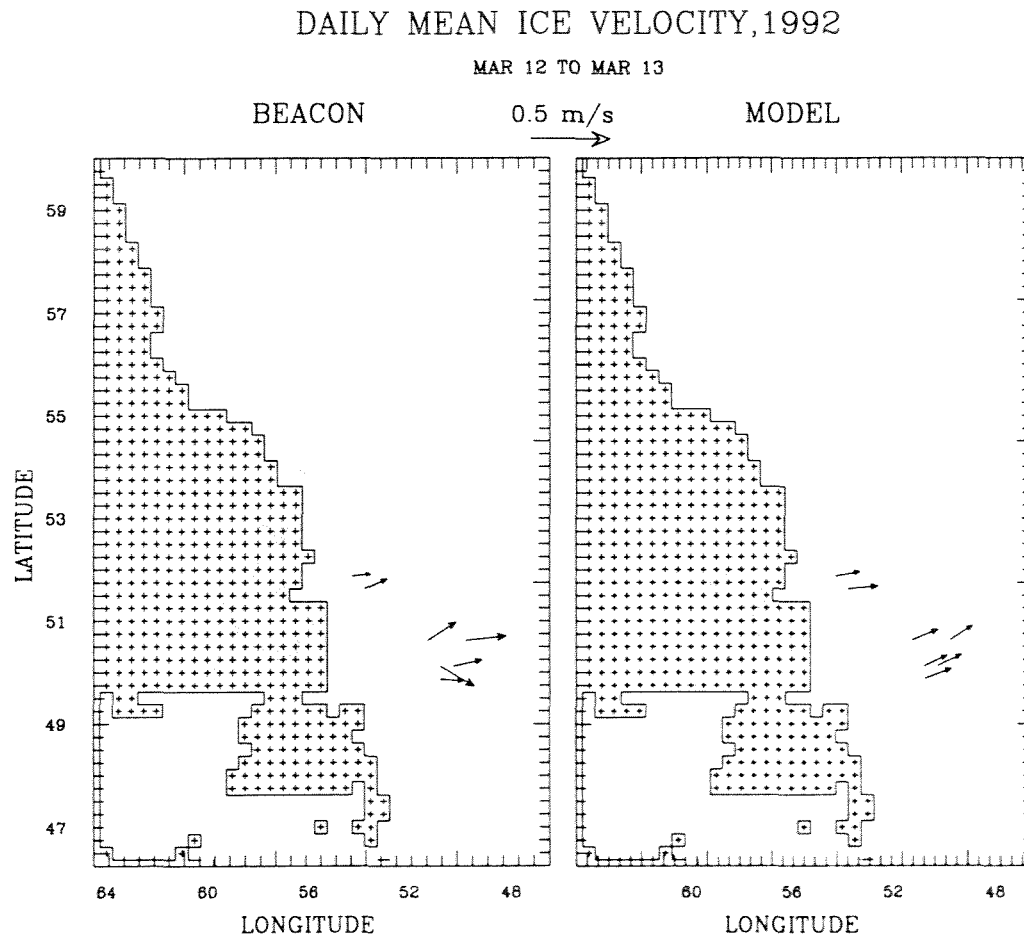


Fig. 3.4 Comparison of daily mean ice velocities of beacon data and model simulations for Mar. 13, 1992.

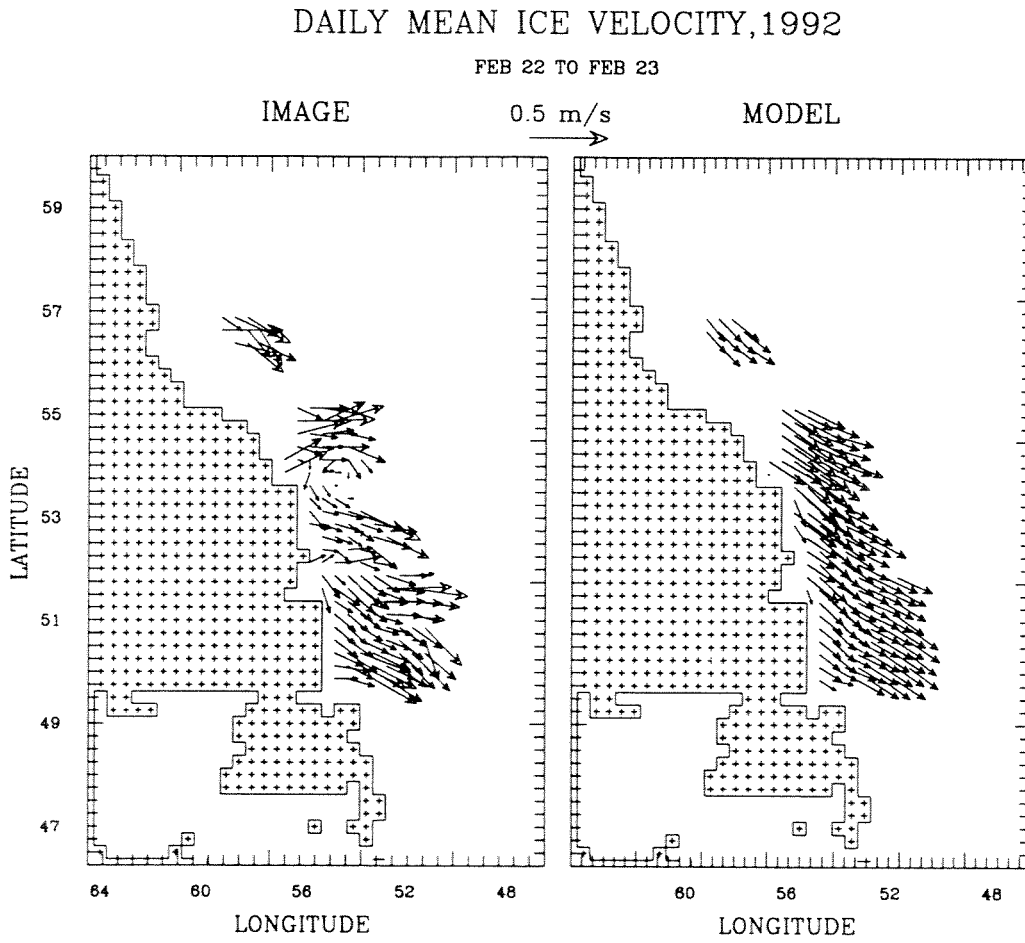


Fig. 3.5 Comparison of daily mean ice velocities of image data and model simulations for Feb. 23, 1992.





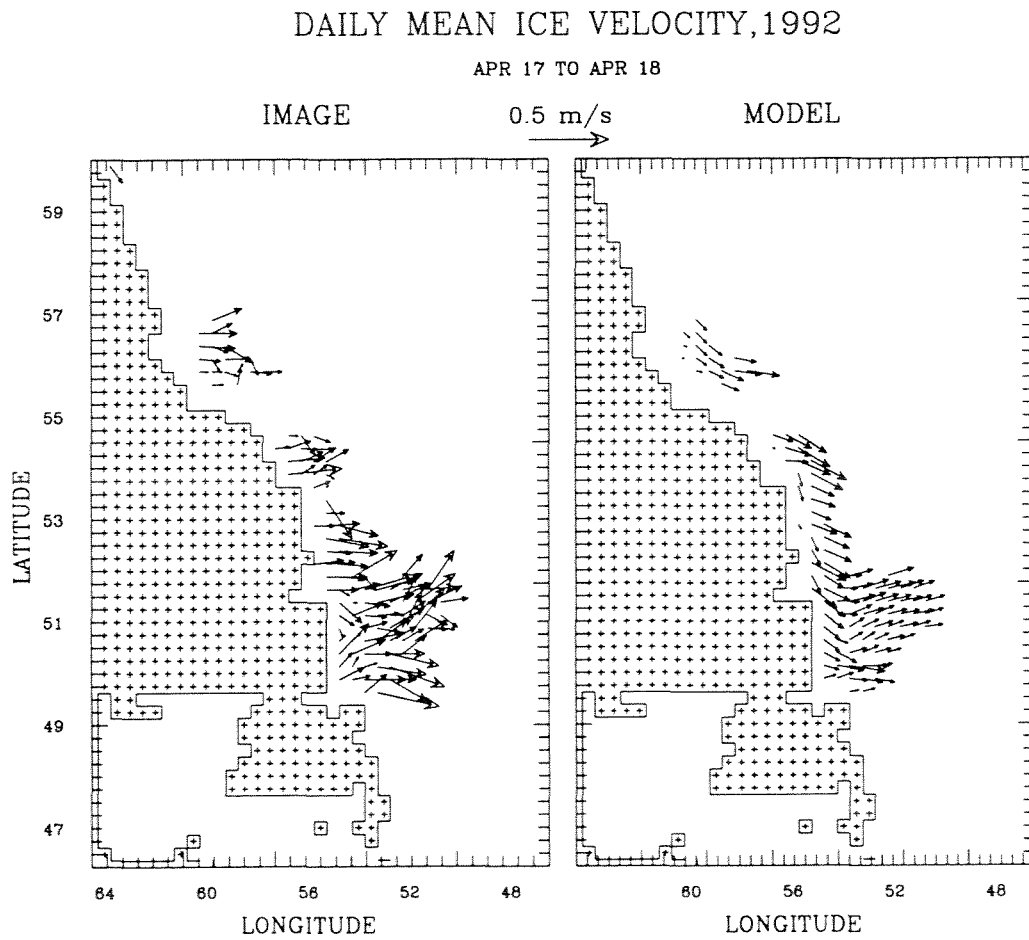


Fig. 3.8 Comparison of daily mean ice velocities of image data and model simulations for Apr. 18, 1992.

SCATTER PLOT OF ICE VELOCITY, FEB., 1992, 64 SAMPLES

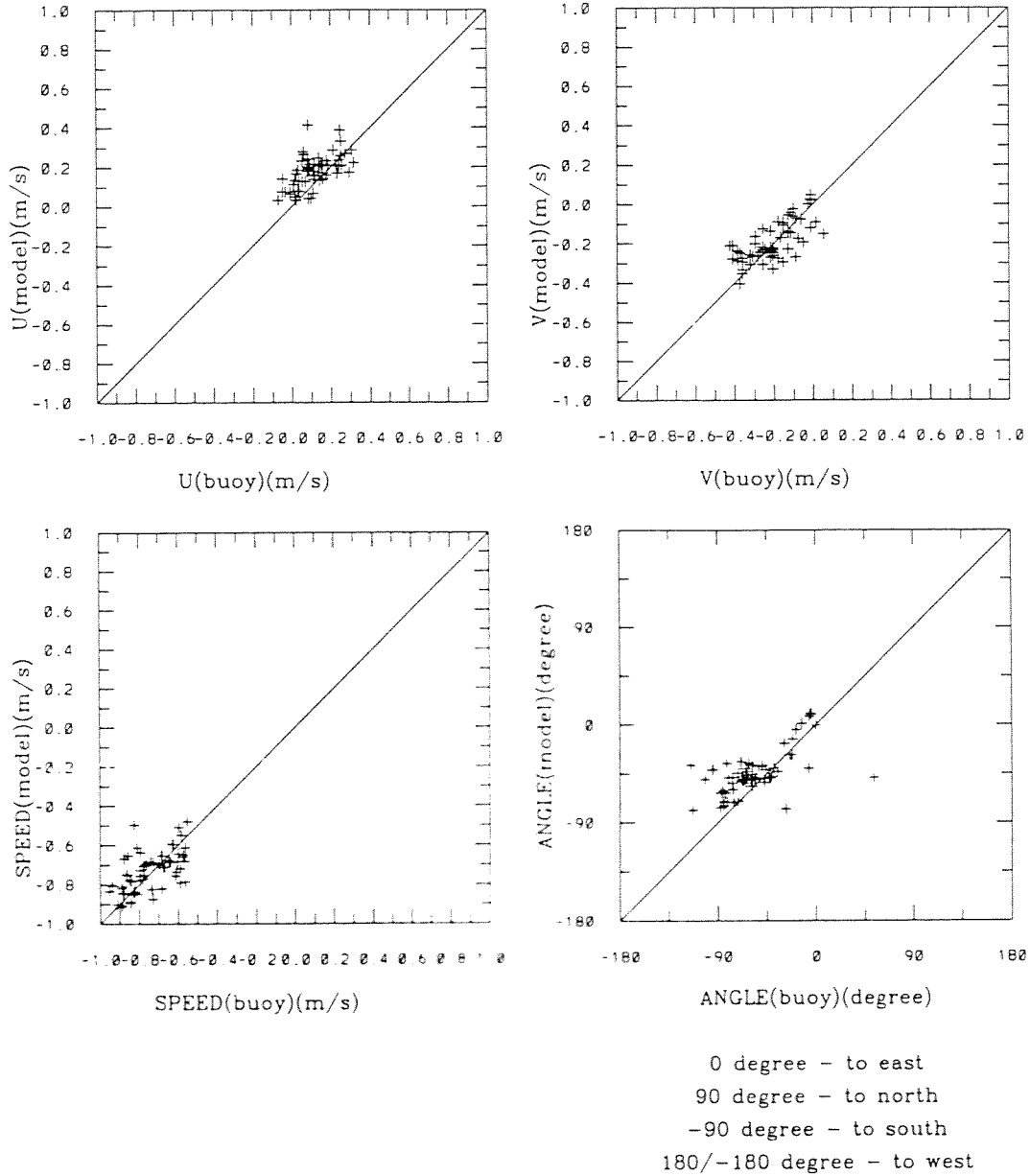


Fig. 3.9a Ice velocity scatter plot of beacon data and model simulations for Feb., 1992.

SCATTER PLOT OF ICE VELOCITY, FEB., 1992, 140 SAMPLES

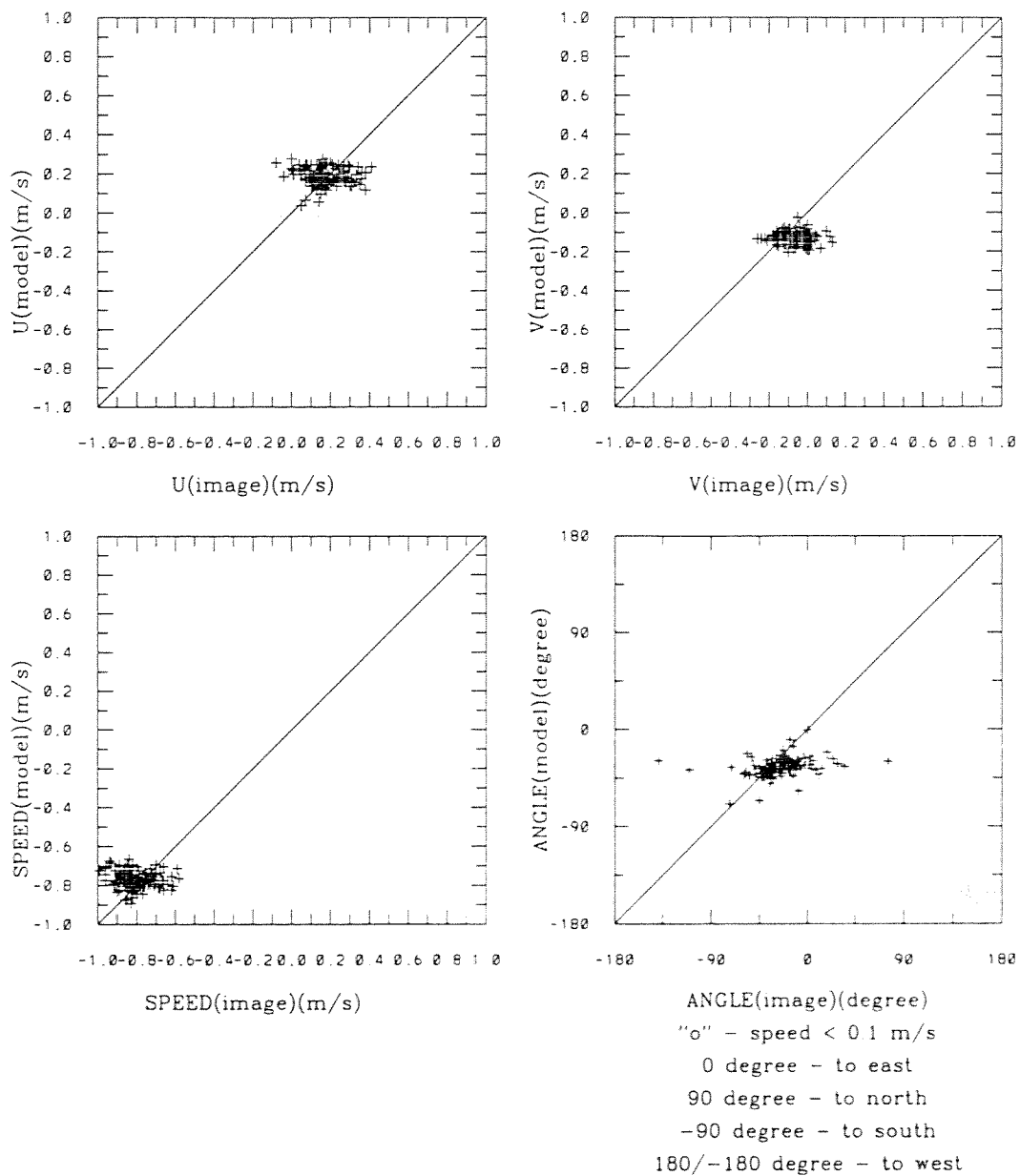


Fig. 3.9b Ice velocity scatter plot of image data and model simulations for Feb., 1992.

SCATTER PLOT OF ICE VELOCITY, MAR., 1992, 149 SAMPLES

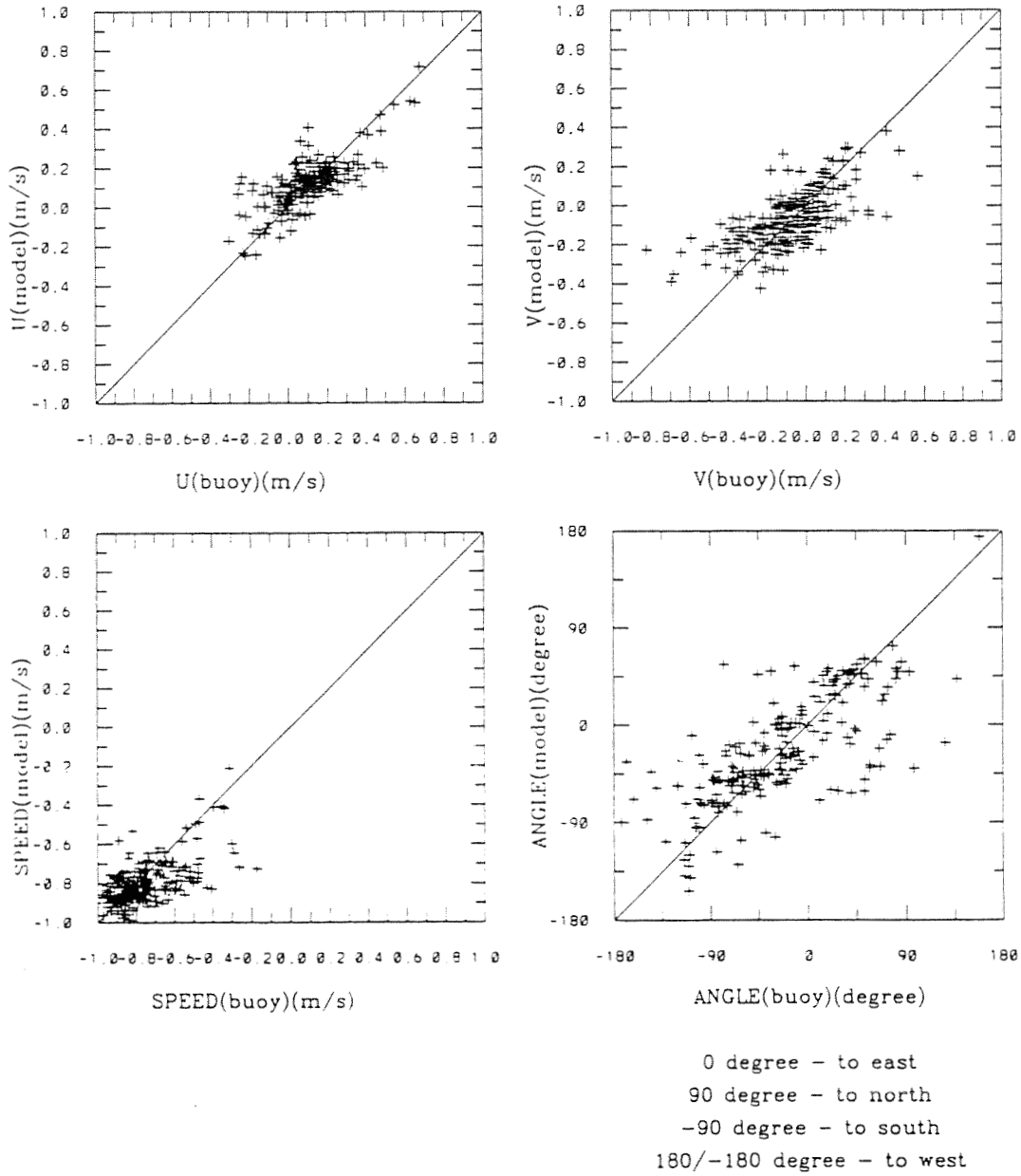


Fig. 3.10a Ice velocity scatter plot of beacon data and model simulations for Mar., 1992.

SCATTER PLOT OF ICE VELOCITY, MAR., 1992, 148 SAMPLES

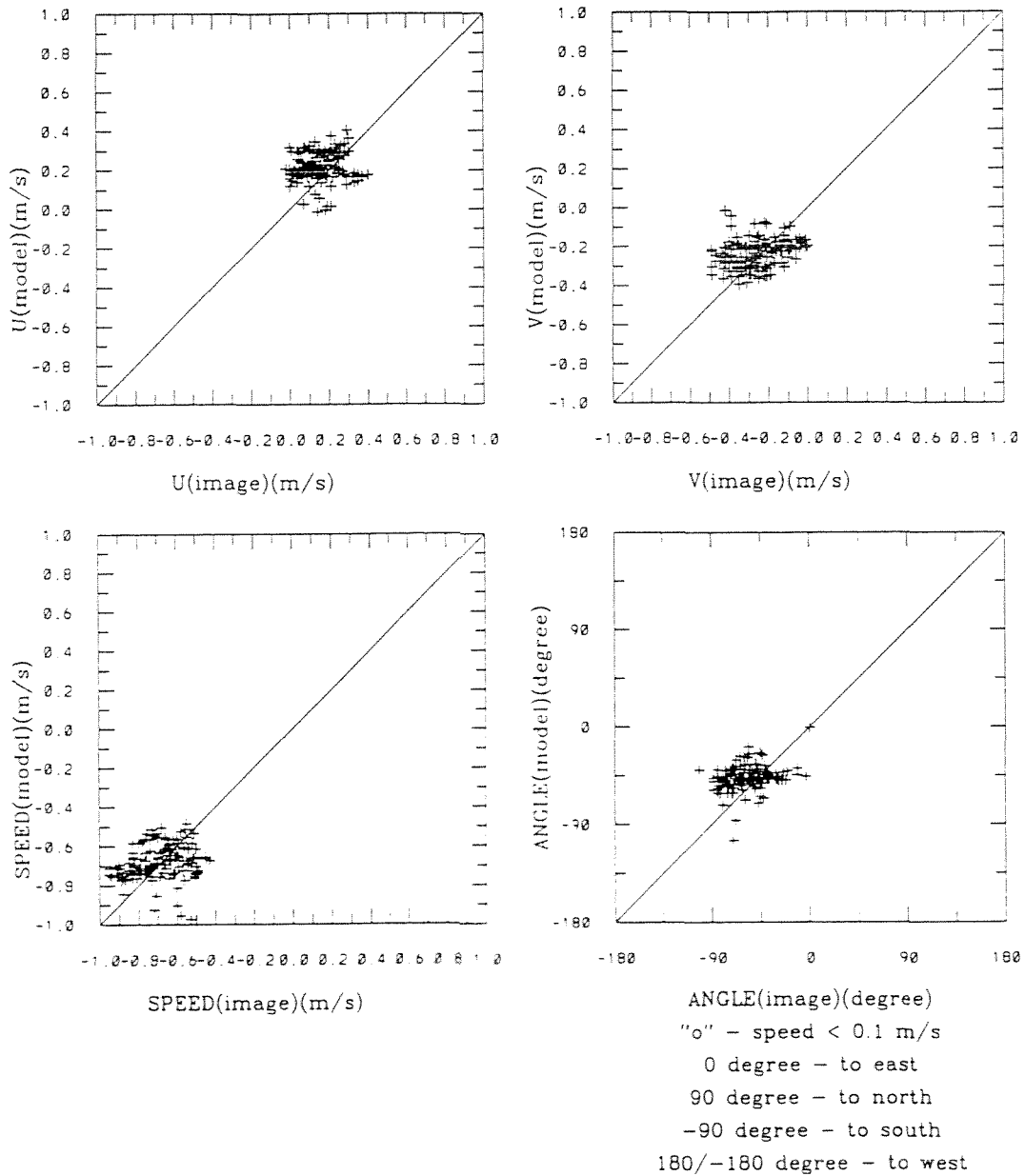


Fig. 3.10b Ice velocity scatter plot of image data and model simulations for Mar., 1992.

SCATTER PLOT OF ICE VELOCITY, APR., 1992, 165 SAMPLES

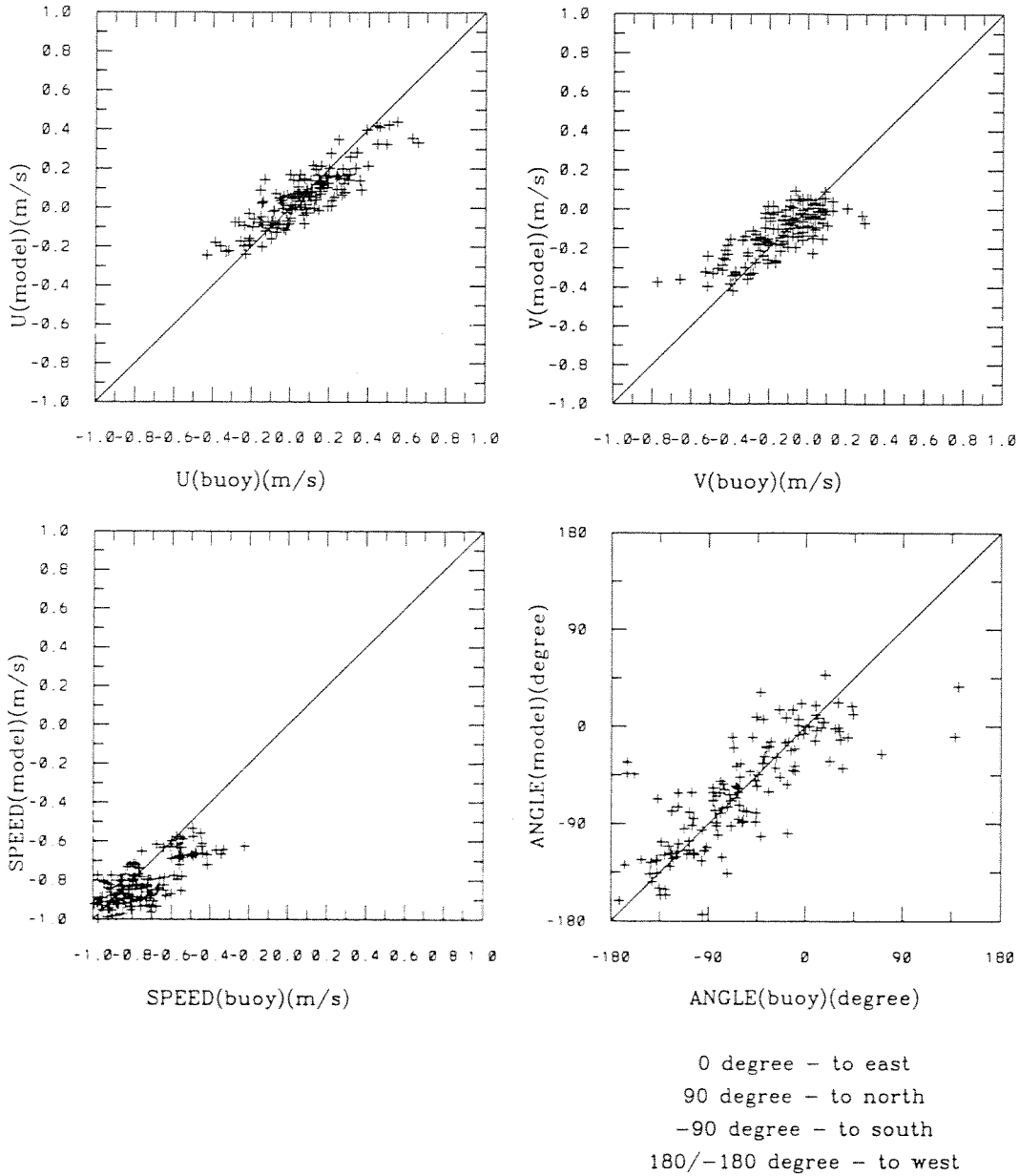


Fig. 3.1 la Ice velocity scatter plot of beacon data and model simulations for Apr. 1992.

SCATTER PLOT OF ICE VELOCITY, APR., 1992, 334 SAMPLES

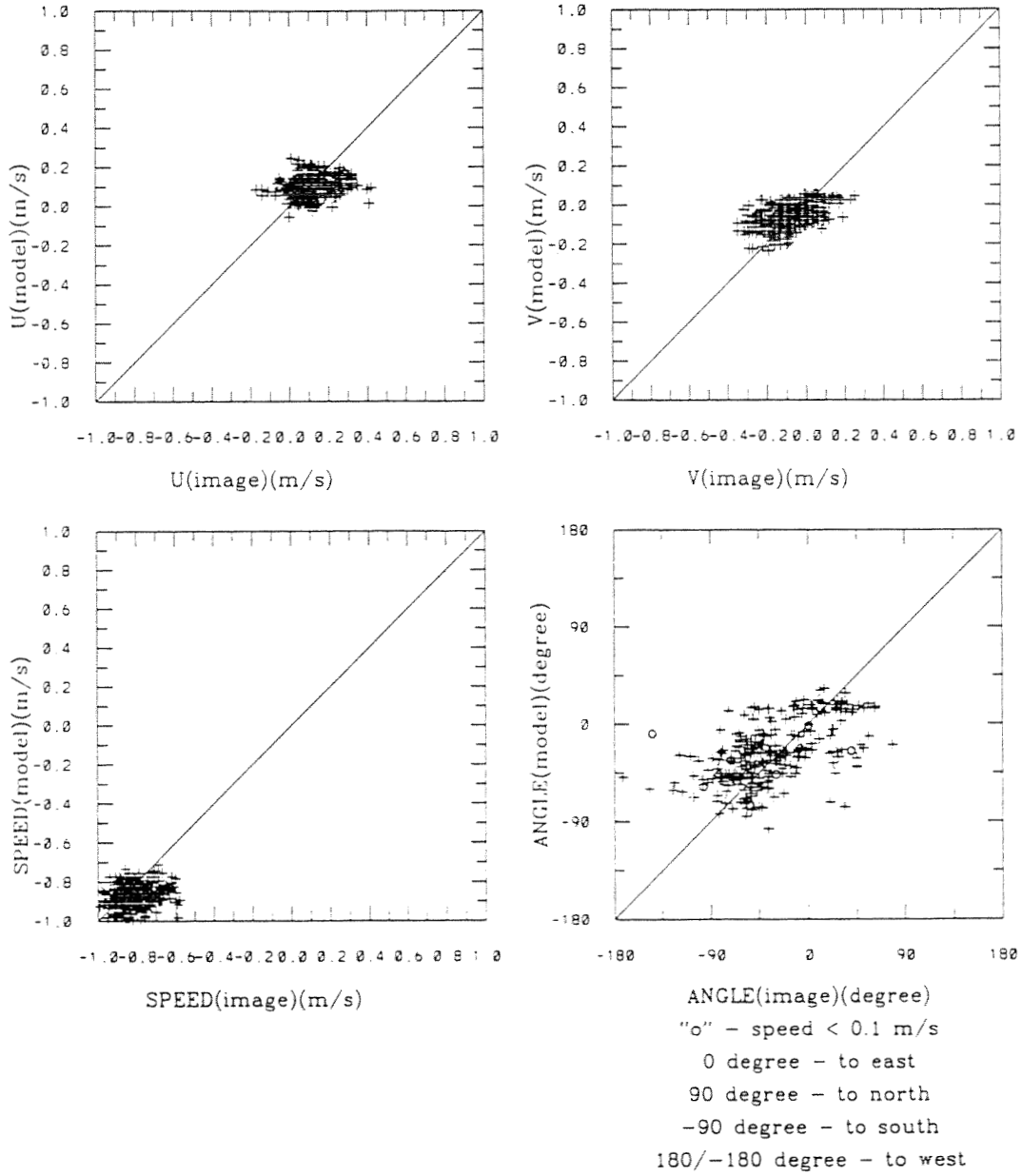


Fig. 3.11b Ice velocity scatter plot of image data and model simulations for Apr. 1992.

SCATTER PLOT OF ICE VELOCITY  
 FEB 22 TO MAY 22, 1994, 170 SAMPLES

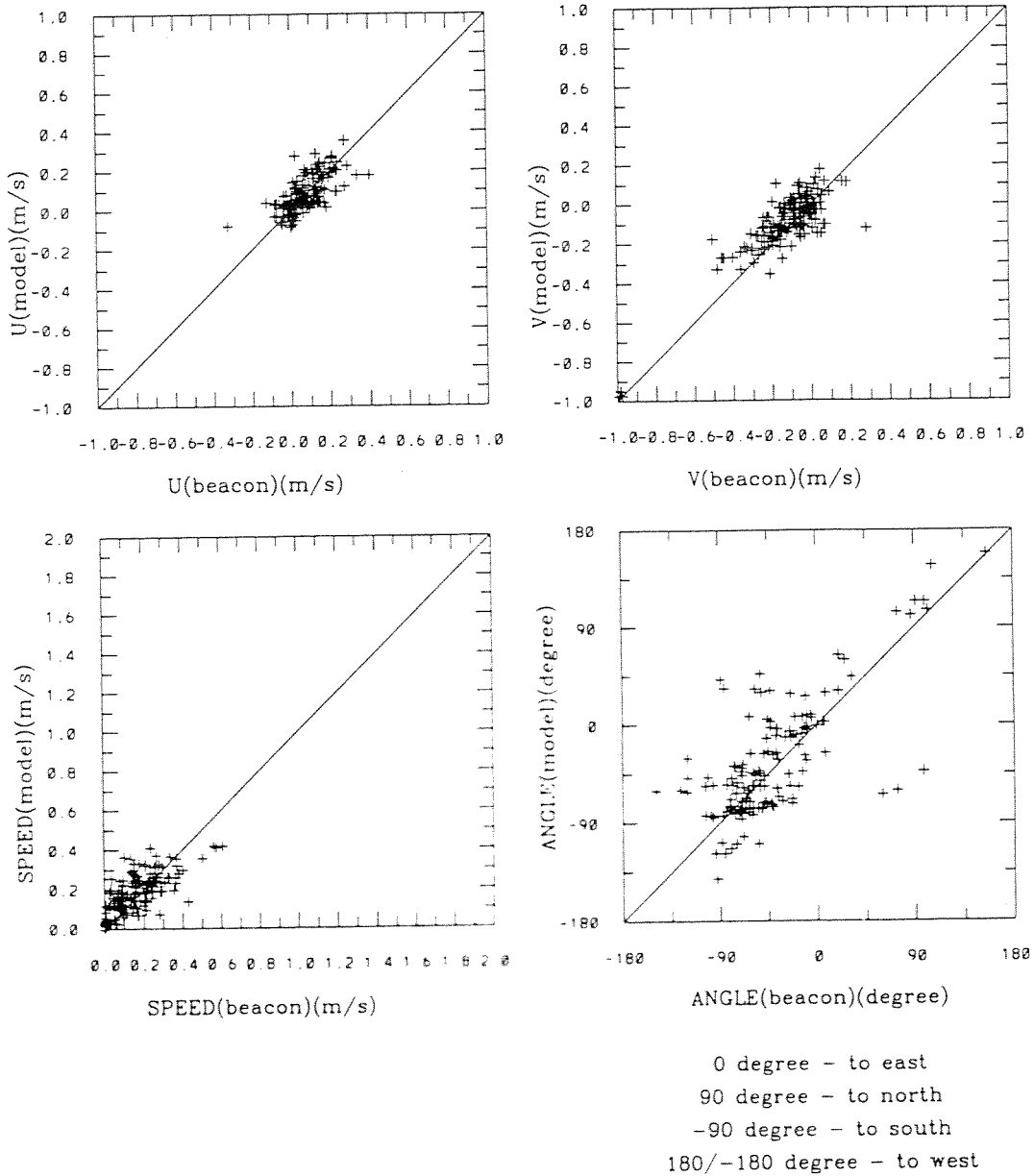


Fig. 3.12 Ice velocity scatter plot of beacon data and model simulations for Feb. 22 to May 22, 1994.

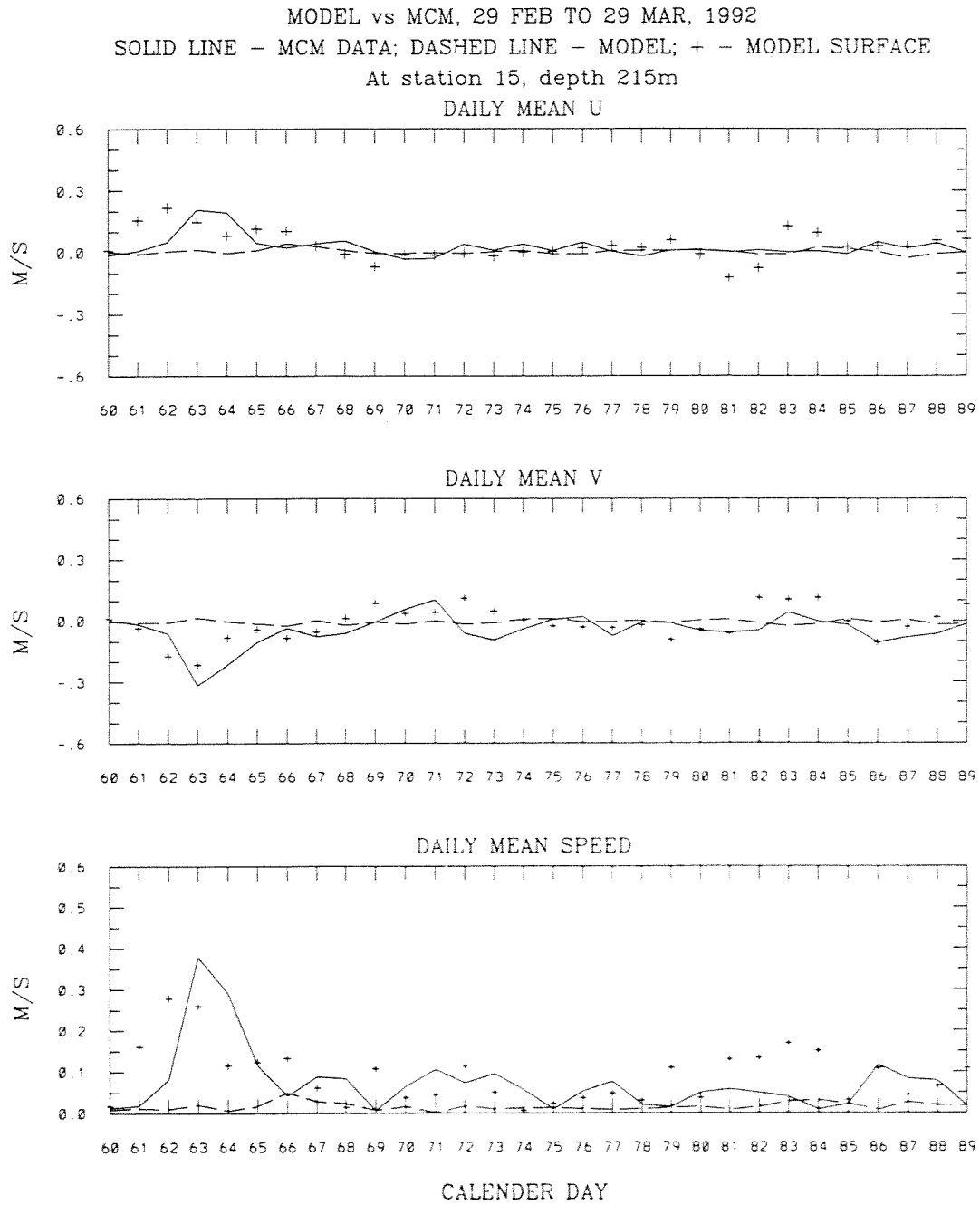


Fig. 3.13a Comparison of daily mean ocean velocities and speeds of MCM data and model simulations at Station 15 for Feb. 29 to Mar. 29, 1992.

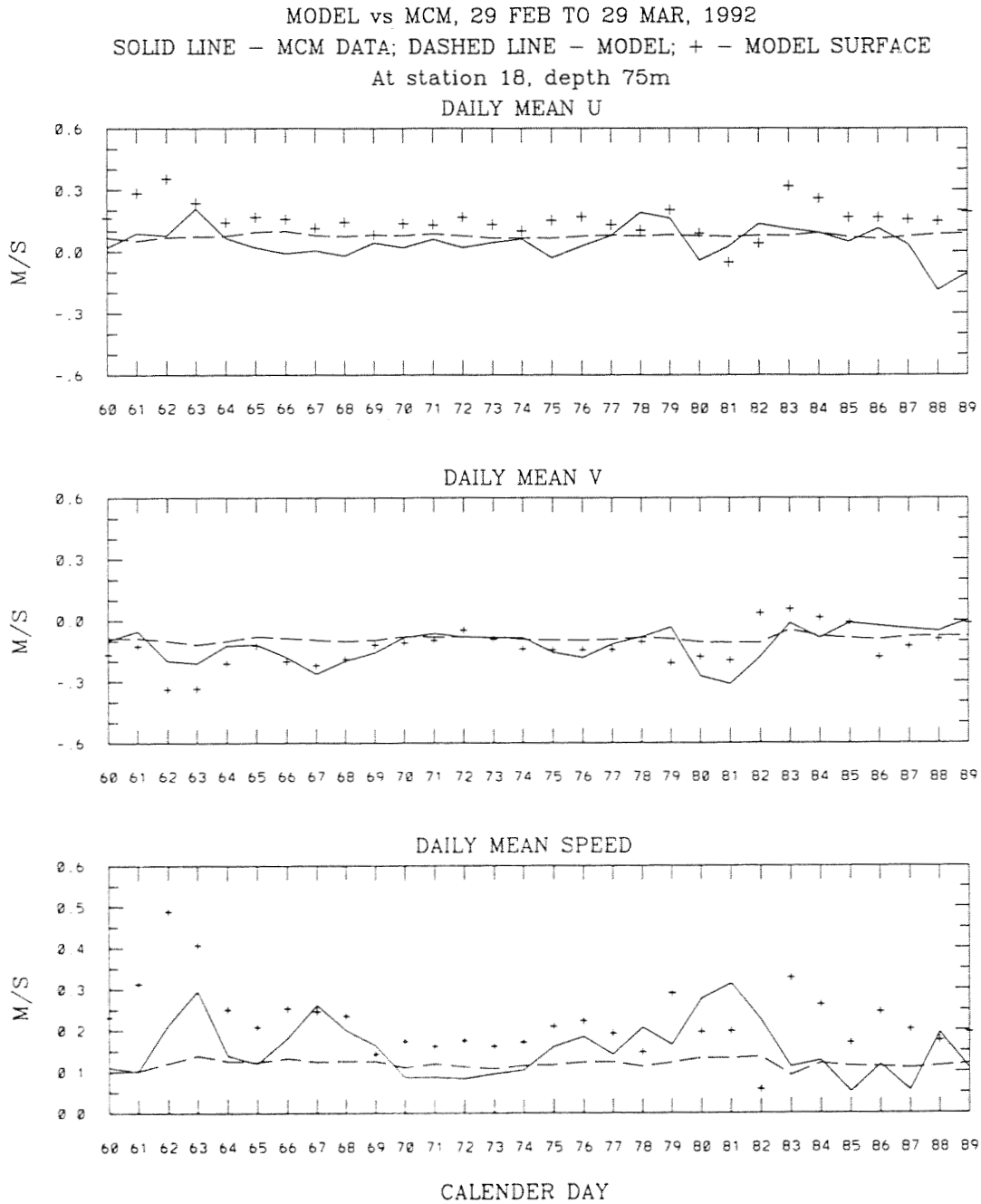


Fig. 3.13b Comparison of daily mean ocean velocities and speeds of MCM data and model simulations at Station 18 for Feb. 29 to Mar. 29, 1992.

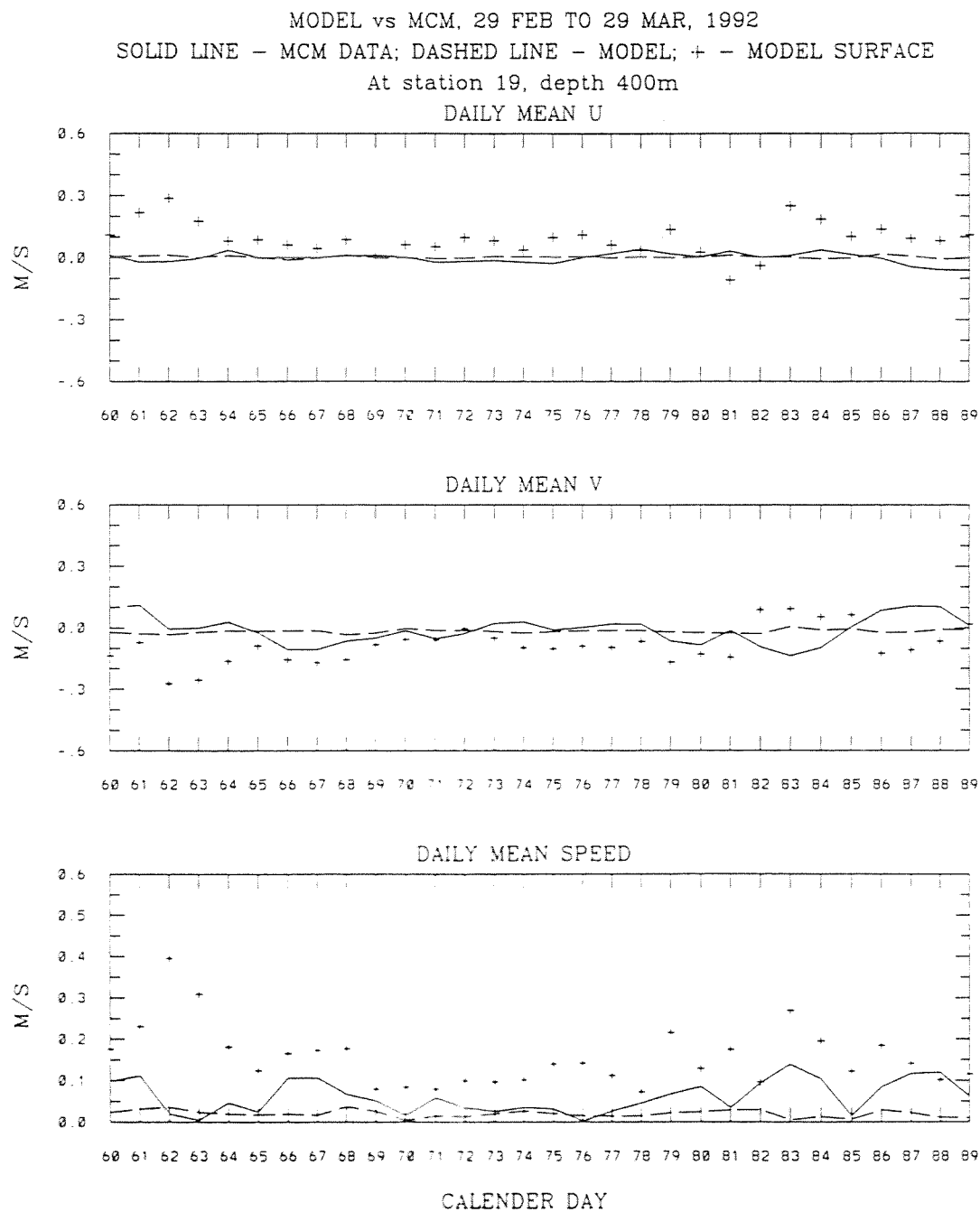


Fig. 3.13c Comparison of daily mean ocean velocities and speeds of MCM data and model simulations at Station 19 for Feb. 29 to Mar. 29, 1992.

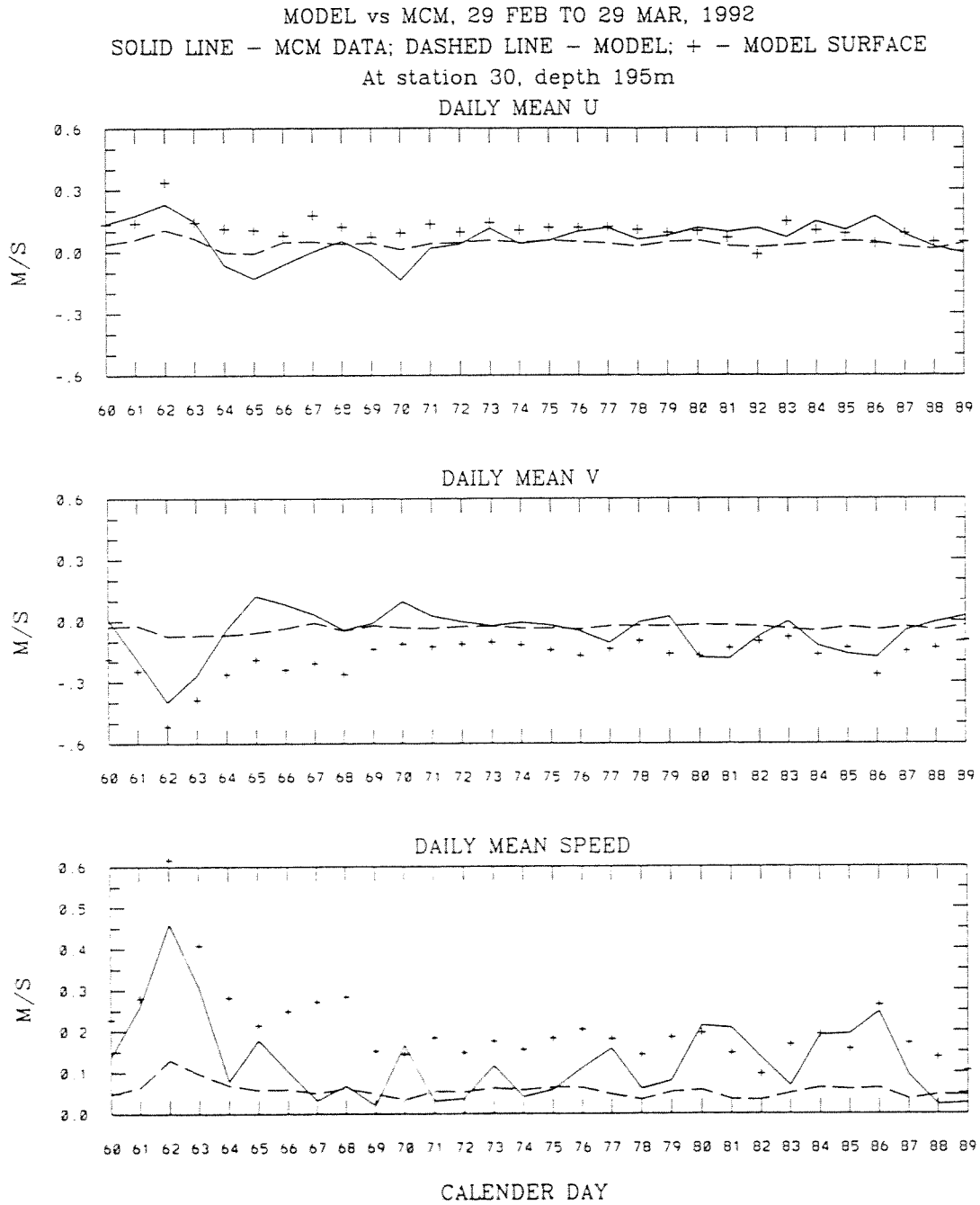
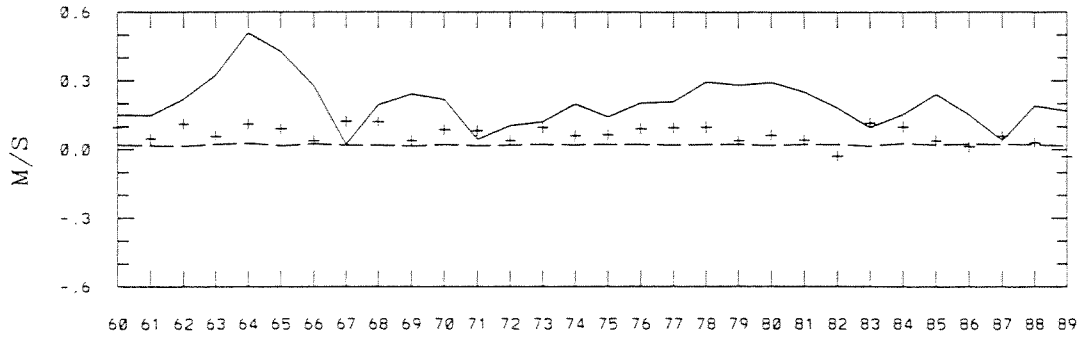
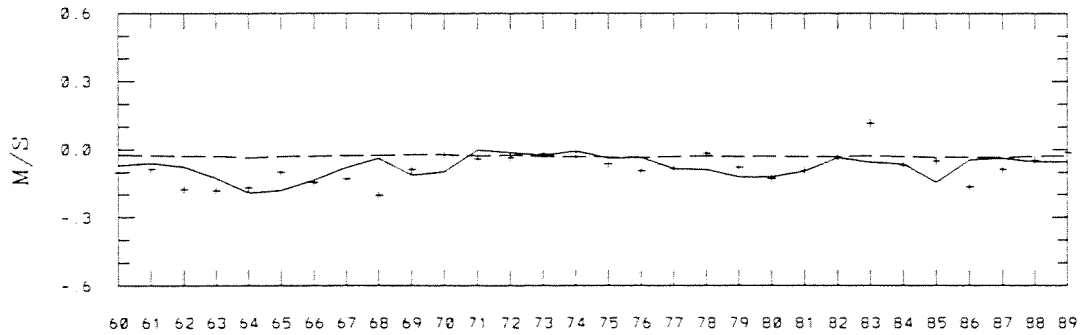


Fig. 3.13d Comparison of daily mean ocean velocities and speeds of MCM data and model simulations at Station 30 for Feb. 29 to Mar. 29, 1992.

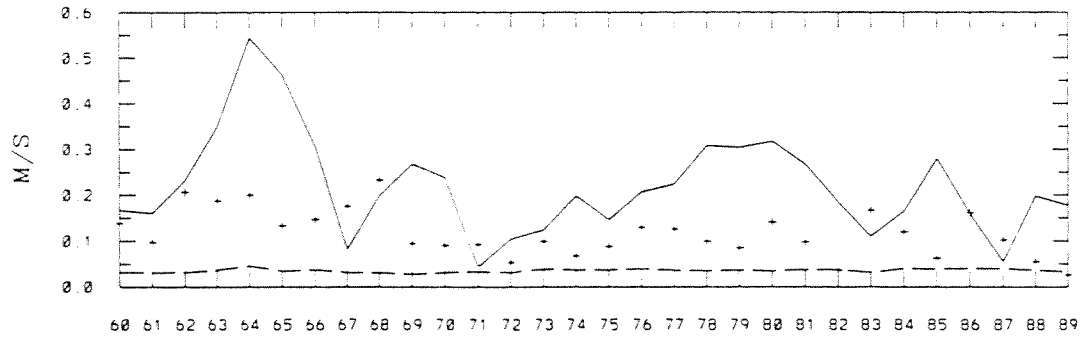
MODEL vs MCM, 29 FEB TO 29 MAR, 1992  
 SOLID LINE - MCM DATA; DASHED LINE - MODEL; + - MODEL SURFACE  
 At station 40, depth 400m  
 DAILY MEAN U



DAILY MEAN V



DAILY MEAN SPEED



CALENDER DAY

Fig. 3.13e Comparison of daily mean ocean velocities and speeds of MCM data and model simulations at Station 40 for Feb. 29 to Mar. 29, 1992.

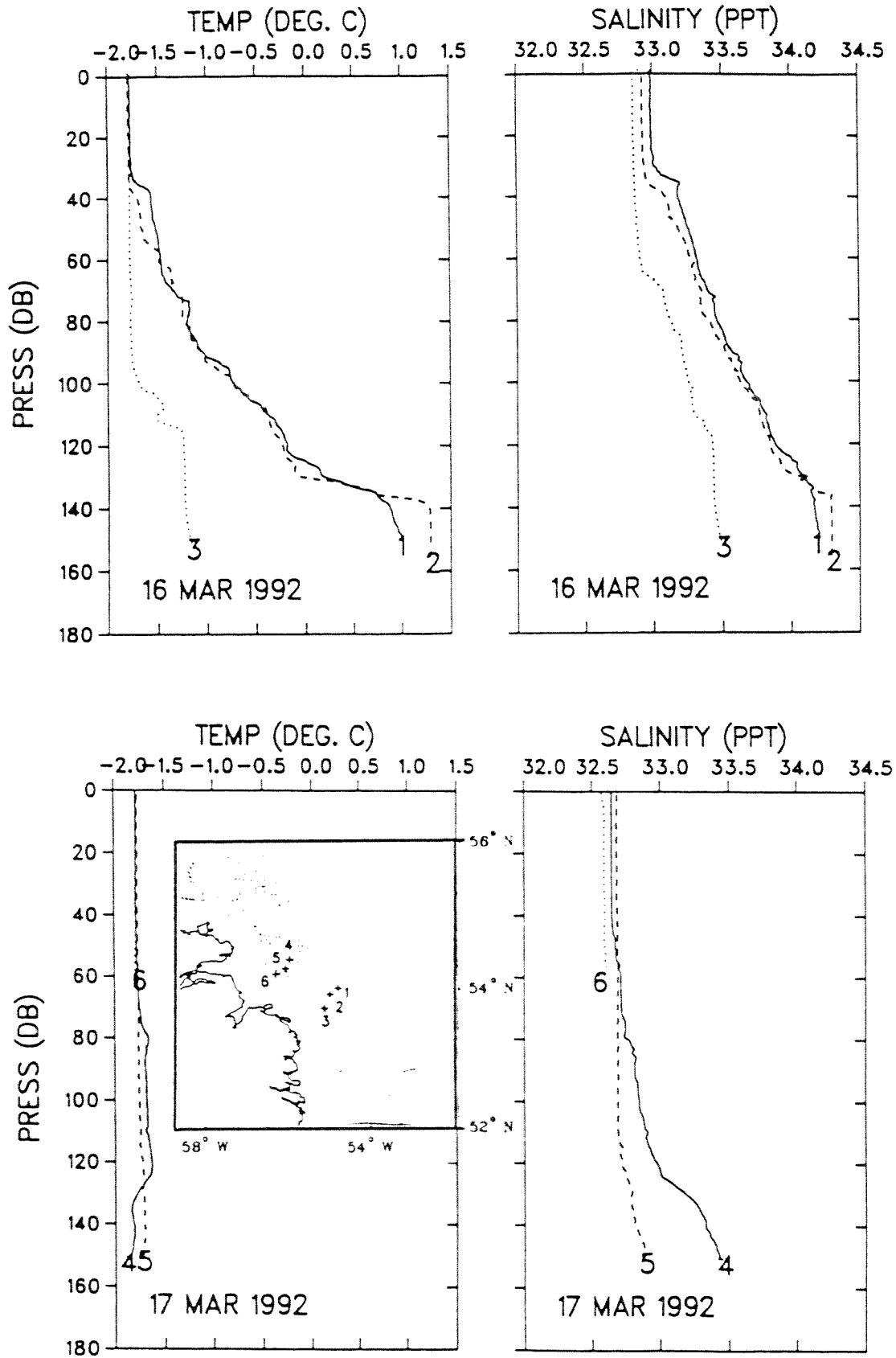


Fig. 3.14 March 1992 salinity and temperature profiles from Hamilton Bank stations 1-3, and from Cartwright Saddle stations 4-6.

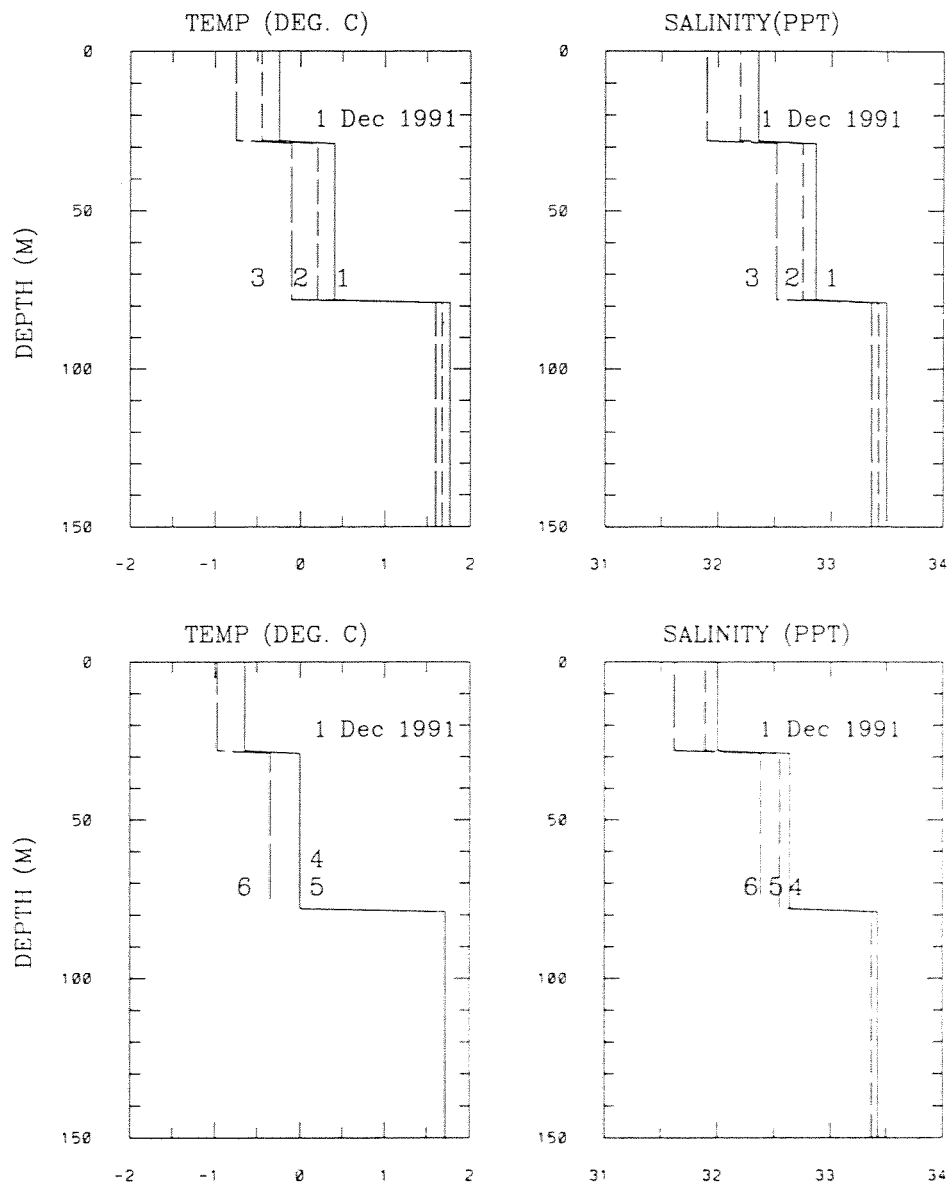
INITIAL TEMPERATURE AND SALINITY OF THE MODEL  
AT LOCATIONS 1, 2, 3, 4, 5, AND 6

Fig. 3.15 Initial temperature and salinity profiles used by the model at stations 1-6.

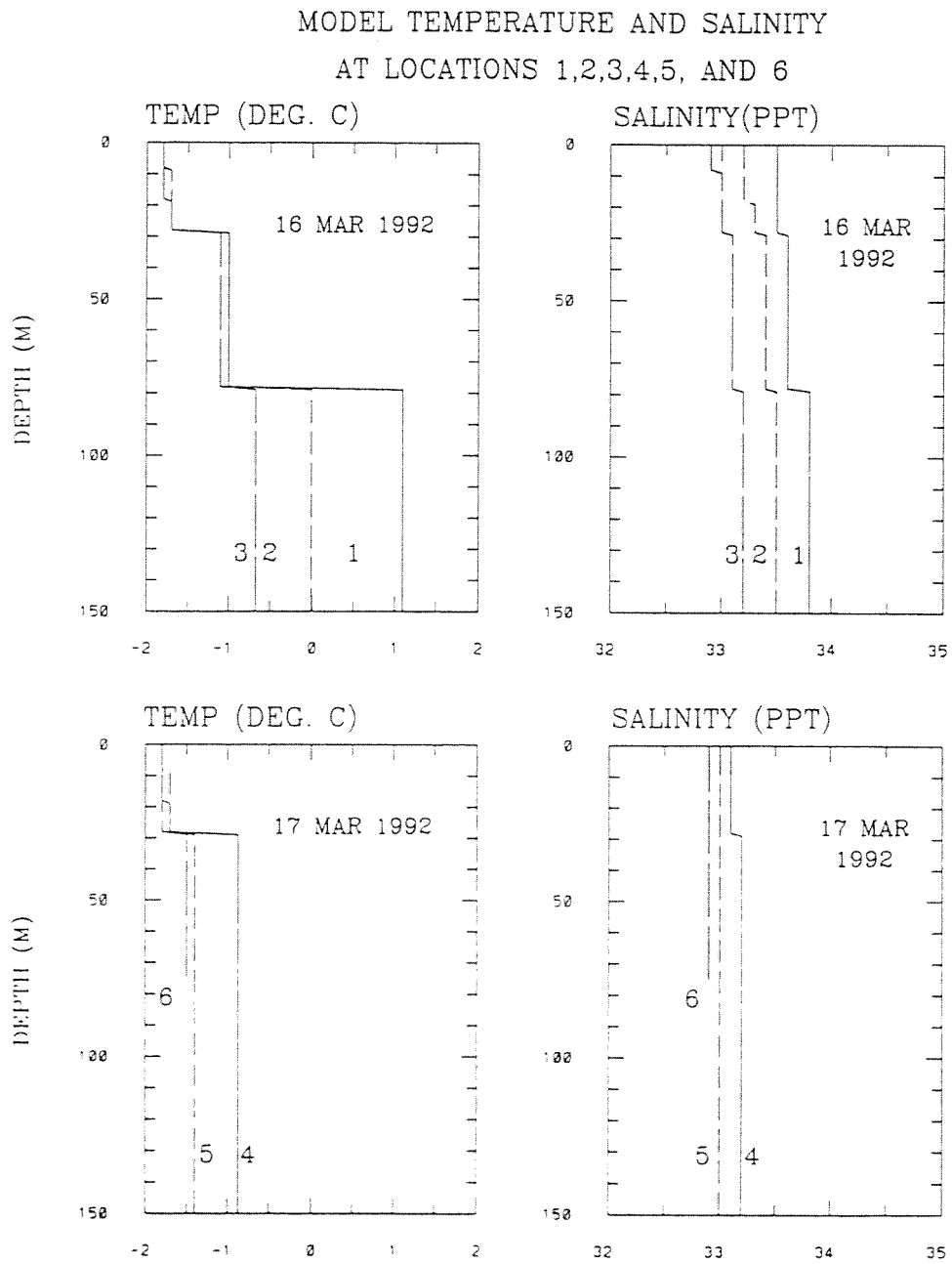
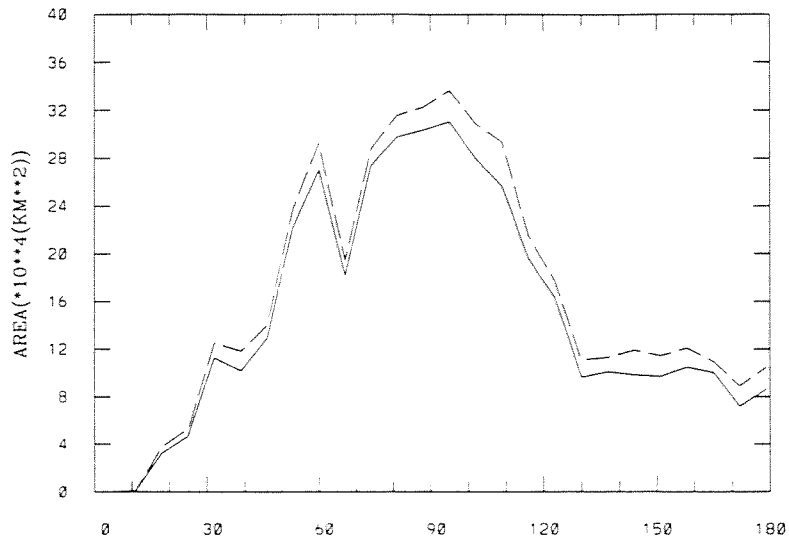


Fig. 3.16 March 1992 model simulated temperature and salinity profiles at stations 1-6.

OBSERVED DATA AND MODEL IN 91/92 ICE SEASON  
solid line - total area, dashed line - total ice extent  
AT SOUTH OF 55 N  
OBSERVED DATA (WEEKLY)



MODEL BASIC CASE (DAILY)

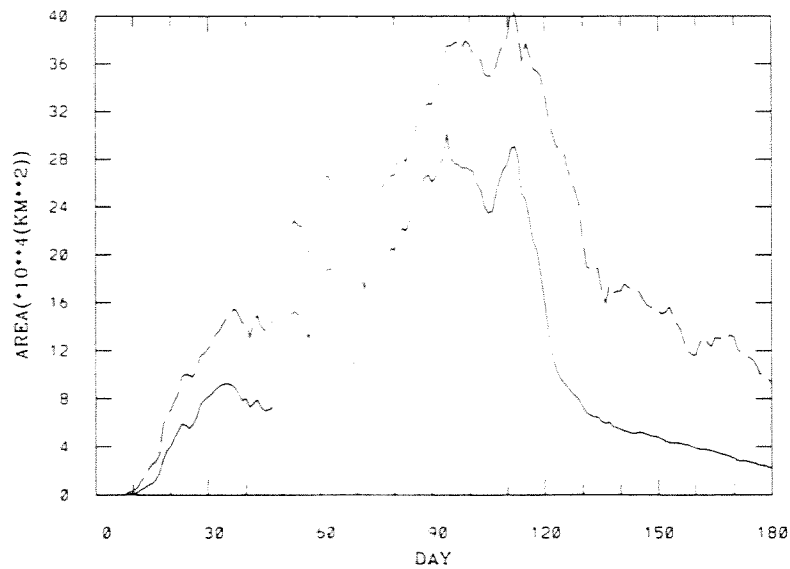


Fig. 3.17 Comparison of weekly data and 10-category ice model for 1991/92 ice season.



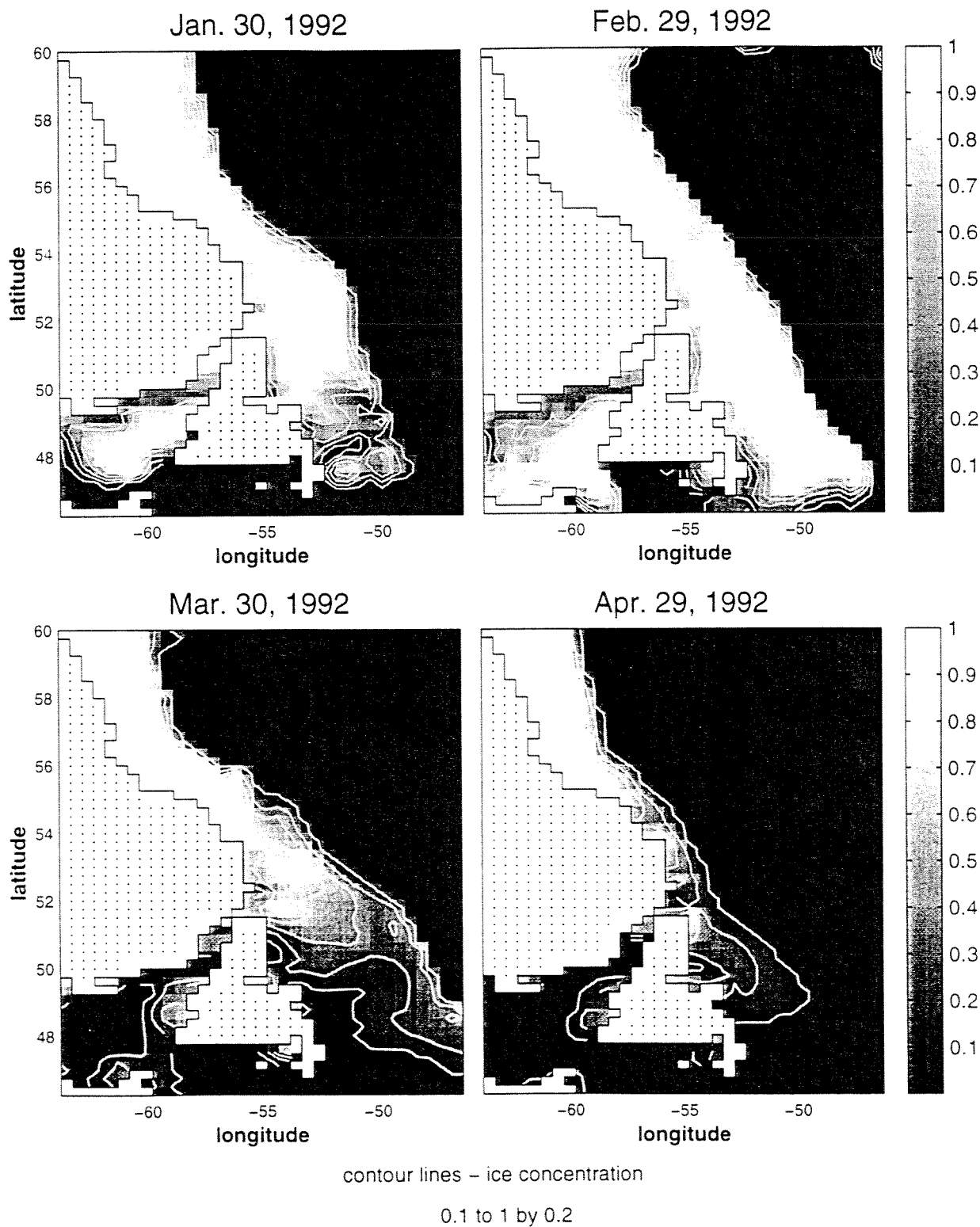


Fig.3.19 Concentrations of 10-category ice model for Jan. 30, Feb. 29, Mar. 30 and Apr. 29. 1992